AEDC-TR-75-62

cy2

STUDY OF MODEL AEROELASTIC CHARACTERISTICS IN THE PROPOSED HIGH REYNOLDS NUMBER TRANSONIC WIND TUNNEL (HIRT) IN REFERENCE TO THE AEROELASTIC NATURE OF THE FLIGHT VEHICLE

GENERAL DYNAMICS CORPORATION
CONVAIR AEROSPACE DIVISION
SAN DIEGO, CALIFORNIA 92111

October 1975

Final Report for Period April through December 1973

Approved for public release; distribution unlimited.

Prepared for

ARNOLD ENGINEERING DEVELOPMENT CENTER (DY)
AIR FORCE SYSTEMS COMMAND
ARNOLD AIR FORCE STATION, TENNESSEE 37389

NOTICES

When U. S. Government drawings specifications, or other data are used for any purpose other than a definitely related Government procurement operation, the Government thereby incurs no responsibility nor any obligation whatsoever, and the fact that the Government may have formulated, furnished, or in any way supplied the said drawings, specifications, or other data, is not to be regarded by implication or otherwise, or in any manner licensing the holder or any other person or corporation, or conveying any rights or permission to manufacture, use, or sell any patented invention that may in any way be related thereto.

Qualified users may obtain copies of this report from the Defense Documentation Center.

References to named commercial products in this report are not to be considered in any sense as an endorsement of the product by the United States Air Force or the Government.

This final report was submitted by General Dynamics Corporation, Convair Aerospace Division, San Diego, CA 37389, under contract F40600-72-C-0015, with Arnold Engineering Development Center, Arnold Air Force Station, TN 37389. Mr. Ross G. Roepke was the AEDC technical representative.

This report has been reviewed by the Information Office (OI) and is releasable to the National Technical Information Service (NTIS). At NTIS, it will be available to the general public, including foreign nations.

APPROVAL STATEMENT

This technical report has been reviewed and is approved for publication.

FOR THE COMMANDER

ROSS G. ROEPKE
Requirements Planning
Division
Directorate of Technology

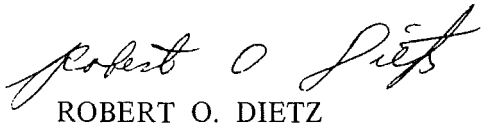

ROBERT O. DIETZ
Director of Technology

REPORT DOCUMENTATION PAGE		READ INSTRUCTIONS BEFORE COMPLETING FORM
1. REPORT NUMBER AEDC-TR-75-62	2. GOVT ACCESSION NO.	3. RECIPIENT'S CATALOG NUMBER
4. TITLE *(and Subtitle)* STUDY OF MODEL AEROELASTIC CHARACTERISTICS IN THE PROPOSED HIGH REYNOLDS NUMBER TRANSONIC WIND TUNNEL (HIRT) IN REFERENCE TO THE AEROELASTIC NATURE OF THE FLIGHT VEHICLE		5. TYPE OF REPORT & PERIOD COVERED Final Report - April through December 1973 6. PERFORMING ORG. REPORT NUMBER CASD-AFS-73-008
7. AUTHOR(s) R. L. Holt, G. J. Fatta, S. P. Tyler		8. CONTRACT OR GRANT NUMBER(s) F40600-72-C-0015
9. PERFORMING ORGANIZATION NAME AND ADDRESS General Dynamics Corporation Convair Aerospace Division San Diego, California 92111		10. PROGRAM ELEMENT, PROJECT, TASK AREA & WORK UNIT NUMBERS Program Element 65802F
11. CONTROLLING OFFICE NAME AND ADDRESS Arnold Engineering Development Center(DYFS) Air Force Systems Command Arnold Air Force Station, Tennessee 37389		12. REPORT DATE October 1975 13. NUMBER OF PAGES 128
14. MONITORING AGENCY NAME & ADDRESS*(if different from Controlling Office)*		15. SECURITY CLASS. *(of this report)* UNCLASSIFIED 15a. DECLASSIFICATION/DOWNGRADING SCHEDULE N/A

16. DISTRIBUTION STATEMENT *(of this Report)*

Approved for public release; distribution unlimited.

17. DISTRIBUTION STATEMENT *(of the abstract entered in Block 20, if different from Report)*

18. SUPPLEMENTARY NOTES

Available in DDC

19. KEY WORDS *(Continue on reverse side if necessary and identify by block number)*

high Reynolds number testing
aeroelasticity
model aeroelastic effects

20. ABSTRACT *(Continue on reverse side if necessary and identify by block number)*

The need for a High Reynolds Number Transonic Wind Tunnel (HIRT) has been recognized throughout the industry for some years. The proposed HIRT facility at Arnold Engineering Development Center will provide a much needed tool for the study of phenomena sensitive to Reynolds number. The usefulness of the HIRT facility will be largely influenced by the ability of industry to design and build wind tunnel models for an acceptable cost capable of operating within the

DD FORM 1 JAN 73 1473 EDITION OF 1 NOV 65 IS OBSOLETE

20. ABSTRACT (Continued)

severe environment of the tunnel.

This task has been examined and it has been shown that models can be built at a reasonable cost with present day techniques and materials. Accompanying the task, however, are several problems which must be considered involving the simulation of the representative aircraft shape. The objective of this study is to determine the effect of aeroelastic distortions of the wind tunnel model on the resulting aerodynamic data.

A test plan, which encompasses several critical conditions within the flight envelope, was developed for two configurations. Full-size aircraft loads and aeroelastic distortions were computed and compared with models being tested under HIRT conditions. Longitudinal aerodynamic increments are presented for the models under the various flight conditions. HIRT model wings were jig twisted to match a selected flight condition of altitude, load factor, and Mach number.

The study concludes that the incremental aeroelastic deformations from a selected flight condition, with corresponding proper model design, do not result in significant effects on the aerodynamic data. Aeroelastic differences between the model and the airplane were less than differences resulting from a rigid model. For a majority of the conditions considered during the study, the fabrication of one wing was found to be adequate. Tunnel Reynolds number and temperature controls were found to offer attractive methods of further minimizing the aerodynamic corrections due to aeroelasticity.

AFSC
Arnold AFS Tenn

PREFACE

This report describes the work performed on Air Force contract F-40600 -72-C-0015 by the Convair Aerospace Division of General Dynamics Corporation, San Diego operation, San Diego, California. This report is identified by contractor's number CASD-AFS-73-008.

The work was administered by the Department of the Air Force, Headquarters, Arnold Engineering Development Center (TMP), Arnold Air Force Station, Tennessee. Mr. Ross G. Roepke, AEDC (DYX), is the Air Force technical representative.

This program was conducted in the research and engineering department of Convair and was managed by S. A. Griffin with W. K. Alexander as coordination engineer. The work was accomplished between April and December 1973.

Principal contributors to the study include:

Dynamics	R. L. Holt
Aerodynamics	G. J. Fatta, S. P. Tyler

The reproducibles used in the reproduction of this report were supplied by the author.

TABLE OF CONTENTS

TABLE OF CONTENTS (cont'd)

LIST OF FIGURES

LIST OF FIGURES (Cont'd)

LIST OF FIGURES (Cont'd)

LIST OF FIGURES (Cont'd)

LIST OF FIGURES, Contd

LIST OF FIGURES, Contd

LIST OF FIGURES, Contd

LIST OF TABLES

SECTION 1

INTRODUCTION

The international concern over the inability of existing wind tunnel facilities to approach or match full-scale Reynolds numbers has led to the development of a variety of plans to construct high Reynolds number transonic wind tunnels. One proposed facility is HIRT, a large Ludwieg tube tunnel with an 8 by 10 foot test section. The facility is to be located at Arnold Engineering Development Center, Arnold Air Force Station, Tennessee (References 1 and 2).* The High Reynolds Number Transonic Tunnel (HIRT) will operate from Reynolds number levels of present wind tunnels to full-scale values for future aircraft.

This study is one of four conducted by General Dynamics for Arnold Engineering Development Center, addressing several problem areas unique to the proposed HIRT facility. An initial study conducted by General Dynamics (Reference 3) covered the feasibility of designing and building models capable of withstanding the loads and environmental conditions of the facility. The initial study concluded that models capable of being tested in the HIRT facility could be built at a reasonable cost with present-day techniques and materials. The additional studies have examined the feasibility of multipiece flow-through wind tunnel models for the HIRT facility, (Reference 4), six-component internal strain gage balance designs for the HIRT facility (Reference 5), and the expected precision of test data in the HIRT facility (Reference 6).

---

1. J. D. Whitfield, C. J. Schueler, and R. F. Starr, ARO, Inc., "High Reynolds Number Transonic Wind Tunnels — Blowdown or Ludwieg Tube", AGARD-CP-83 -71, April 1971.
2. R. G. Roepke, "The High Reynolds Number Transonic Wind Tunnel HIRT Proposal as Part of the National Aeronautical Facilities Program,"AIAA Paper No. 72-1035, September 1972.
3. W. K. Alexander, S. A. Griffin and R. L. Holt, General Dynamics Convair Aerospace Division, "Wind Tunnel Model Parametric Study for Use in the Proposed 8 Ft × 10 Ft High Reynolds Number Transonic Wind Tunnel (HIRT) at Arnold Engineering Development Center," AEDC Report TR-73-47, March 1973.
4. W. K. Alexander, A. E. Brady and S. A. Griffin, "Study of Multipiece Flow-through Wind Tunnel Model for HIRT" AEDC Report TR-75-60, July 1974.
5. M. L. Kuszewski, P. J. Mole and S. A. Griffin, "Study of Six-Component Internal Strain Gage Balances for Use in the HIRT Facility," AEDC Report TR-75-63, July 1974.
6. J. Picklesimer, and W. H. Lowe, "A Study of Expected Precision In the Proposed AEDC HIRT Facility," AEDC Report TR-75-61, July 1974.

---

*Since completion of this report by Convair, a final decision was made not to construct the HIRT at AEDC in favor of a continuous cryogenic wind tunnel, site as yet undetermined.

The high loads imposed on the models in the HIRT facility will produce considerable aeroelastic deformations to the primary aerodynamic surfaces. An undesired wing twist distribution will cause a disturbed span loading, which alters the configuration-induced drag characteristics. Lift and pitching moment characteristics are also altered and lead to errors in trim characteristics caused by a reduced lift curve slope and a more unstable configuration.

The objective of this task was to study the effects of model wing deformations obtained in the HIRT facility. These deformations were analyzed to obtain the effect on the longitudinal aerodynamic characteristics of related full size aircraft. Two study configurations were analyzed. First, a large transport-type aircraft, the Advanced Technology Transport, was analyzed; second, a variable-sweep wing supersonic fighter type aircraft (F-111) was analyzed.

The arrangement of this report is as follows. Section II describes the study program organization. Section III describes the test conditions that were considered for evaluating the aeroelastic and aerodynamic characteristics. Aeroelastic methods and analysis are presented in Section IV. For the aeroelastic analysis, a modified form of the Weissinger L-method was used. An aerodynamic influence coefficient matrix and a structural flexibility influence coefficient matrix were used to determine the elastic properties, deformations, and rotations of the airplane structure. Section V provides the aerodynamic methods and analysis, with a description of the study aircraft. Incremental longitudinal aerodynamic characteristics were determined from the differential aeroelastic deformation of the aircraft and the wind tunnel model. Conclusions are presented in Section VI and references in Section VII. An additional study was conducted to obtain the aeroelastic characteristics of an airplane composite wing and to assess the HIRT model/airplane wing deformation differences on the longitudinal aerodynamic characteristics. This additional study is presented in Appendix A.

SECTION II

PROGRAM ORGANIZATION

Convair Aerospace division established a program team within its research and engineering department to conduct further study of four particular problem areas associated with testing in the proposed high Reynolds number transonic wind tunnel (HIRT). The team organized to conduct the studies was led by Mr. S. A. Griffin, who reports to Mr. W. T. MacCarthy, manager of wind tunnels. The entire organization is under the senior management of the division vice president of research and engineering, Mr. R. H. Widmer.

The program operations chart, Figure 1, illustrates the flow of information from the various technical groups to the final report.

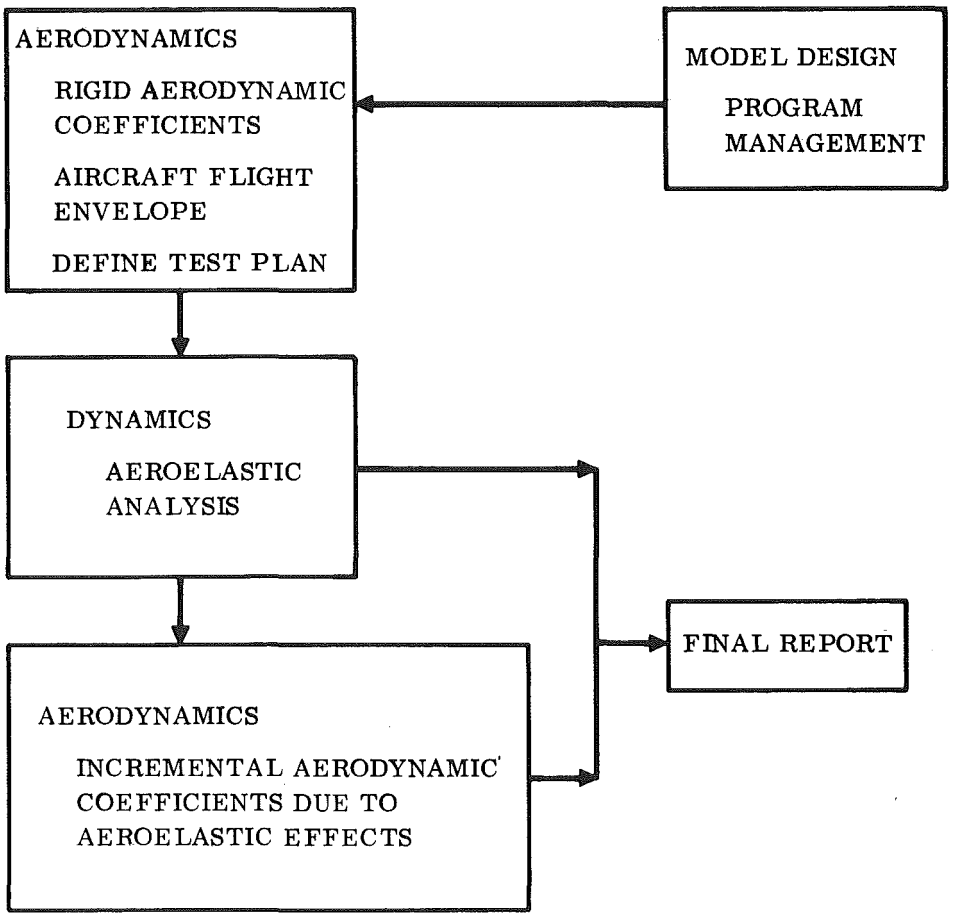

Figure 1. Program Organization

SECTION III

TEST PLAN

3.1 TUNNEL USE

It is anticipated that a great demand for test time in the HIRT facility will result in a situation where testing will necessarily be restricted to tests that are very Reynolds number dependent. Hence, use of the HIRT facility will be somewhat unlike that of current transonic wind tunnels in that plans will probably be much more operating envelope oriented or will concentrate on one particular test problem. It is current practice to test a configuration without particular regard to its envelope so that data is obtained beyond the limits that the flight vehicle can achieve. Such practice cannot be justified for HIRT testing because of the impact of high model loads and model deformations. HIRT testing will best be carried out by testing in critical areas of the operating envelope to obtain the configuration performance (typically design point cruise and maneuvering parameters).

3.2 OPERATING ENVELOPES

For the purpose of this study, selected points within the operating envelope were considered for analysis with a typical cruise condition selected to establish the airplane wing deflection and the jig twist for the HIRT models. The model test conditions were considered at full-scale Reynolds number with the tunnel operating nominally at ambient conditions. Reduced Reynolds numbers and temperature effects were also considered. Reynolds number ranges for the aircraft covered in this test plan are illustrated in Figure 2.

Flight vehicle operational envelopes for the two study configurations are shown in Figures 3 and 4. Two plots are presented for each configuration. The first plot illustrates $R_{e_{MAC}C_L}$ as a function of Mach number and altitude up to the structural limit load factor. The second plot illustrates the HIRT dynamic pressures for the equivalent envelope.

3.3 TEST PLAN DEVELOPMENT

Tables 1 and 2 respectively present summaries of the model and full-size conditions that were analyzed to determine:

a. Wing distortions (vertical deflection and twist).
b. Wing bending moments.
c. Wing pitching moments.
d. Wing shear loads.
e. Wing loading.
f. Wing section properties (EI, GJ).
g. Model angle of attack.

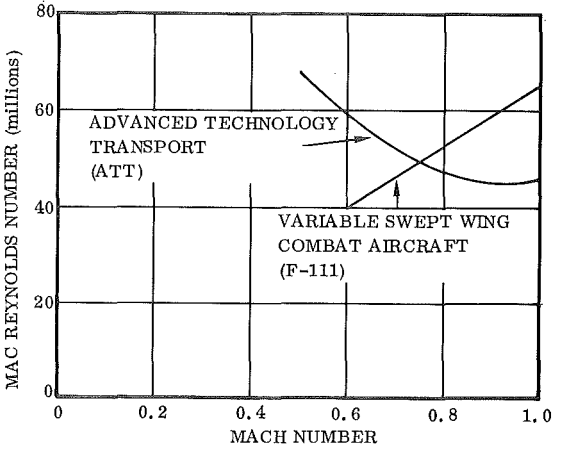

Figure 2. Reynolds Number Ranges for Aircraft in the Test Plan

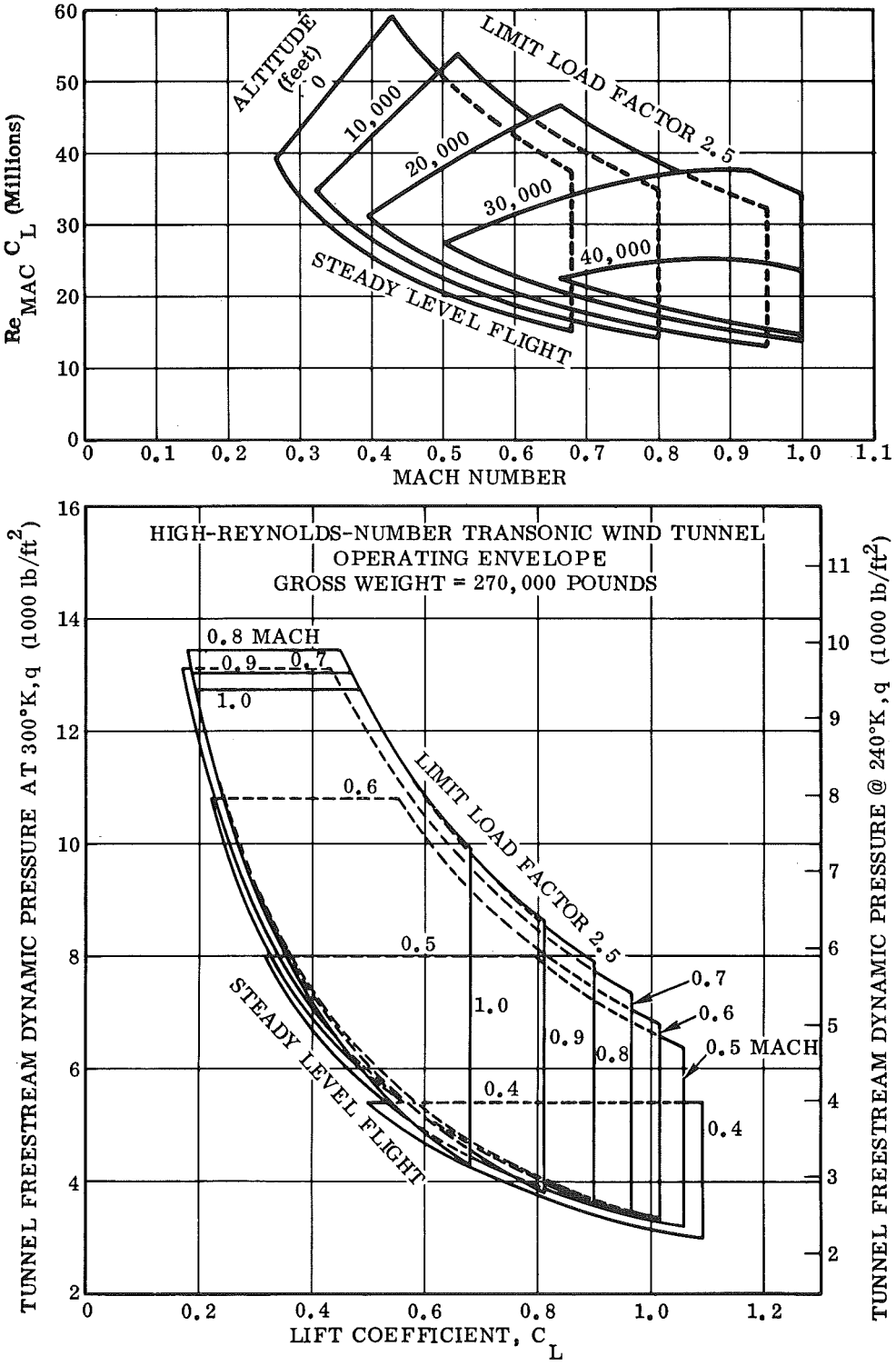

Figure 3. ATT Operating Envelope

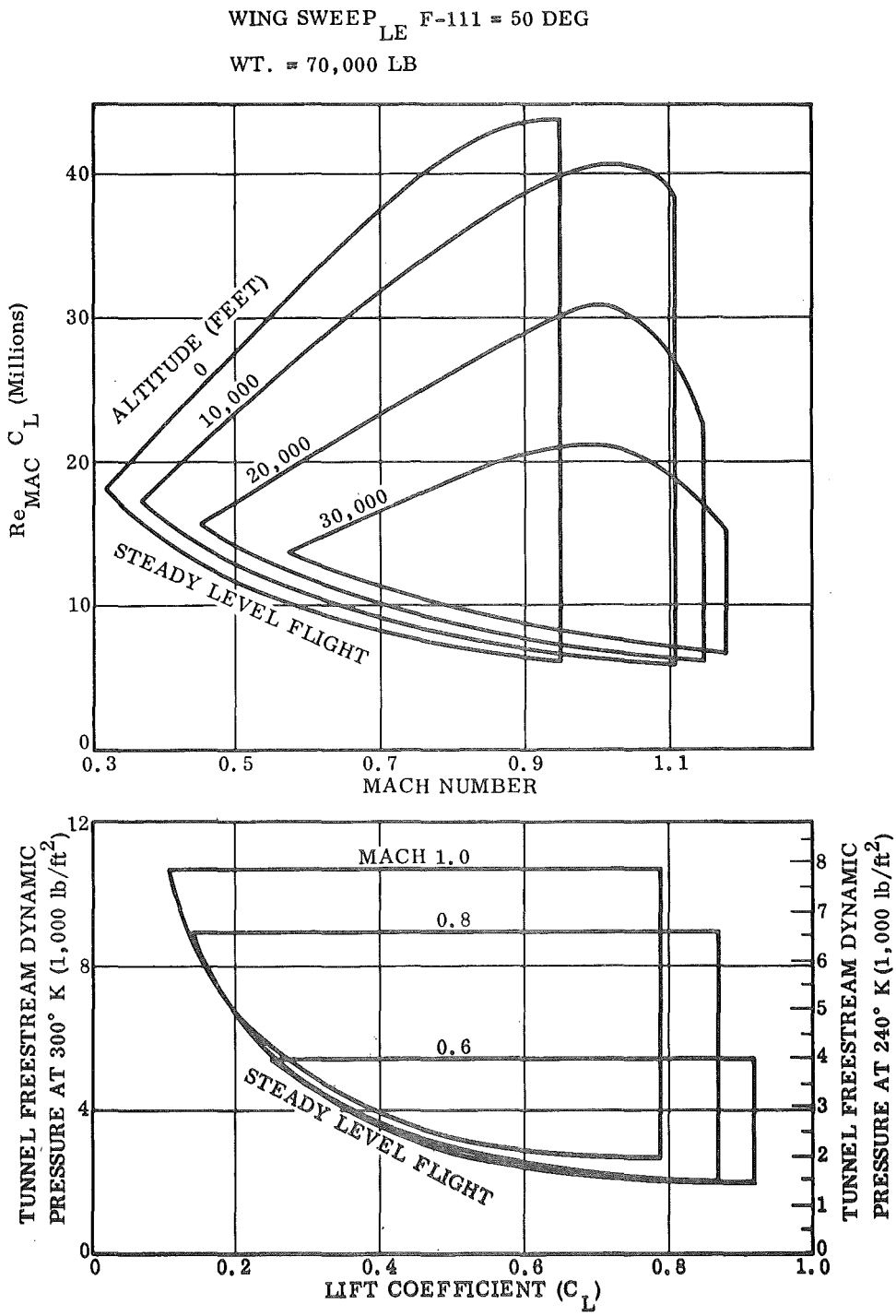

Figure 4. F-111 Operating Envelope (50 Deg Sweep)

Computer run no.	Mach number M	Altitude 10^3 (ft)	Load factor (g)	Flight dyn pres (psf)	Flight C_L	Model α (deg)	Tunnel dyn pres (psf)	Tunnel temp (°K)	Tunnel R_e/ft (10^6)	Tunnel Storage Pres (psia)	Wing struct cross sect (%)
A1	0.98	36	1.0	320	0.320	6.0	7805	300	54.5	240	65
A2	↓	↓	1.5	↓	0.480	7.8	↓	↓	↓	↓	↓
A3	↓	↓	2.0	↓	0.640	9.6	↓	↓	↓	↓	↓
A4	↓	↓	2.88	↓	0.923	12.9	↓	↓	↓	↓	↓
B1	0.80	25	1.0	352	0.336	4.2	8309	↓	64.6	300	↓
B2	↓	↓	1.5	↓	0.505	7.2	↓	↓	↓	↓	↓
B3	↓	↓	2.0	↓	0.673	10.2	↓	↓	↓	↓	↓
B4	↓	↓	2.5	↓	0.841	13.1	↓	↓	↓	↓	↓
C1	0.60	10	1.0	367	0.322	4.6	8092	↓	77.0	410	↓
C2	↓	↓	1.5	↓	0.484	6.6	↓	↓	↓	↓	↓
C3	↓	↓	2.0	↓	0.645	8.7	↓	↓	↓	↓	↓
C4	↓	↓	2.5	↓	0.806	10.8	↓	↓	↓	↓	↓
D1	0.98	36	1.0	320	0.320	6.0	7805	↓	54.5	240	52
D2	↓	↓	1.5	↓	0.480	7.8	↓	↓	↓	↓	↓
D3	↓	↓	2.0	↓	0.640	9.6	↓	↓	↓	↓	↓
D4	↓	↓	2.88	↓	0.923	12.9	↓	↓	↓	↓	↓
E1	0.95	20	1.0	614	0.193	4.0	12500	↓	89.8	390	65
E2	↓	↓	1.5	↓	0.289	5.4	↓	↓	↓	↓	↓
E3	↓	↓	2.0	↓	0.385	6.9	↓	↓	↓	↓	↓
E4	↓	↓	2.5	↓	0.482	8.3	↓	↓	↓	↓	↓
G1	0.50	20	1.0	170	0.695	8.4	4399	↓	47.0	320	↓
G2	↓	↓	1.5	↓	1.043	13.4	↓	↓	↓	↓	↓
G3	↓	↓	2.0	↓	1.391	19.4	↓	↓	↓	↓	↓
G4	↓	↓	2.5	↓	1.738	23.9	↓	↓	↓	↓	↓

Table 1. ATT HIRT Model Test Plan

Computer run no.	Mach number M	Altitude 10^3 (ft)	Load factor (g)	Flight dyn pres (psf)	Flight C_L	Model α (deg)	Tunnel dyn pres (psf)	Tunnel temp (°K)	Tunnel R_e/ft (10^6)	Tunnel Storage Pressure (psia)	Wing struct cross sect (%)
A1	0.90	30	1.0	357	0.366	4.90	4248	300	30.8	150	100
A2	↓	↓	1.5	↓	0.549	7.20	↓	↓	↓	↓	↓
A3	↓	↓	2.0	↓	0.732	9.40	↓	↓	↓	↓	↓
B1	↓	10	1.0	824	0.158	2.40	7891	↓	57.7	260	↓
B2	↓	↓	2.0	↓	0.316	4.40	↓	↓	↓	↓	↓
B3	↓	↓	3.0	↓	0.474	6.40	↓	↓	↓	↓	↓
B4	↓	↓	4.0	↓	0.631	8.35	↓	↓	↓	↓	↓
B5	↓	↓	5.0	↓	0.789	10.30	↓	↓	↓	↓	↓
C1	0.70	↓	1.0	498	0.261	3.80	5256	↓	44.9	330	↓
C2	↓	↓	2.0	↓	0.522	7.70	↓	↓	↓	↓	↓
C3	↓	↓	3.0	↓	0.783	11.50	↓	↓	↓	↓	↓
C4	↓	↓	3.4	↓	0.887	13.20	↓	↓	↓	↓	↓
D1	0.90	20	1.0	551	0.236	3.40	5900	↓	43.3	205	↓
D2	↓	↓	2.0	↓	0.473	6.40	↓	↓	↓	↓	↓
D3	↓	↓	3.0	↓	0.709	9.40	↓	↓	↓	↓	↓
D4	↓	↓	4.0	↓	0.945	12.40	↓	↓	↓	↓	↓
E1	0.70	↓	1.0	333	0.390	5.50	3700	↓	31.5	170	↓
E2	↓	↓	1.5	↓	0.586	8.10	↓	↓	↓	↓	↓
E3	↓	↓	2.0	↓	0.781	11.60	↓	↓	↓	↓	↓
E4	↓	↓	2.5	↓	0.976	14.30	↓	↓	↓	↓	↓
F1	0.90	10	1.0	824	0.158	2.40	5846	↓	43.2	205	↓
F2	↓	↓	2.0	↓	0.316	4.40	↓	↓	↓	↓	↓
F3	↓	↓	3.0	↓	0.474	6.40	↓	↓	↓	↓	↓
F4	↓	↓	4.0	↓	0.631	8.35	↓	↓	↓	↓	↓
F5	↓	↓	5.0	↓	0.789	10.30	↓	↓	↓	↓	↓
G1	↓	↓	1.0	↓	0.158	2.40	4100	↓	28.9	140	↓
G2	↓	↓	2.0	↓	0.316	4.40	↓	↓	↓	↓	↓
G3	↓	↓	3.0	↓	0.474	6.40	↓	↓	↓	↓	↓
G4	↓	↓	4.0	↓	0.631	8.35	↓	↓	↓	↓	↓
G5	↓	↓	5.0	↓	0.789	10.30	↓	↓	↓	↓	↓
H1	↓	↓	1.0	↓	0.158	2.40	5846	240	57.7	200	↓
H2	↓	↓	2.0	↓	0.316	4.40	↓	↓	↓	↓	↓
H3	↓	↓	3.0	↓	0.474	6.40	↓	↓	↓	↓	↓
H4	↓	↓	4.0	↓	0.631	8.35	↓	↓	↓	↓	↓
H5	↓	↓	5.0	↓	0.789	10.30	↓	↓	↓	↓	↓

Table 2. F-111 HIRT Model Test Plan

SECTION IV

AEROELASTIC ANALYSIS

4.1 METHODS

Considerable aeroelastic deformation of models in the HIRT facility is a certainty. A means of accounting for the model aeroelasticity is necessary before the test data can be applied to the full size design problem. A simultaneous solution of equations that contain both the aerodynamic influence functions and the structural influence functions are necessary for this task. A method based on a modification of the Weissinger L-Method was used to accomplish this analysis. The method and digital program (Reference 7) was written for computing steady-state spanwise load distributions on an elastic airplane wing for specified airplane weights and load factors. The Weissinger L-Method, originally developed for subsonic flow, is valid for supersonic flow providing that the flow over the wing is subsonic (this is a case where the leading edge of a swept wing is behind the shock cone).

The modified Weissinger L-Method used in this analysis was from the work of Gray and Schenk (Reference 8). Additional information was used from the works of Schindel (Reference 9), Borland (Reference 10) and Blackwell (Reference 11).

The aeroelastic program was used to determine the loads for each flight condition of the airplane and the resulting wing twist and bending. Model deformation and loads were also determined for the equivalent Reynolds number test condition in the HIRT facility. Prior to the determination of the airplane/model loading conditions, rigid aerodynamic characteristics of the airplane configurations were determined through the use of wind tunnel test data and DATCOM (Reference 12).

---

7. "Application of Lifting Line Theory to Aircraft Aeroelastic Loads Analysis," General Dynamics Convair Report No. GDC-ERR-AN-1128, February 1968.
8. W. L. Gray and K. M. Schenk, Boeing Aircraft Co., "A Method for Calculating the Subsonic Steady-State Loading on an Airplane with a Wing of Arbitrary Planform and Stiffness," NACA TN 3030, December 1953.
9. L. H. Schindel, "An Evaluation of Procedures for Calculating Aerodynamic Loads," AFFDL-TR-65-18, May 1965.
10. C. J. Borland, "Methods of Calculating Aerodynamic Loads on Aircraft Structures," AFFDL-TR-66-37, August 1966.
11. J. A. Blackwell, Jr., "A Finite Step Method for Calculation of Theoretical Load Distribution for Arbitrary Lifting – Surface Arrangements at Subsonic Speeds," NASA TND-5335, 1969.
12. "USAF Stability and Control DATCOM," AFFDL.

Each flight condition presented in Tables 1 and 2 was analyzed through the use of the aeroelastic program. This section presents the spanwise variation of the elastic wing twist and the wing vertical deflection for the study configurations. Estimated incremental aerodynamic characteristics are presented in Section V of this report for the resulting wing twist differences between the airplane and the HIRT model under equivalent Reynolds number testing. Model and full-size geometric data used in the aeroelastic analysis are presented in Figure 5 with an illustration of the wing geometry strip arrangement.

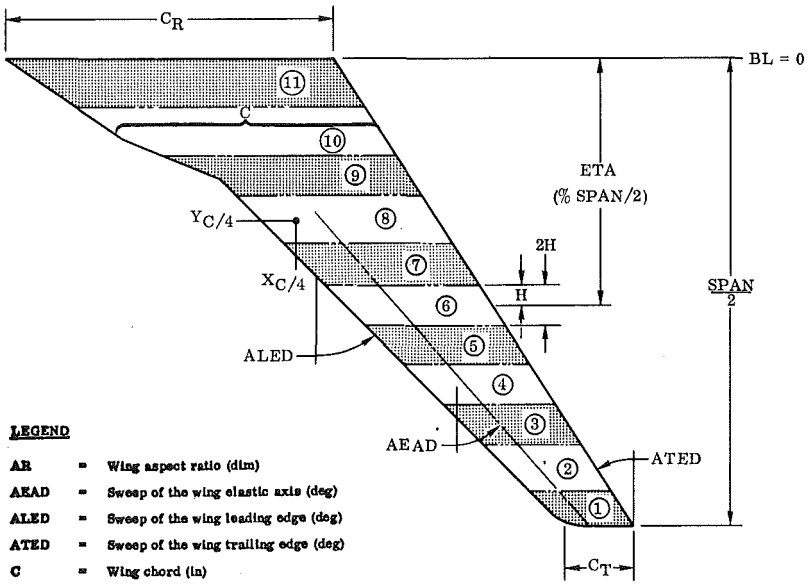

Figure 5 Aerolastic Program Geometry

FULL SIZE ATT

ETA	C	2H	XC4	YC4	ZC4	EA	ALED	AEAD	ATED
ND	IN	IN	IN	IN	IN	ND	DEG	DEG	DEG
.96	120.80	70.12	1551.22	775.54	193.20	.40	43.50	40.66	36.00
.87	136.39	70.12	1498.58	705.42	193.20	.40	43.50	40.66	36.00
.78	151.98	70.04	1425.98	635.35	193.20	.40	43.50	40.66	36.00
.70	167.56	70.12	1363.38	565.27	193.20	.40	43.50	40.66	36.00
.61	183.15	70.04	1300.78	495.20	193.20	.40	43.50	40.66	36.00
.52	198.74	70.12	1238.17	425.12	193.20	.40	43.50	40.66	36.00
.44	214.32	70.04	1175.57	355.04	193.20	.40	43.50	40.66	36.00
.35	258.61	80.01	1113.41	280.02	193.20	.40	45.00	32.23	5.00
.25	350.70	71.98	1037.70	204.03	193.20	.40	58.50	45.18	5.00
.16	503.93	77.57	916.23	129.25	193.20	.40	69.00	57.76	5.00
.06	640.55	90.46	806.42	45.23	193.20	.40	43.50	30.97	5.00

CR=679.51 CT=113.00 SPAN= 1621.20 WINGA= 450341.70 AR= 5.84

CALCULATED CBAR=380.521 AT(X=979.77 Y=278.27 Z=193.20)

1/24 SCALE ATT

ETA	C	2H	XC4	YC4	ZC4	EA	ALED	AEAD	ATED
ND	IN	IN	IN	IN	IN	ND	DEG	DEG	DEG
.96	5.03	2.92	64.63	32.31	8.05	.40	43.50	40.66	36.00
.87	5.68	2.92	62.02	29.39	8.05	.40	43.50	40.66	36.00
.78	6.33	2.92	59.42	26.47	8.05	.40	43.50	40.66	36.00
.70	6.98	2.92	56.81	23.55	8.05	.40	43.50	40.66	36.00
.61	7.63	2.92	54.20	20.63	8.05	.40	43.50	40.66	36.00
.52	8.28	2.92	51.59	17.71	8.05	.40	43.50	40.66	36.00
.44	8.93	2.92	48.98	14.79	8.05	.40	43.50	40.66	36.00
.35	10.78	3.33	46.39	11.67	8.05	.40	45.00	32.23	5.00
.25	14.61	3.00	43.24	8.50	8.05	.40	58.50	45.18	5.00
.16	21.00	3.23	38.18	5.39	8.05	.40	69.00	57.76	5.00
.06	26.69	3.77	33.60	1.89	8.05	.40	43.50	30.97	5.00

CR= 28.31 CT= 4.71 SPAN= 67.55 WINGA= 781.84 AR= 5.84

CALCULATED CBAR= 15.855 AT(X= 40.82 Y= 11.59 Z= 8.05)

Figure 5 Aerolastic Program Geometry (cont'd)

FULL SIZE F-111, 50° SWEEP

ETA	C	2H	XC4	YC4	ZC4	EA	ALED	AEAD	ATED
NO	IN	IN	IN	IN	IN	NO	DEG	DEG	DEG
.95	70.98	25.99	692.48	269.50	202.70	.44	50.00	44.29	35.00
.86	83.76	26.02	664.68	243.50	202.25	.44	50.00	44.29	35.00
.77	96.54	25.99	636.89	217.50	201.80	.44	50.00	44.29	35.00
.68	109.32	25.99	609.11	191.51	201.34	.44	50.00	44.29	35.00
.59	122.10	26.02	581.31	165.50	200.89	.44	50.00	44.29	35.00
.49	134.88	25.99	553.52	139.50	200.43	.44	50.00	44.29	35.00
.40	147.66	25.99	525.74	113.51	199.98	.44	50.00	44.29	35.00
.33	169.40	14.46	495.27	93.28	199.63	.44	70.50	62.11	35.00
.28	201.35	15.62	460.77	78.24	199.37	.44	70.50	62.11	35.00
.19	252.46	32.52	405.58	54.17	198.95	.44	70.50	62.11	35.00
.07	327.24	37.91	324.84	18.96	198.33	.44	70.50	62.11	35.00

CR=367.50 CT= 64.59 SPAN= 565.00 WINGA= 92196.09 AR= 3.46

CALCULATED CBAR=206.330 AT(X=423.25 Y=101.96 Z=199.79)

1/12 SCALE F-111, 50° SWEEP

ETA	C	2H	XC4	YC4	ZC4	EA	ALED	AEAD	ATED
NO	IN	IN	IN	IN	IN	NO	DEG	DEG	DEG
.95	5.93	2.16	57.65	22.42	16.89	.44	50.00	44.29	35.00
.86	7.00	2.16	55.34	20.26	16.85	.44	50.00	44.29	35.00
.77	8.06	2.16	53.02	18.09	16.82	.44	50.00	44.29	35.00
.68	9.12	2.16	50.71	15.93	16.78	.44	50.00	44.29	35.00
.59	10.19	2.16	48.40	13.77	16.74	.44	50.00	44.29	35.00
.49	11.25	2.16	46.09	11.60	16.70	.44	50.00	44.29	35.00
.40	12.31	2.16	43.78	9.44	16.66	.44	50.00	44.29	35.00
.33	14.12	1.20	41.24	7.76	16.64	.44	70.50	62.11	35.00
.28	16.78	1.30	38.37	6.51	16.61	.44	70.50	62.11	35.00
.19	21.03	2.70	33.78	4.51	16.58	.44	70.50	62.11	35.00
.07	27.25	3.15	27.07	1.58	16.53	.44	70.50	62.11	35.00

CR= 30.60 CT= 5.40 SPAN= 47.00 WINGA= 639.36 AR= 3.46

CALCULATED CBAR= 17.185 AT(X= 35.26 Y= 8.49 Z= 16.65)

Figure 5 Aerolastic Program Geometry (cont'd)

4.2 AEROELASTIC EQUATIONS

The three most basic equations in this aeroelastic analysis are as follows.

Kutta-Joukowsky Relationship

$$\ell = \rho V \Gamma$$

where

ℓ = span loading

V = velocity

ρ = fluid density

$\Gamma = \oint w_p \, ds$ = circulation

Biot-Savart Law of Vorticity

This law was applied to the bound vortex and the trailing vortices at each wing strip to calculate the aerodynamic influence functions:

$$w_p = \frac{\Gamma(\cos \alpha - \cos \beta)}{4 \pi R}$$

where α and β are the angles between the direction of the vortex segment and lines joining the ends of the segment to the control point (sketch). The control point in this theory is located at the .75c location of each strip. W_p is the velocity induced normal to the plane of the wing.

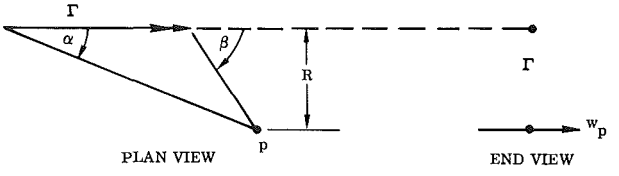

Castigliano Theorem

A part of the general Castigliano Theorem was used that related the twisting of a structure to the applied bending and torsional moments by means of virtually applied moments. Structural properties are induced by the EI and GJ terms.

$$\alpha_s = \int \frac{m \, M \, ds}{EI} + \int \frac{t \, T \, ds}{GJ}$$

where

α_s = Elastic angle of attack change due to bending and torsional moments along the elastic axis.

m = Beam bending moment per unit pitching moment applied at the station at which θ is to be determined.

t = Torsional moment around the elastic axis per unit pitching moment.

ds = Incremental distance along elastic axis.

EI = Effective beam stiffness around the axis of the bending moments M and m.

GJ = Effective torsional stiffness around the axis of the torsional moments T and t.

Angle-of-attack definitions and positive sign convention are as follows:

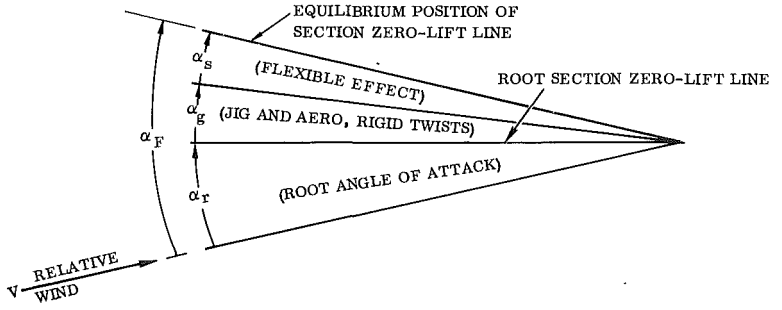

Angle of Attack at Each Strip:

$$\{\alpha_F\} = (\alpha_r) + \{\alpha_g\} + \{\alpha_s\} \tag{1}$$

where:

$$\{\alpha_F\} = \left[[I] - QS\,[E_A] + \left[\frac{\Delta V_z}{V_z}\right]\right] \times \left[\frac{1}{4\,m_o}\right] \times \left[[A_W] + [A_F]\right] \times \{c_\ell c\}$$

$$\{\alpha_S\} = \int_o^\eta \frac{m\,M\,ds}{EI} + \int_o^\eta \frac{t\,T\,ds}{GJ} = Q\,[S] \times \{c_\ell c\}$$

$$\{\alpha_g\} = \left[\frac{\Delta V_z}{V_z}\right] \times (\alpha_r) - \{\alpha_g/P_T\} \times P_T + \alpha_T + (\alpha_{o}L_{root}) - \{\alpha_o L_{sect}\}$$

$$+ (\alpha_{inc_{fus}}) + \alpha_o L_{root}) \left[\frac{\Delta V_z}{V_z}\right] \left\{ \frac{\alpha_{o}L_{body} + \alpha_{inc}}{\alpha_{o}L_{root} + \alpha_{inc}} \begin{matrix} \text{sect} \quad \text{body} \\ \text{fus} \end{matrix} \right\} + \left\{\frac{\alpha}{\delta_{FL}}\right\}\delta_{FL} + \left\{\frac{\alpha}{\delta_{SP}}\right\} \delta_{SP}$$

$$+ \left\{\frac{\alpha}{\delta_{SL}}\right\} \delta_{SL} + \alpha_{g_I} + \alpha_{g_{II}}$$

(α_r) = root angle of attack

Vertical Force on Both Wings:

$$\underbrace{4QH \times \{c_{\ell} c\}}_{\text{wings}} + 2QS \sum_{1}^{n} \left(C_{L_{E_\alpha}}\right)_n \times \underbrace{\left[\frac{1}{4m_o}\right]}_{\text{stores}} \times [A_W + A_F] \times \{c_{\ell} c\} + \underbrace{QS\, C_{L_{F_\alpha}} \alpha_r}_{\text{fuselage}} + \underbrace{P_T}_{\text{tail}}$$

$$= \underbrace{n_z W}_{\text{inertia}} - QS\left(C_{L_{F_o}} + C_{L_{F_\alpha}}\left(\alpha_{\substack{\text{inc} \\ \text{fus}}} + \alpha_{\substack{oL \\ \text{root}}}\right)\right) - \underbrace{2QS \sum_{1}^{n} \left(C_{L_{E_o}}\right)_n}_{\text{stores}} \qquad (2)$$

Moments on Both Wings at $\bar{c}/4$

$$\underbrace{-4QH(XC4 - \bar{X}C4)\ \{c_{\ell} c\}}_{\text{wings}} - 2QS \sum_{1}^{n} \left[\left(C_{L_{E_\alpha}}\right)_n (XE - XC4) + C_{D_{E_\alpha}}{}_n \bar{c}\right]$$

$$\underbrace{\times \left[\frac{1}{4m_o}\right] \times [A_W + A_F] \times \{c_{\ell} c\}}_{\text{stores}} + QS\left(C_{L_{F_\alpha}} (\bar{X}C4 - X\text{fus}) + C_{M_{F_\alpha}} \bar{c}\right.$$

$$\left. - C_{L_{\alpha_{\text{tail}}}} \left(1 - \frac{d\epsilon}{d\alpha}\right)(XDE)\right) \times \alpha_r - \underbrace{(X\text{tail} - XC4 - XDE) \times P_T}_{\text{tail}} =$$

$$\underbrace{I_{Y_{CG}} \ddot{\theta}_{CG} - {}_z W (XCG - \bar{X}C4)}_{\text{inertia}} - \underbrace{4Q\left[HC^2 I\right]\{C_{m_o}\}}_{\text{wing } C_{m_o}}$$

$$+ QS\left(C_{L_{F_o}} + \left(C_{L_{F_\alpha}}\right)\left(\alpha_{\substack{\text{inc} \\ \text{fus}}} + \alpha_o L_R\right)\right) \times (X\text{fus} - \bar{X}C4)$$

$$\underbrace{- QS\left(C_{M_{F_o}} + \left(C_{M_{F_\alpha}}\right)\left(\alpha_{\substack{\text{inc} \\ \text{fus}}} + \alpha_o L_R\right)\right) \bar{c}}_{\text{fuselage}} + \underbrace{\Delta C_{D_{\text{fus}}} (\bar{Z}C4 - ZCD_{\text{fus}})}_{\text{fus drag}}$$

$$\underbrace{+ \Delta C_{D_{\text{tail}}} (\bar{Z}C4 - ZCD_{\text{tail}})}_{\text{tail drag}} + 2QS \sum_{1}^{n} \left(\left(C_{L_{E_o}}\right)_n (XE - \bar{X}C4) - \left(C_{M_{E_o}}\right)_n \bar{c}\right.$$

$$\left. + \left(\Delta C_{D_E}\right)_n (\bar{Z}C4 - ZE)\right) + \underbrace{QS\, C_{L_{\alpha_{\text{tail}}}} \times \alpha_{\substack{\text{inc} \\ \text{tail}}} \times XDE}_{\text{stores}} \qquad (3)$$

4.3 TUNNEL OPERATING CONDITIONS

Tunnel operating conditions were obtained from a set of estimated flow property curves for the proposed HIRT facility (Reference 13). These curves were supplied by the government for use in this study. Tunnel dynamic pressures as a function of Reynolds number per foot are presented in Figures 6 and 7 for storage temperatures of 300°K and 240°K. Since Reynolds number is sensitive to freestream temperature, a significant reduction of dynamic pressure can be obtained by using a cooled freestream temperature.

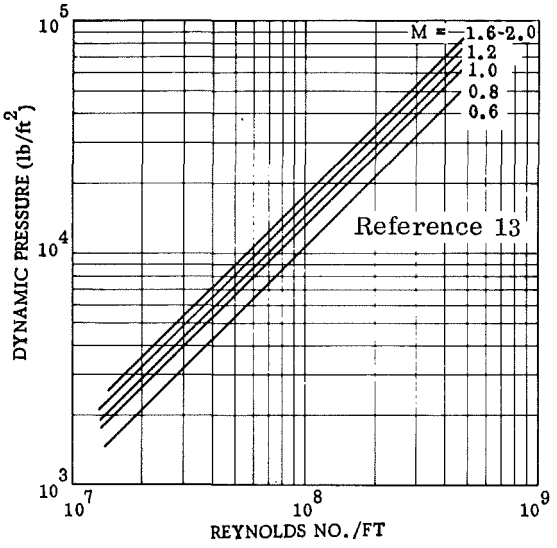

Figure 6. Tunnel Reynolds Number and Dynamic Pressure Characteristics at 300°K

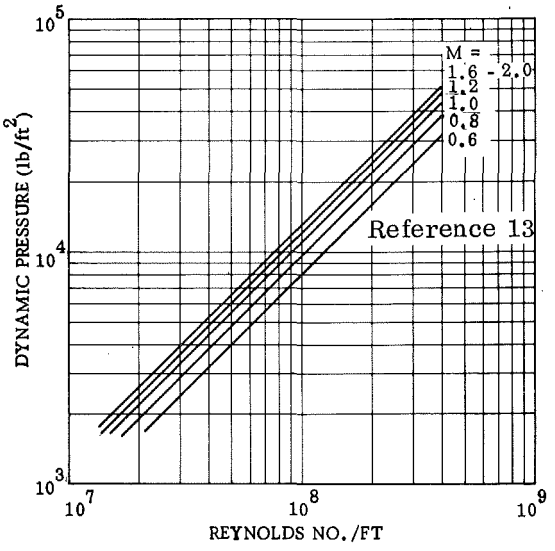

Figure 7. Tunnel Reynolds Number and Dynamic Pressure Characteristics at 240°K

13. "Curves of Flow Properties for HIRT Operation," USAF, June 1972.

4.4 F-111 AIRPLANE AEROELASTIC ANALYSIS

The F-111 airplane wing deformation characteristics were obtained from data presented in References 14, 15 and 16. Structural properties (EI and GJ), elastic axis location, airplane geometry, and inertia distribution were obtained from Reference 16. The wing bending and torsional stiffness properties were modified to account for the leading and trailing edge portions of the wing section. The wing bending moment of inertia and the polar moment of inertia characteristics of the F-111 airplane are presented in Figure 8 for a wing sweep of 50 degrees.

Figure 9 shows the airplane wing jig twist distribution for the 50 degree wing sweep. Using the data presented in Reference 16 and the data shown in Figures 8 and 9, the aeroelastic program was used to obtain the deformation characteristics of the F-111 airplane at selected flight conditions.

Figure 10 shows the elastic wing twist distribution for the F-111 airplane at an altitude of 10,000 feet and Mach 0.90 for several flight load factors. Figure 11 illustrates the elastic wing twist distribution as a function of load factor for a flight condition of 20,000 feet and Mach 0.90. Figure 12 illustrates the elastic wing twist distribution at an altitude of 30,000 feet and Mach 0.90 for several flight load factors. From Figures 10, 11 and 12 at a load factor of 2.0, the effect of increasing dynamic pressure, as shown in Figure 13, results in a more negative wing twist (wash-out). Figure 14 illustrates the non-dimensional vertical deflection of the airplane wing at load factors of 1.0, 2.0, 3.0 and 4.0 for a flight condition at 20,000 feet and Mach 0.90. A flight condition at 20,000 feet and Mach 0.70 was analyzed resulting in the wing elastic distributions shown in Figure 15. Figure 16 shows the wing elastic distributions as a function of the load factor for the airplane at an altitude of 10,000 feet and Mach 0.70.

14. "F-111 Wing Aeroelastic Analysis for the Safe Life Steel Wing Carry-Through-Box," General Dynamics Convair Aerospace Division, Report No. FZS-12-1030, January 1970.

15. "F-111C Wing Aeroelastic Analysis for the Safe Life Steel Wing Carry-Through-Box," General Dynamics Convair Aerospace Division Report No. FZS-12-5003, April 1971.

16. "F-111 A/B Basic Data Report," General Dynamics Convair Aerospace Division Report No. FZS-12-157, January 1966.

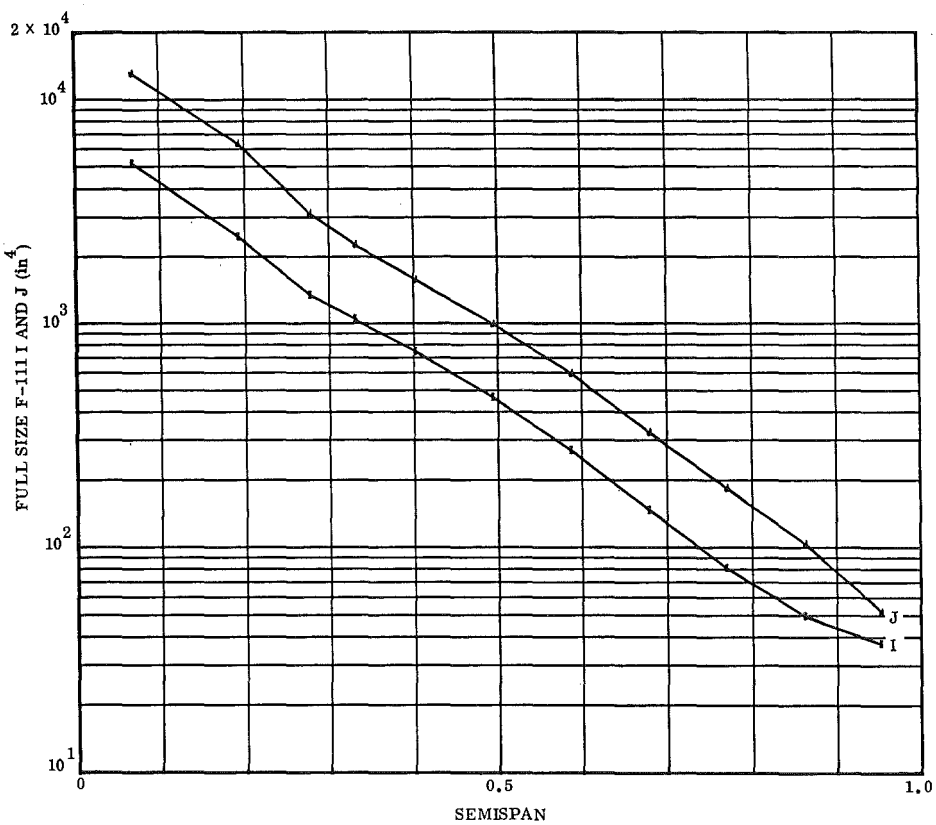

Figure 8. Wing Bending Moment of Inertia and Polar Moment of Inertia for the F-111 Wing.

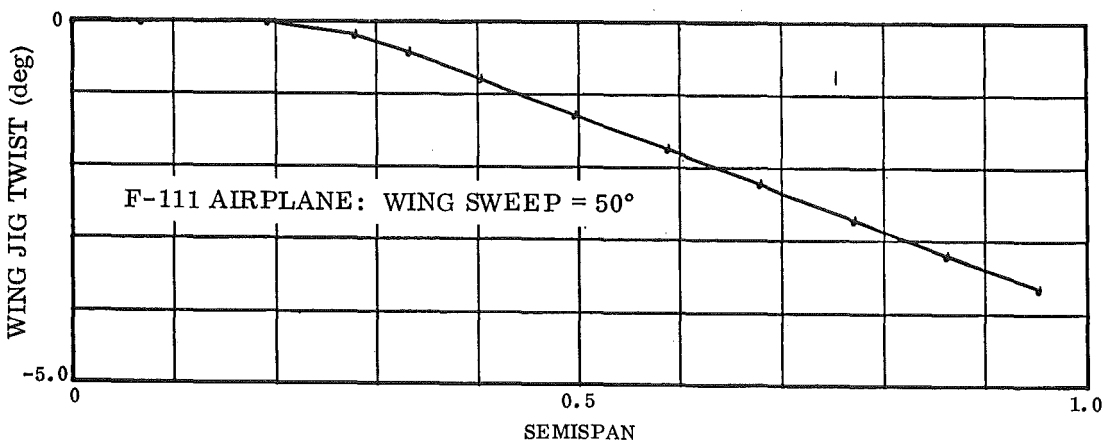

Figure 9. Wing Jig Twist Distribution for the F-111 Airplane.

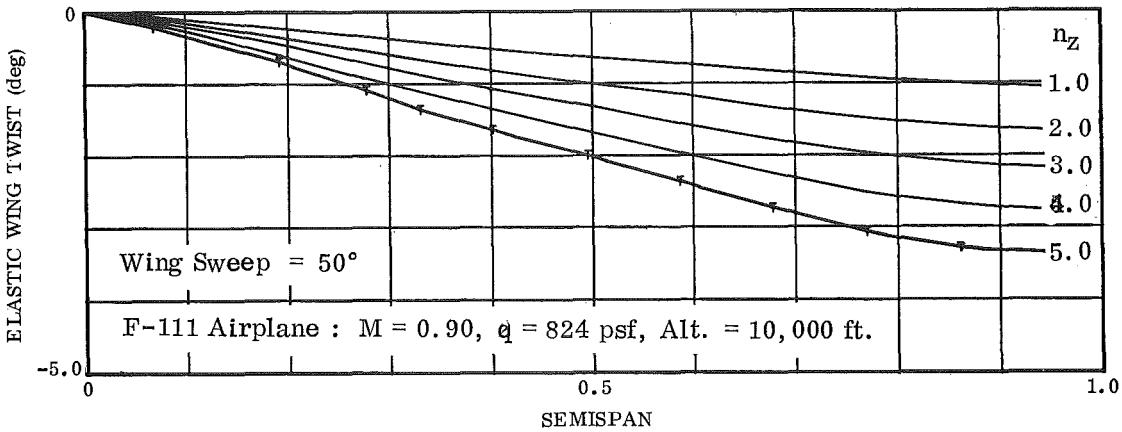

Figure 10. Effect of Load Factor on the F-111 Wing Twist at Mach 0.90 (Altitude = 10,000 ft.)

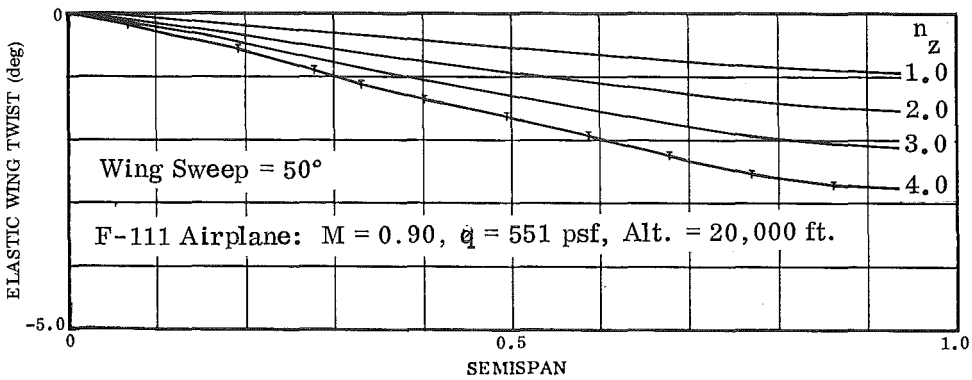

Figure 11. Effect of Load Factor on the F-111 Wing Twist at Mach 0.90 (Altitude=20,000 ft.)

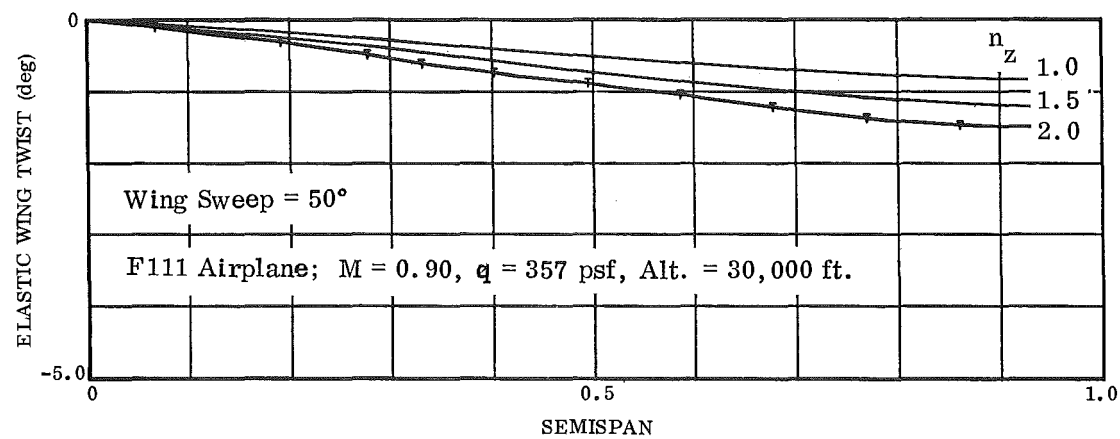

Figure 12. Effect of Load Factor on the F-111 Wing Twist at Mach 0.90 (Altitude = 30,000 ft.)

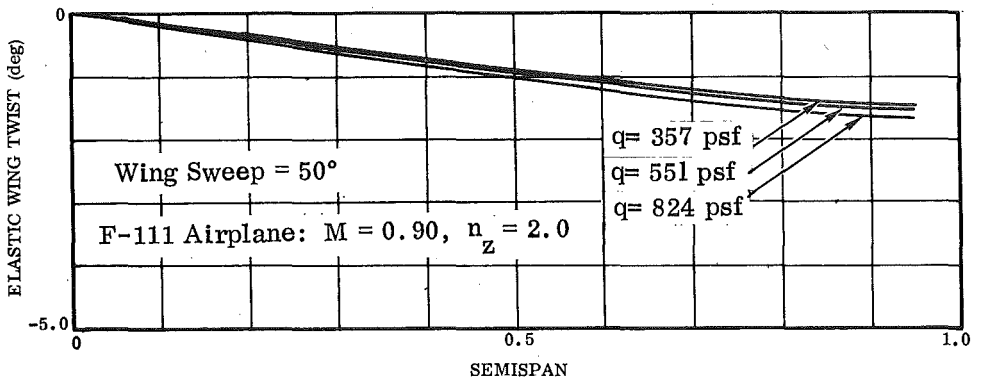

Figure 13. Effect of Dynamic Pressure on the F-111 Wing Twist at Mach 0.90 for a Load Factor of 2.0

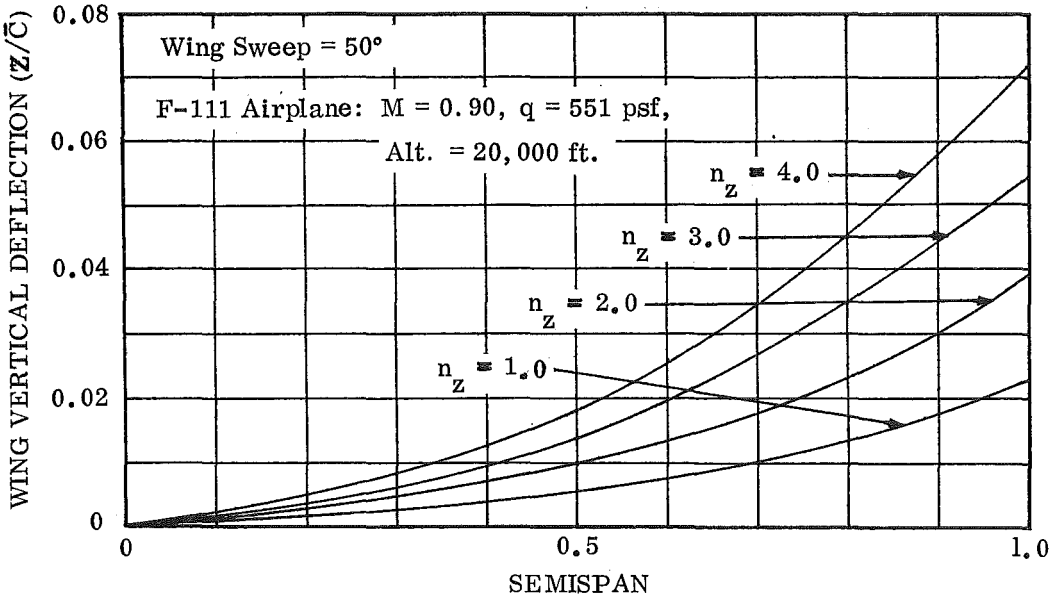

Figure 14. Effect of Load Factor on the F-111 Wing Vertical Deflection Characteristics at Mach 0.90 (Altitude = 20,000 ft.)

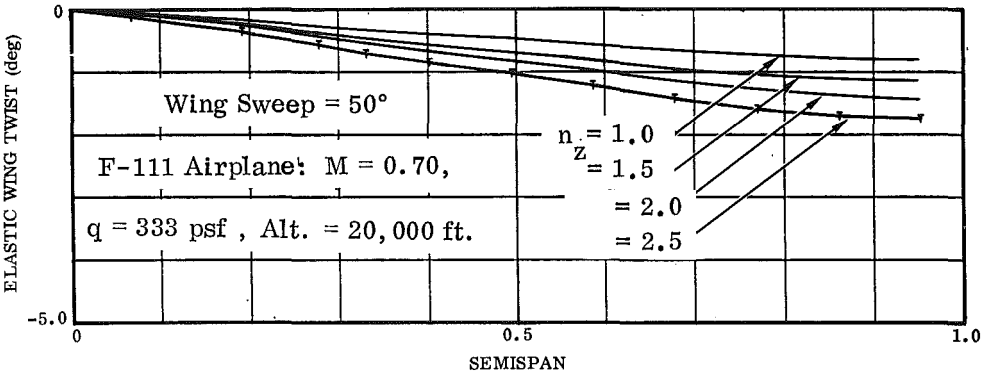

Figure 15. Effect of Load Factor on the F-111 Wing Twist at Mach 0.70 (Altitude = 20,000 ft.)

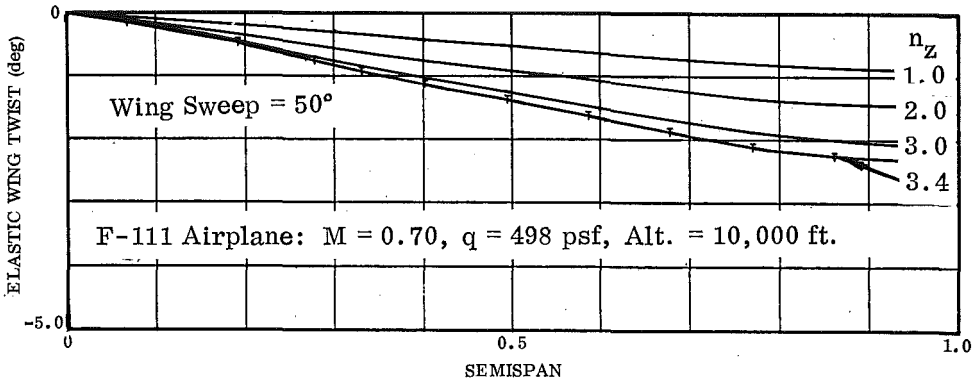

Figure 16. Effect of Load Factor on the F-111 Wing Twist at Mach 0.70 (Altitude = 10,000 ft.)

Table 3 gives the shear, bending moment, and pitching torque of the wing at the centerline for the conditions of Table 2.

Condition No.	A	B	C	D	E
	Shear Load, Air+Inertia (thousands of lb)				
1	23.57	30.28	24.72	26.34	22.27
2	32.07	46.50	40.87	43.01	30.48
3	40.58	62.73	57.01	59.69	38.69
4	-	78.95	63.46	76.36	46.90
5	-	95.17	-	-	-
	Bending Moment (millions of in-lb)				
1	5.50	6.73	5.71	6.02	5.23
2	7.56	10.58	9.61	10.03	7.24
3	9.63	14.44	13.50	14.04	9.23
4	-	18.30	15.06	18.05	11.23
5	-	22.15	-	-	-
	Pitching Torque (thousands of in-lb)				
1	0.90	0.98	0.90	0.93	0.87
2	1.29	1.72	1.64	1.70	1.25
3	1.68	2.46	2.39	2.46	1.63
4	-	3.19	2.69	3.22	2.01
5	-	3.93	-	-	-

Table 3. F-111 Airplane Shear, Bending Moment and Pitching Torque

4.5 ATT AIRPLANE AEROELASTIC ANALYSIS

The wing bending moment of inertia and the polar moment of inertia characteristics of the ATT airplane are presented in Figure 17. Figure 18 shows the airplane wing jig twist distribution for the design cruise point. This distribution produces the most favorable span loading condition.

Figure 19 shows the elastic wing twist distribution for the ATT airplane at an altitude of 36,000 feet and Mach 0.98 for several load factors. Figure 20 illustrates the elastic wing twist distribution as a function of load factor for a flight condition of 25,000 feet and Mach 0.80. Figure 21 illustrates the non-dimensional vertical deflection of the airplane wing at load factors of 1.0, 1.5, 2.0, and 2.5 for a flight condition at 25,000 feet and Mach 0.80. The vertical deflection is interrelated with the elastic wing twist, but is not critical to the wing design since the drag increment is more readily identified with the wing lift.

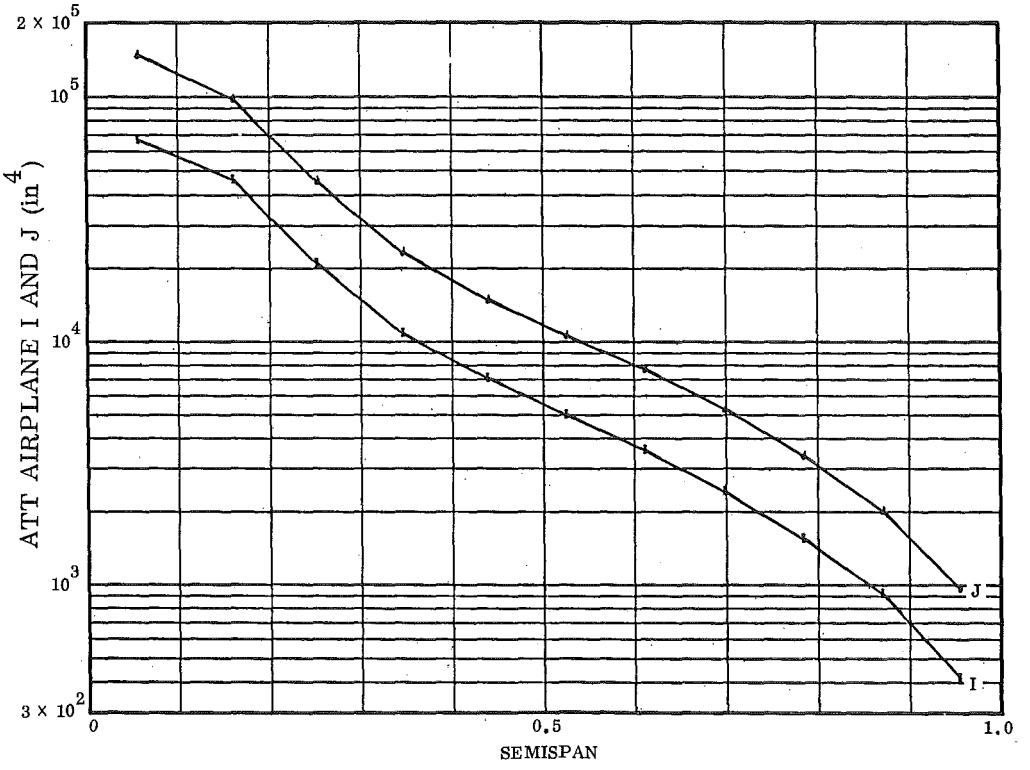

Figure 17. Wing Bending Moment of Inertia and Polar Moment of Inertia for the ATT Wing

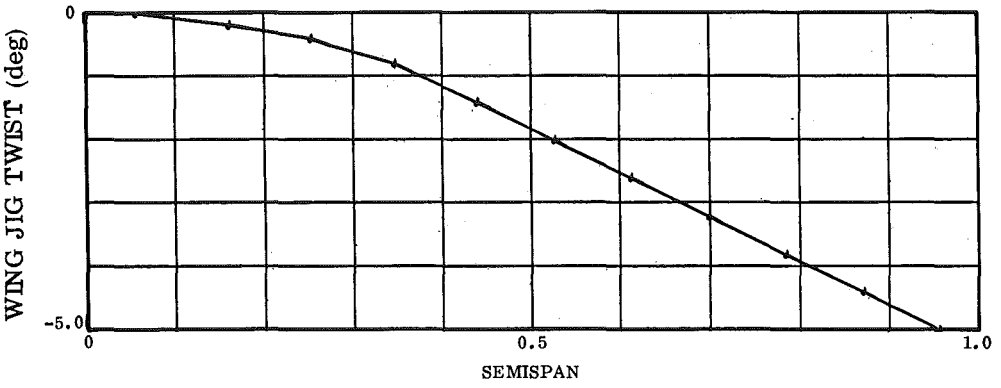

Figure 18. Wing Jig Twist Distribution for the ATT Airplane

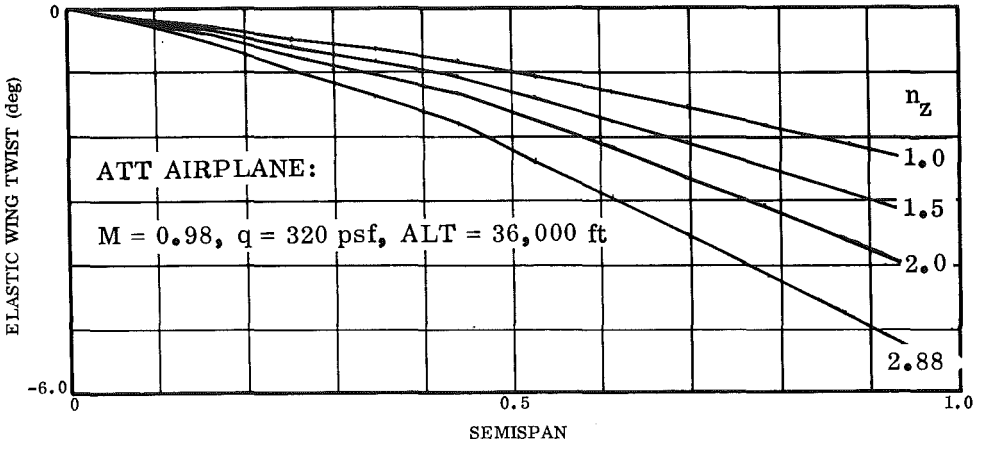

Figure 19. Effect of Load Factor on the ATT Wing Twist at Mach 0.98 (Altitude = 36,000 ft)

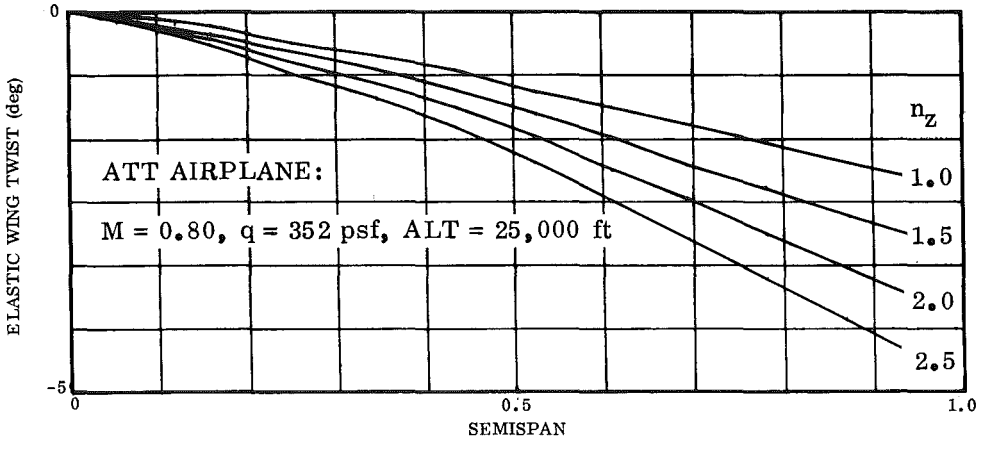

Figure 20. Effect of Load Factor on the ATT Wing Twist at Mach 0.80 (Altitude = 25,000 ft)

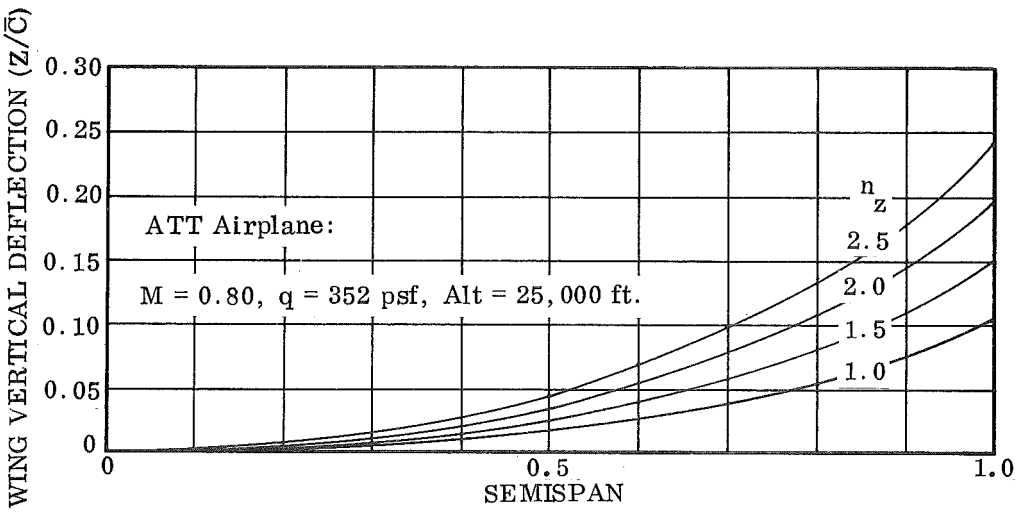

Figure 21. Effect of Load Factor on the Wing Vertical Deflection of the ATT Airplane at Mach 0.80 (Altitude =25,000 ft)

The effect of load factor on the wing twist of the ATT airplane is presented in Figure 22 for a flight condition of Mach 0.60 at an altitude of 10,000 feet. Figure 23 illustrates the wing twist of the ATT airplane at Mach 0.95 and at an altitude of 20,000 feet. Figure 24 shows the wing twist as a function of load factor for a flight condition of Mach 0.50 at an altitude of 20,000 feet for the ATT airplane. The effect of dynamic pressure at a load factor of 2.5 for the ATT airplane is presented in Figure 25. Components of the elastic wing twist are also shown. The twist due to aerodynamic loading decreases the washout with increasing dynamic pressure since the center of pressure is forward of the elastic axis. Wing section pitching moment and wing inertia lead to an increase in the wing twist as the dynamic pressure increases. The resulting twist distribution at each load factor becomes nearly independent of dynamic pressure. This is more of a coincidence of the combination of wing sweep, elastic axis location, airfoil characteristics, and structural properties than the expected result of a vehicle to be selected at random for test.

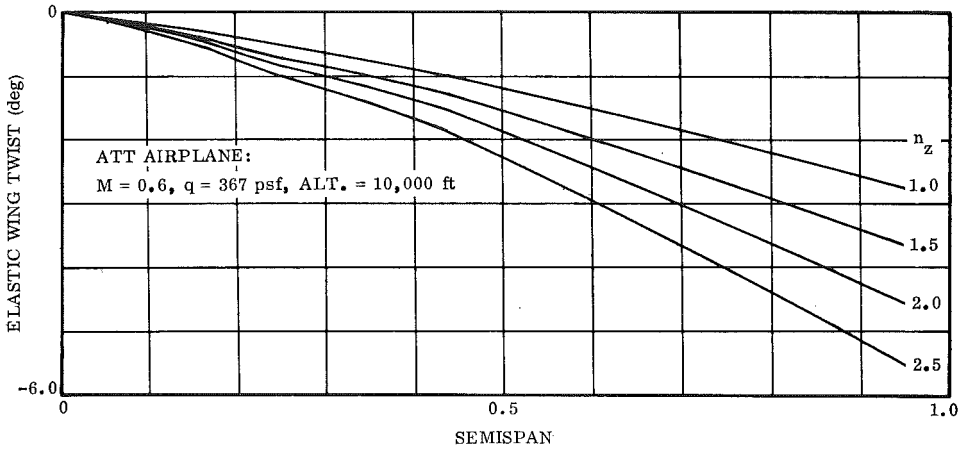

Figure 22. Effect of Load Factor on the ATT Wing Twist at Mach 0.60 (Altitude = 10,000 ft)

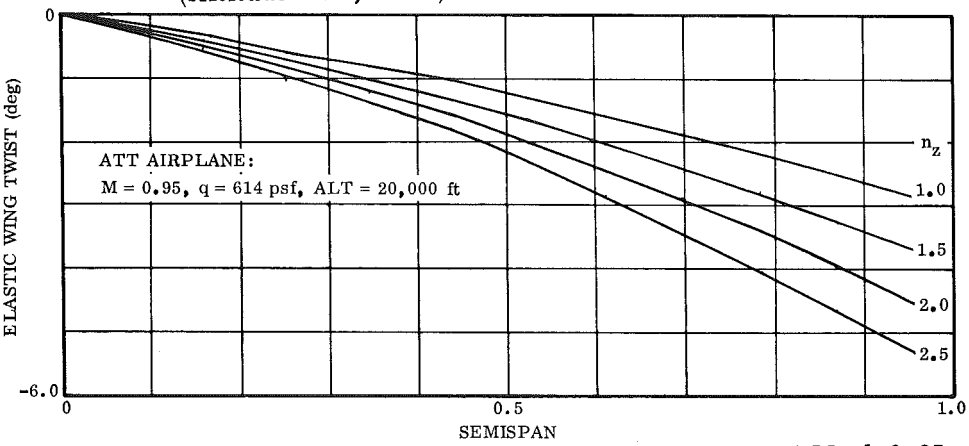

Figure 23. Effect of Load Factor on the ATT Wing Twist at Mach 0.95 (Altitude = 20,000 ft)

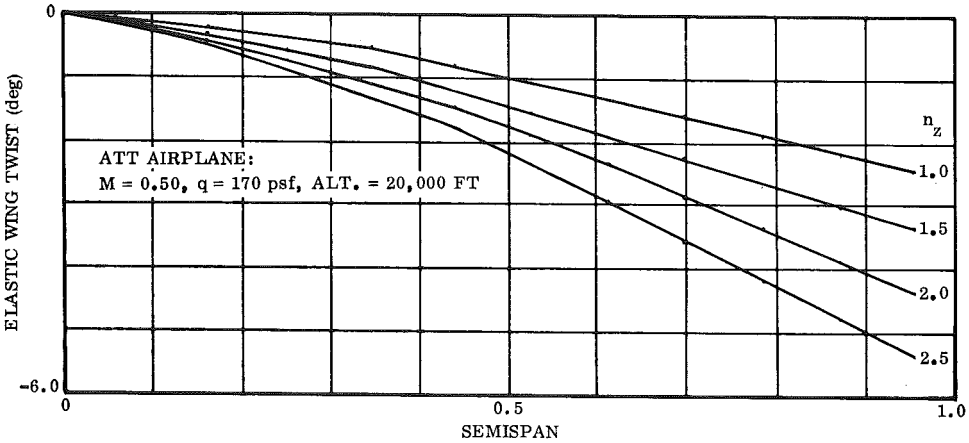

Figure 24. Effect of Load Factor on the ATT Wing Twist at Mach 0.50 (Altitude = 20,000 ft)

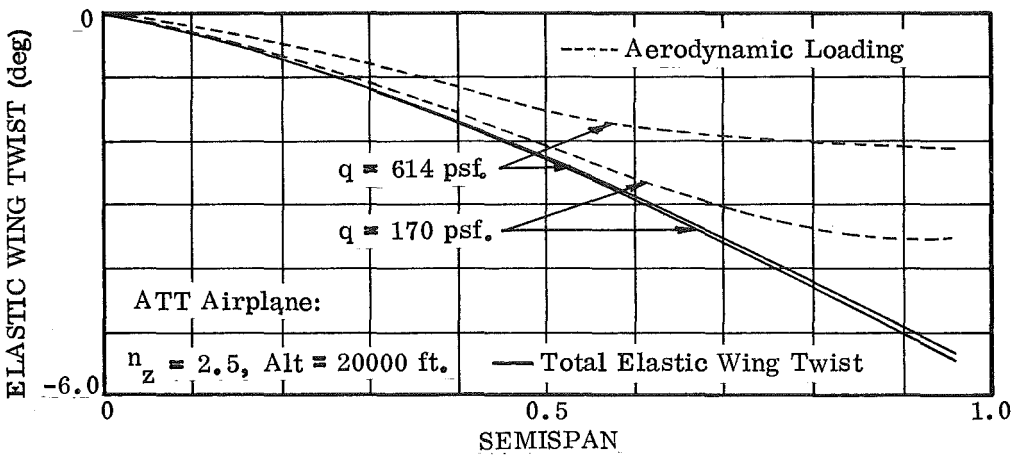

Figure 25. Effect of Dynamic Pressure on the ATT Airplane Wing Twist at a Load Factor of 2.5 (Altitude = 20,000 ft)

The shear, bending moment and torque for the ATT airplane is presented in Table 4. The shear loads and moments are determined along the wing elastic axis.

Table 4. ATT Airplane Shear, Bending Moment and Pitching Torque

Condition No.*	A	B	C	E	G
	Shear Load, Air + Inertia (thousands of lb)				
1	112.8	127.5	126.0	145.7	112.6
2	156.1	177.0	174.4	194.9	161.9
3	199.5	226.6	222.8	244.1	211.1
4	282.0	276.1	271.2	293.3	260.4
	Bending Moment (millions of lb)				
1	60.46	68.01	68.27	70.07	64.29
2	85.55	95.90	95.74	96.52	92.97
3	110.64	123.78	123.22	122.95	121.65
4	152.90	151.66	150.70	149.4	150.33
	Pitching Torque (millions of in-lb)				
1	-27.73	-29.86	-30.45	-37.92	-23.80
2	-35.86	-38.34	-38.89	-46.09	-32.48
3	-43.98	-46.83	-47.33	-54.25	-41.16
4	-54.26	-55.31	-55.77	-62.41	-49.84

*See Table 1, p. 23.

4.6 F-111 HIRT MODEL AEROELASTIC ANALYSIS

The wing bending moment of inertia and the polar moment of inertia characteristics of the 1/12 scale F-111 HIRT model are illustrated in Figure 26. Figure 27 illustrates the model jig twist distribution which causes the combination of elastic twist and jig twist of the model to equal that of the F-111 airplane at the design cruise point.

The effect of load factor on the F-111 HIRT model wing elastic twist and vertical deflection is presented in Figures 28 through 35. Effect of dynamic pressure on the elastic wing twist is presented in Figure 36 for the F-111 HIRT model at Mach 0.90. The effect of section pitching moment (C_{m_o}) is less than the aerodynamic loading due to angle of attack which results in a more positive wing twist with increasing dynamic pressure.

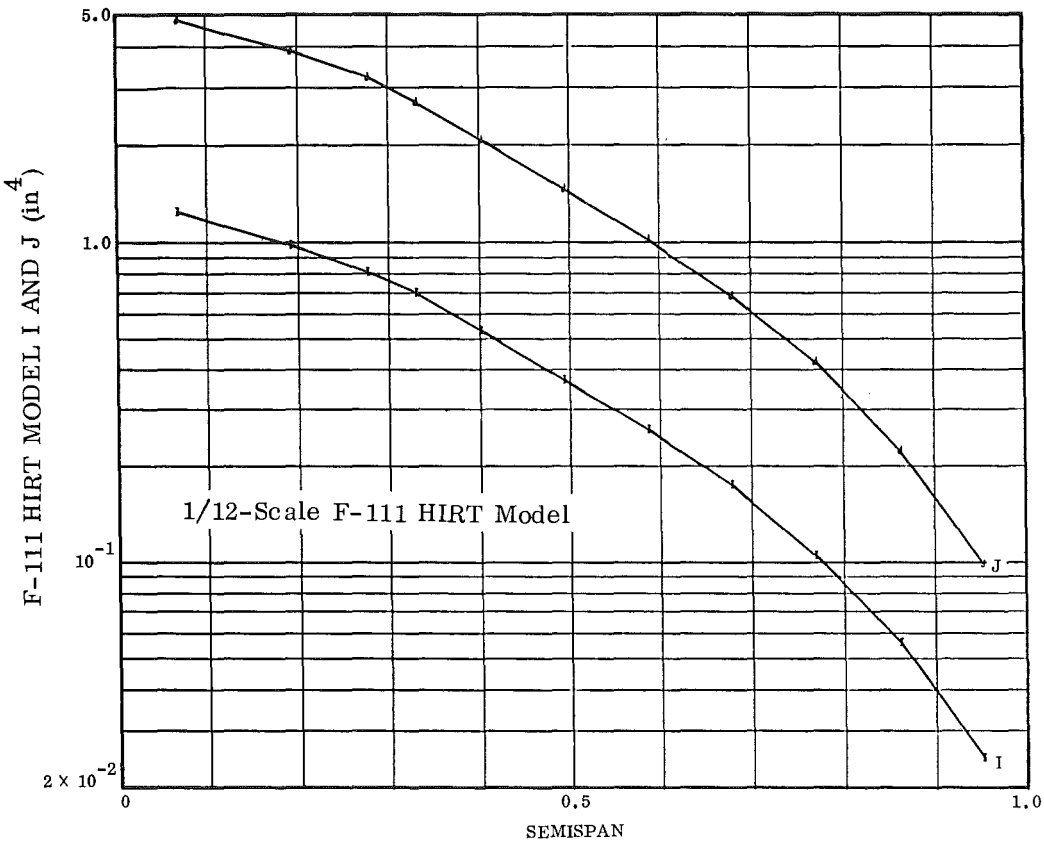

Figure 26. Wing Bending Moment of Inertia and Polar Moment of Inertia for the F-111 HIRT Model Wing

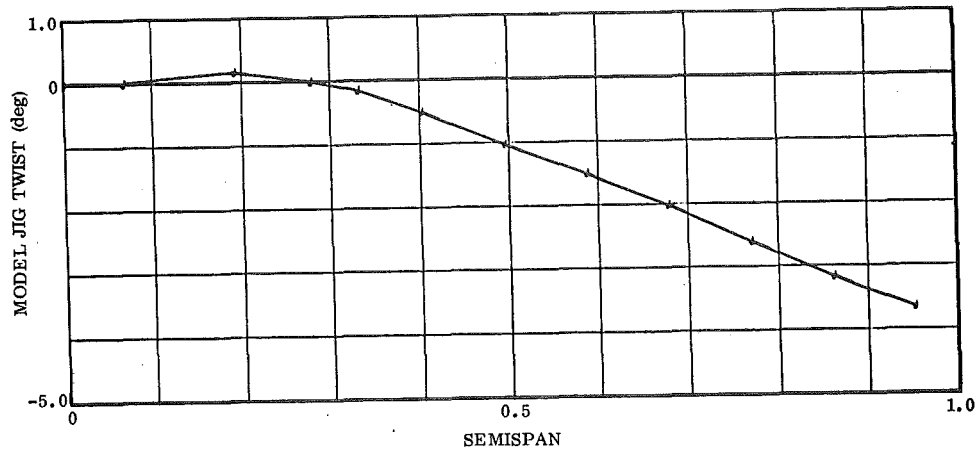

Figure 27. Wing Jig Twist Distribution for the 1/12 Scale F-111 Model

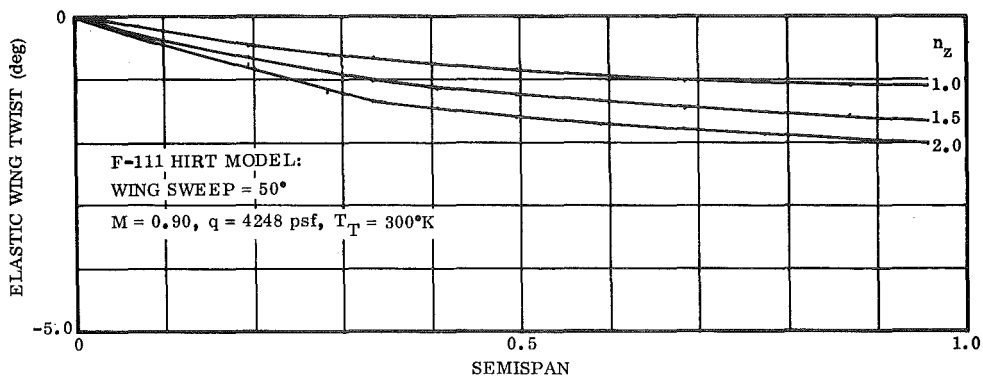

Figure 28. Effect of Load Factor on the F-111 HIRT Model Wing Twist at Mach 0.90 and Full Scale Reynolds Number (Altitude = 30,000 ft)

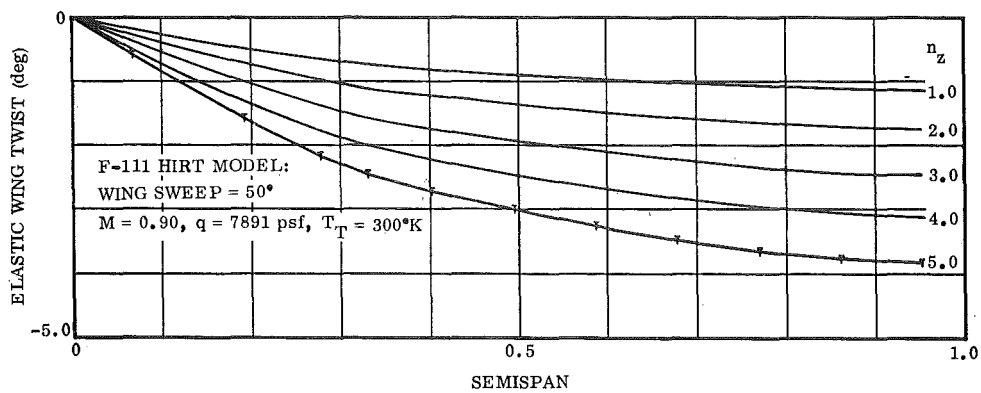

Figure 29. Effect of Load Factor on the F-111 HIRT Model Wing Twist at Mach 0.90 and Full Scale Reynolds Number (Altitude = 10,000 ft)

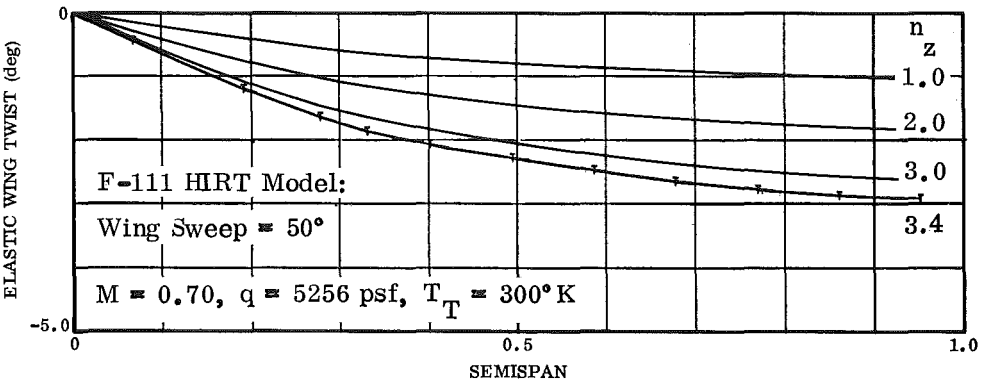

Figure 30. Effect of Load Factor on the F-111 HIRT Model at Mach 0.70 and Full Scale Reynolds Number (Altitude = 10,000 ft)

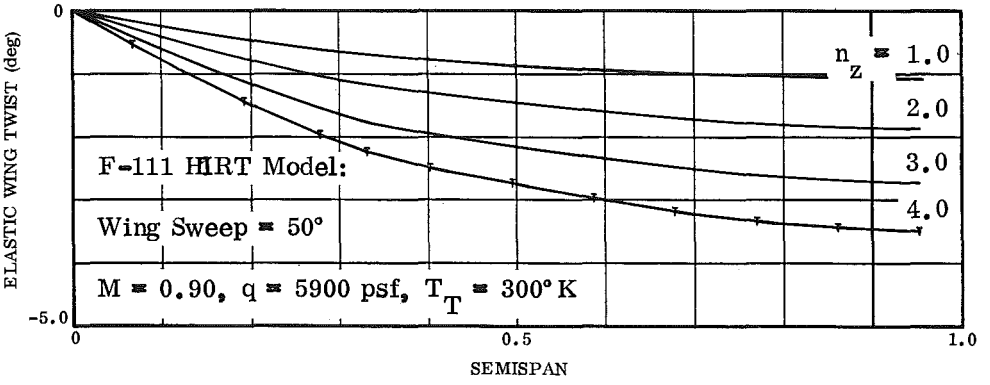

Figure 31. Effect of Load Factor on the F-111 HIRT Model at Mach 0.90 and Full Scale Reynolds Number (Altitude = 20,000 ft)

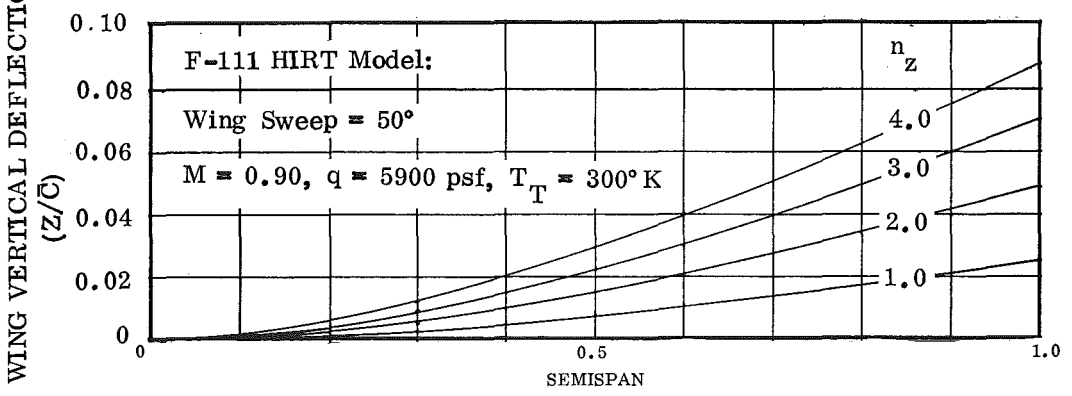

Figure 32. Effect of Load Factor on the Wing Vertical Deflection of the F-111 HIRT Model at Mach 0.90 and Full Scale Reynolds Number (Altitude = 20,000 ft)

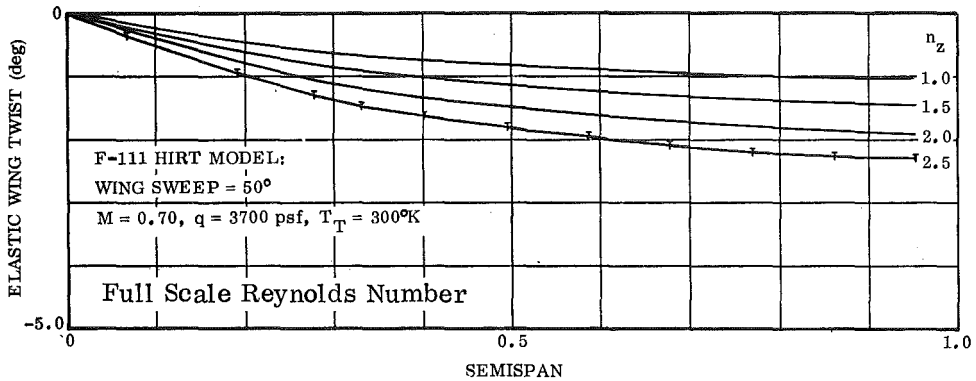

Figure 33. Effect of Load Factor on the F-111 HIRT Model Wing Twist at Mach 0.70 and Full Scale Reynolds Number (Altitude = 20,000 ft)

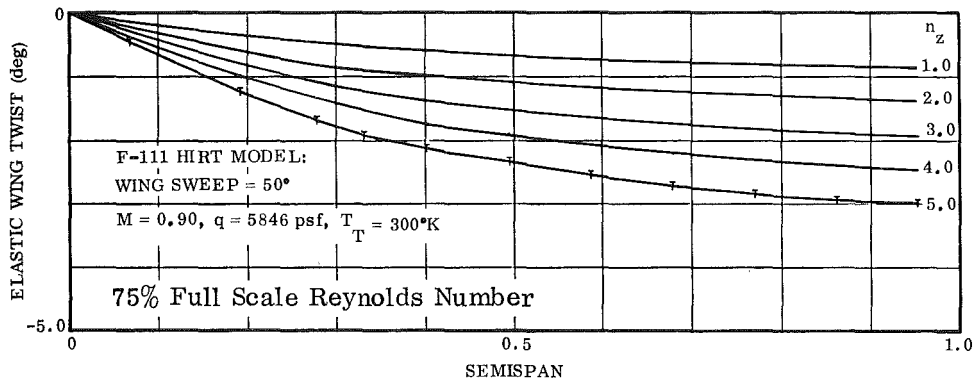

Figure 34. Effect of Load Factor on the F-111 HIRT Model Wing Twist at Mach 0.90 and 75% Full Scale Reynolds Number (Altitude = 10,000 ft)

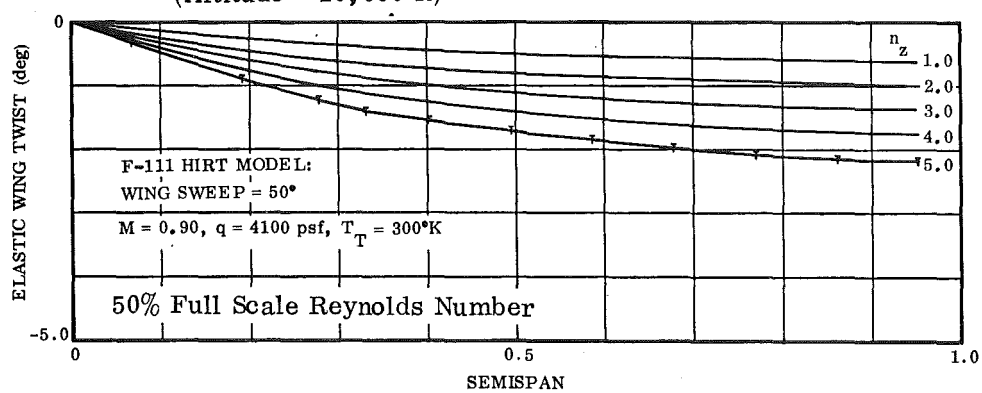

Figure 35. Effect of Load Factor on the F-111 HIRT Model Wing Twist at Mach 0.90 and 50% Full Scale Reynolds Number (Altitude = 10,000 ft)

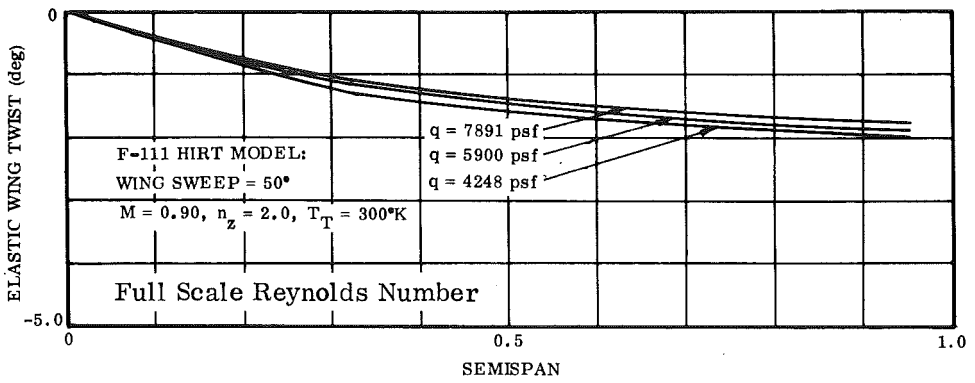

Figure 36. Effect of Dynamic Pressure on the F-111 HIRT Model Wing Twist at Mach 0.90 and Full Scale Reynolds Number

A relatively large effect of Reynolds number reduction is shown in Figure 37. A 50 percent decrease in Reynolds number decreases the twist by 40 percent.

Table 5 presents the shear, bending moment, and pitching torque of the F-111 1/12 scale model at the wing centerline for the conditions of Table 2.

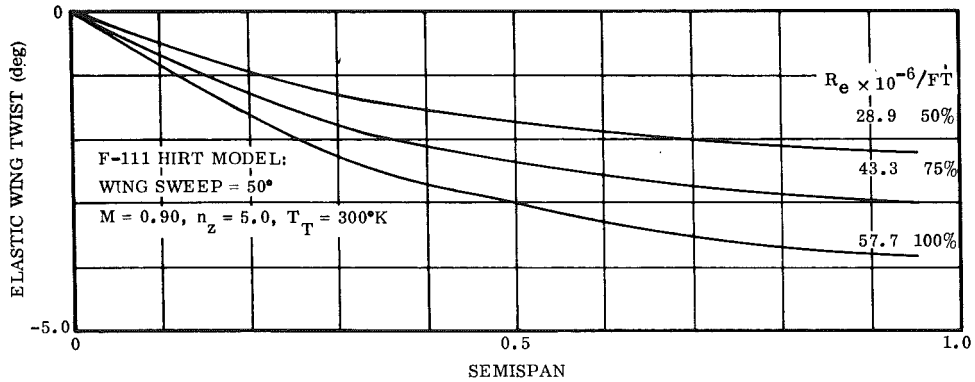

Figure 37. Effect of Reynolds Number on the F-111 HIRT Model Wing Twist at Mach 0.90 and at a Load Factor of 5.0 (Altitude = 10,000 ft)

Table 5. F-111 HIRT Model Shear, Bending Moment and Pitching Torque

Condition No.	A	B	C	D	E	F	G
	Shear Load, Air + Inertia (thousands of lb)						
1	2.24	2.32	2.13	2.28	2.06	1.78	1.28
2	3.08	3.64	3.62	3.80	2.86	2.80	2.03
3	3.93	4.98	5.10	5.33	3.65	3.82	2.78
4	-	6.30	5.69	6.86	4.45	4.85	3.52
5	-	7.63	-	-	-	5.88	4.27
	Bending Moment (thousands of in-lb)						
1	43.92	43.74	41.58	43.89	40.67	33.82	24.59
2	61.12	70.35	71.60	74.69	56.96	54.50	39.74
3	78.38	97.07	101.63	105.56	73.24	75.26	54.94
4	-	123.69	113.61	136.44	89.53	95.94	70.09
5	-	150.31	-	-	-	116.62	85.24
	Pitching Torque (thousands of in-lb)						
1	6.35	5.78	5.83	6.10	5.92	4.52	3.32
2	9.08	10.00	10.58	10.98	8.50	7.79	5.71
3	11.81	14.24	15.34	15.87	11.07	11.08	8.12
4	-	18.46	17.23	20.76	13.65	14.35	10.52
5	-	22.68	-	-	-	17.63	12.91

A comparison of the stiffness ratio (EI/GJ) for the F-111 airplane and the 1/12 scale HIRT model is presented in Figure 38.

It is anticipated that the stiffness ratio for wings fabricated of composite materials will approach a value of 3.0. The aeroelastic analysis for this condition is presented in Appendix A for the F-111 wing.

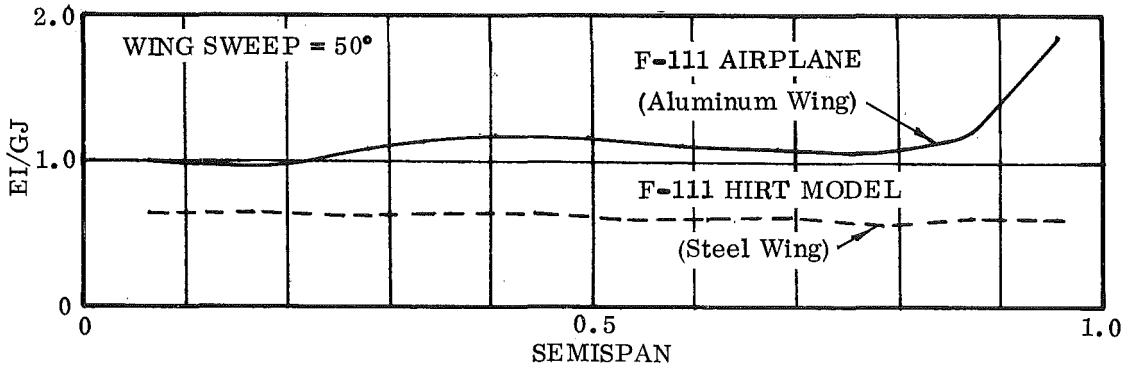

Figure 38. Stiffness Ratio Characteristics of the F-111 Airplane and HIRT Model

The effect of tunnel storage temperature conditions on the elastic wing twist of the F-111 HIRT model is presented in Figure 39 for equivalent Reynolds number test conditions. The reduction in this temperature from 300° K to 240° K results in about a 21 percent reduction in the wing tip twist at a constant load factor. Thus, a reduction in tunnel temperature is an attractive method of controlling the tunnel dynamic pressure and therefore the model wing deformations while maintaining equivalent full scale Reynolds number.

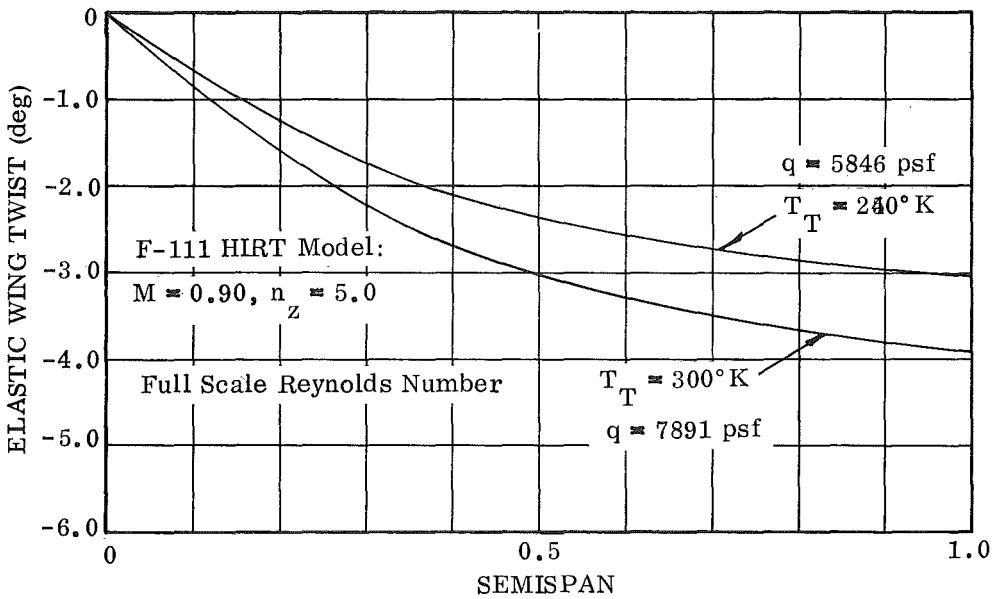

Figure 39. Effect of Tunnel Temperature on the F-111 HIRT Model Wing Twist at Full Scale Reynolds Number

A comparison of the F-111 airplane and the HIRT model wing vertical deflection is presented in Figure 40 for an equivalent Reynolds number condition. The nondimensional vertical deflection ratio at the wing tip for the HIRT model is about 18 percent greater than the F-111 airplane at a constant load factor and an equivalent Reynolds number. The wing vertical deflection, measured along the elastic axis, has been nondimensionalized with respect to the wing mean aerodynamic chord. Wing vertical deflection is an integral portion of the resulting wing twist distribution. For this case, the model wing deflection and twist are greater than the airplane at an equivalent Reynolds number.

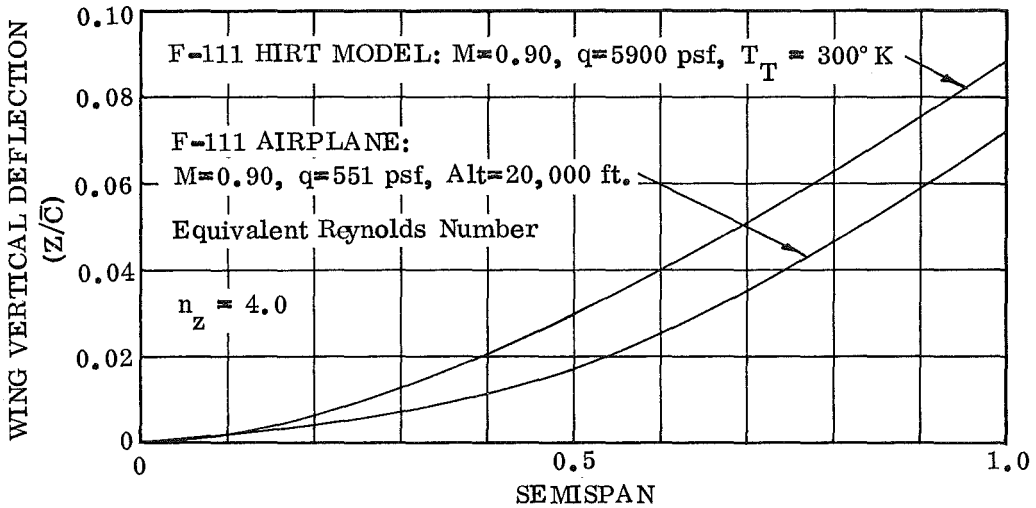

Figure 40. Comparison of the F-111 Airplane and the F-111 HIRT Model Wing Vertical Deflection at Equivalent Reynolds Number.

4.7 ATT HIRT MODEL AEROELASTIC ANALYSIS

The wing bending moment of inertia and the polar moment of inertia characteristics of the steel ATT HIRT model are shown in Figure 41. Figure 42 shows the model wing jig twist distribution which causes the combination of the elastic twist and jig twist of the model to equal that of the airplane wing twist at the design cruise point.

Figure 43 shows the elastic wing twist distribution for the ATT HIRT model at Mach 0.98 for several flight load factors. Tunnel conditions of dynamic pressure and temperature produced the equivalent full scale Reynolds number for a flight condition of Mach 0.98 at an altitude of 36,000 feet.

Figure 44 illustrates the elastic wing twist distribution for the ATT HIRT model as a function of load factor for a flight condition of Mach 0.80.

Effect of load factor on the ATT HIRT model for a flight condition of Mach 0.60 is presented in Figure 45 for full scale Reynolds number conditions. Figures 46, 47 and 48 illustrates the effect of load factor on the ATT HIRT model for equivalent Reynolds number conditions.

Effect of wing stiffness ratio for the ATT HIRT model wing is presented in Figure 49. A solid steel wing would represent a 100 percent structural arrangement. The model wing has been designed with pressure instrumentation within the wing. This results in a structural degradation of the wing cross-sectional properties. The basic model arrangement has a 65 percent wing structural effectiveness. For a reduction in the wing structural characteristics to 52 percent of the solid cross-section causes the wing twist to increase by 15 percent over the basic configuration as shown in Figure 49.

The effect of a tunnel dynamic pressure at a load factor of 2.5 for the ATT HIRT model is presented in Figure 50. Components of the elastic wing twist are also shown. The twist due to aerodynamic loading decreases the washout with increasing dynamic pressure since the center of pressure is forward of the elastic axis. Wing section pitching moment and wing inertia lead to an increase in the washout.

The effect of tunnel dynamic pressure on the ATT HIRT model wing vertical deflection is presented in Figure 51 for a load factor of 2.5 at the equivalent full scale Reynolds number. For the constant load factor, the lower dynamic pressure condition results in larger vertical deflection. Wing vertical deflection as a function of the load factor is presented in Figure 52 for the ATT HIRT model at an equivalent full scale Reynolds number condition.

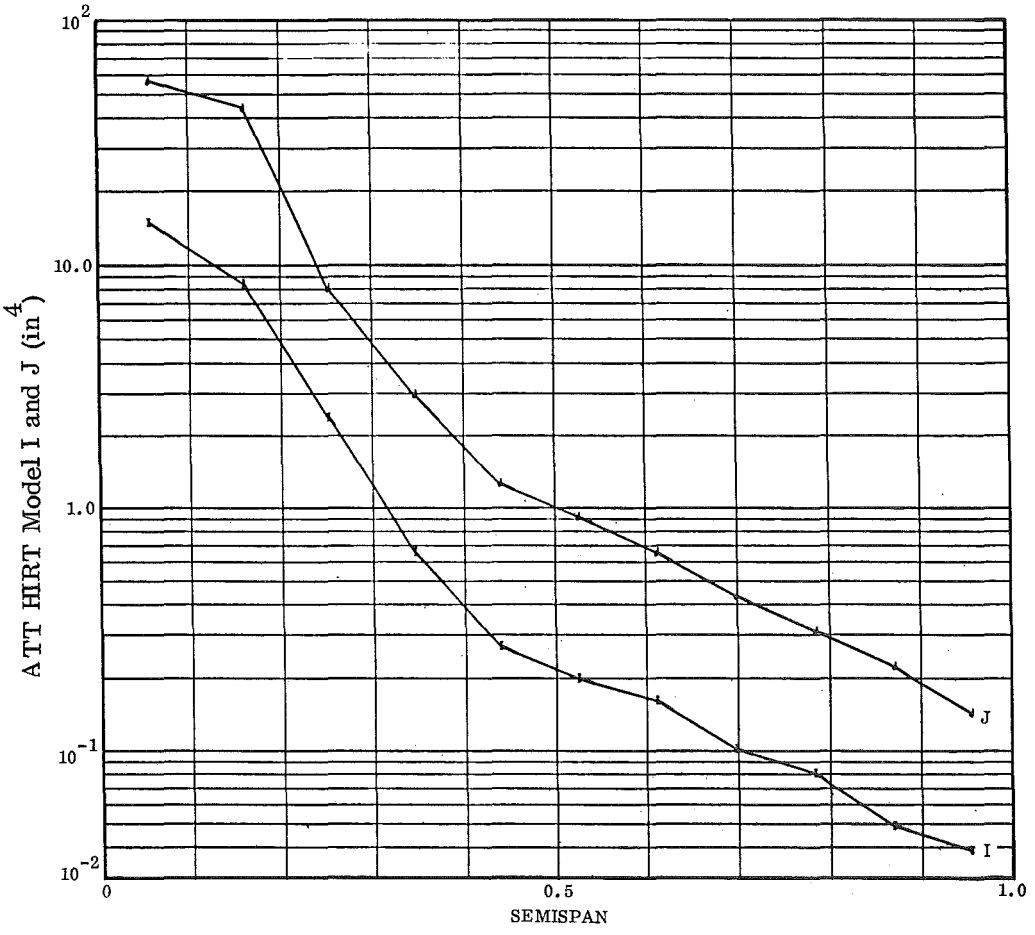

Figure 41. Wing Bending Moment of Inertia and Polar Moment of Inertia for the ATT HIRT Model Wing

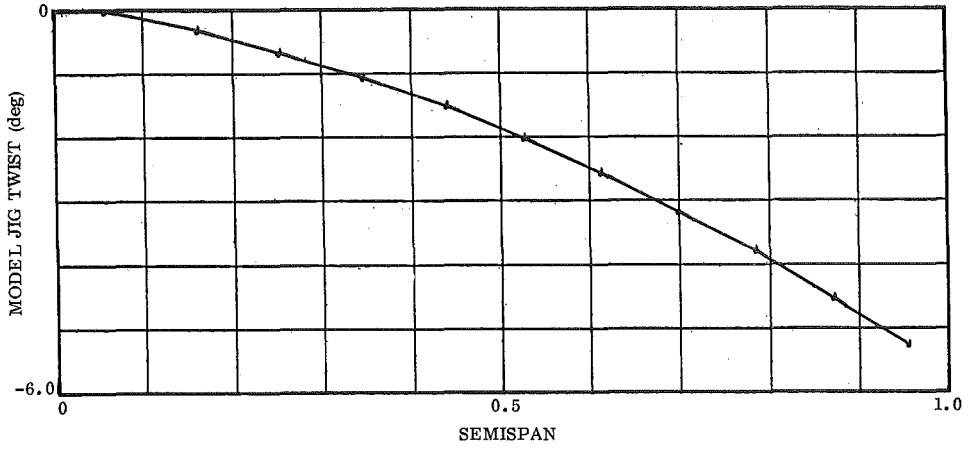

Figure 42. Wing Jig Twist Distribution for the ATT HIRT Model.

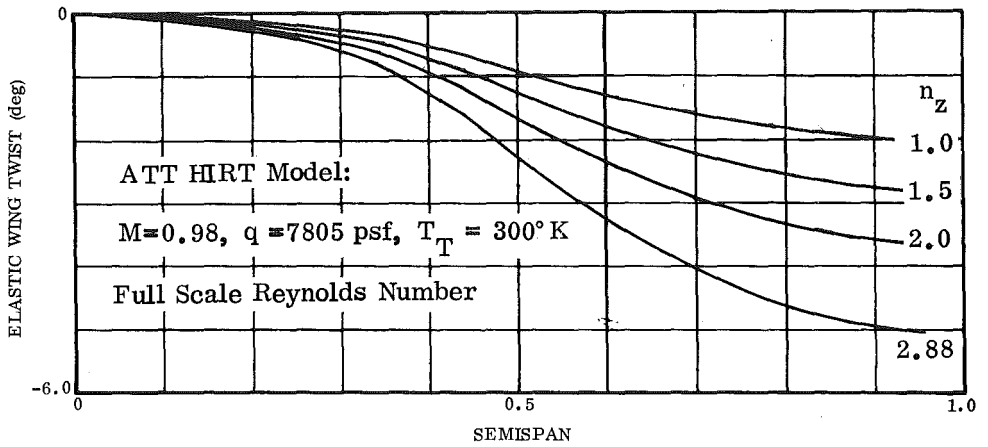

Figure 43. Effect of Load Factor on the ATT HIRT Model at Mach 0.98 and Full Scale Reynolds Number (Altitude =36,000 ft)

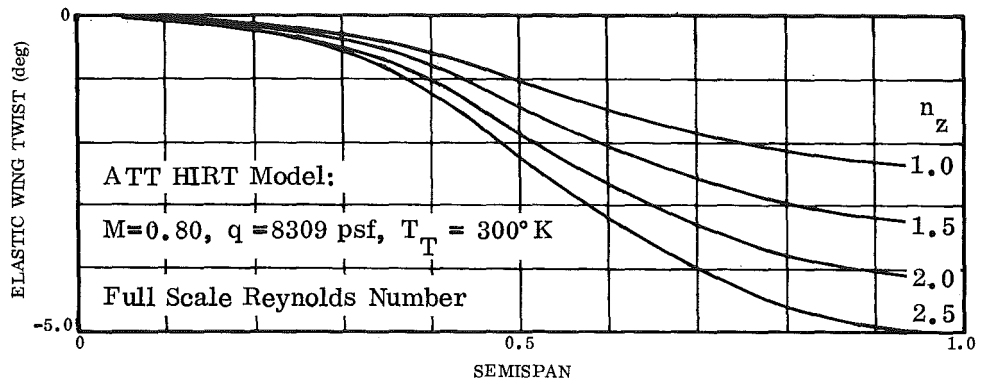

Figure 44. Effect of Load Factor on the ATT HIRT Model at Mach 0.80 and Full Scale Reynolds Number (Altitude =25,000 ft)

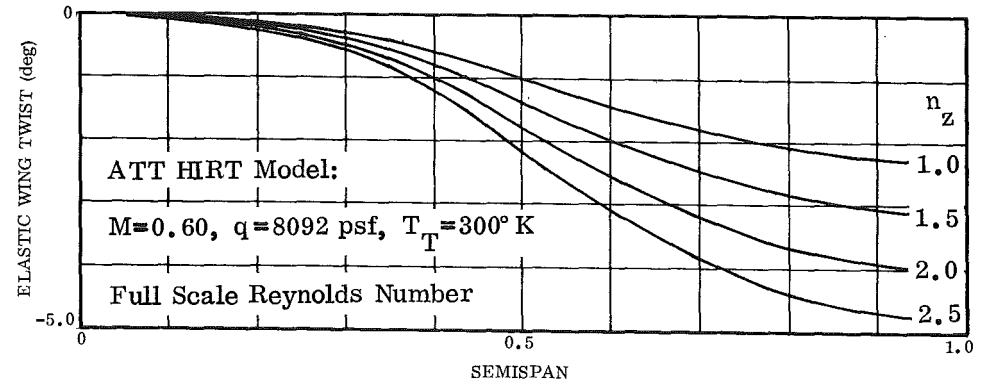

Figure 45. Effect of Load Factor on the ATT HIRT Model at Mach 0.60 and Full Scale Reynolds Number (Altitude=10,000 ft)

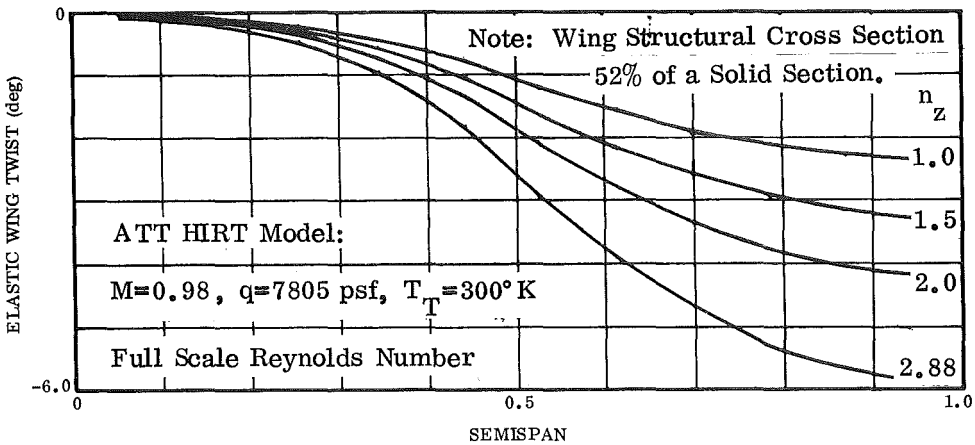

Figure 46. Effect of Load Factor on the ATT HIRT Model at Mach 0.98 and Full Scale Reynolds Number (Altitude=36,000 ft)

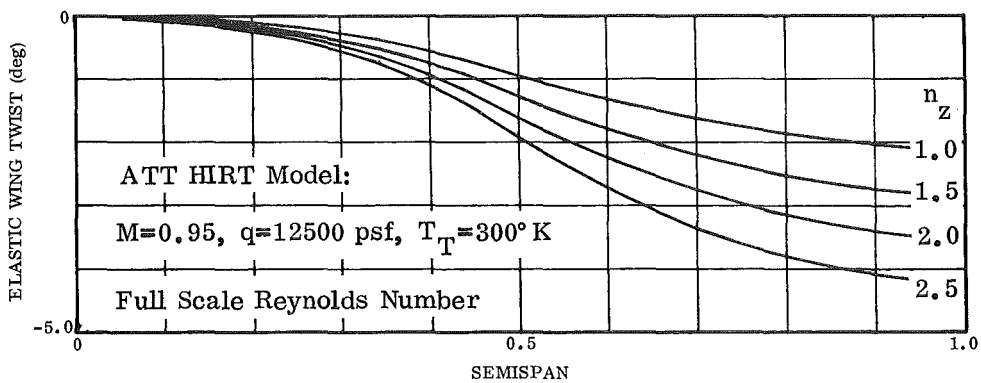

Figure 47. Effect of Load Factor on the ATT HIRT Model at Mach 0.95 and Full Scale Reynolds Number (Altitude=20,000 ft)

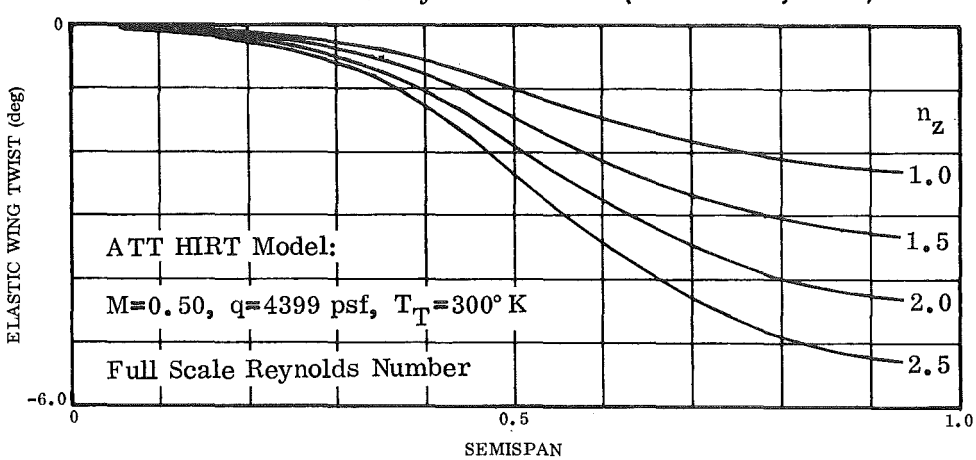

Figure 48. Effect of Load Factor on the ATT HIRT Model at Mach 0.50 and Full Scale Reynolds Number (Altitude=20,000 ft)

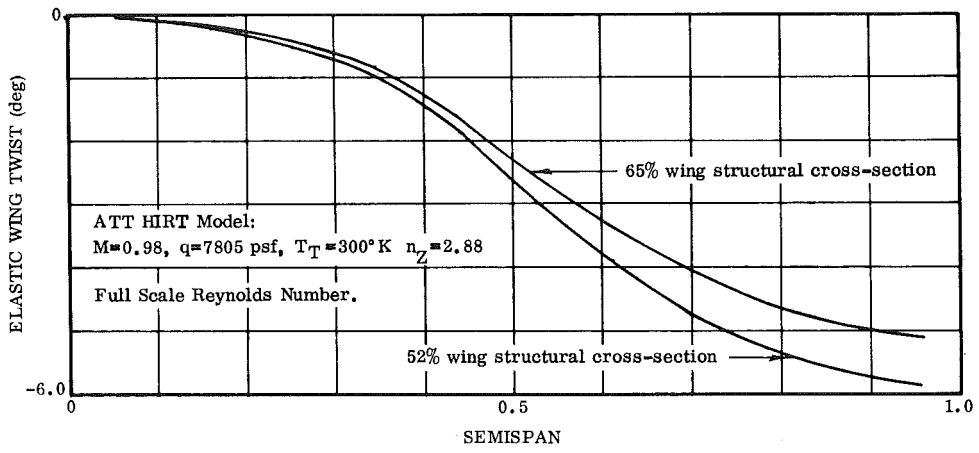

Figure 49. Effect of Wing Stiffness Ratio for the ATT HIRT Model Wing.

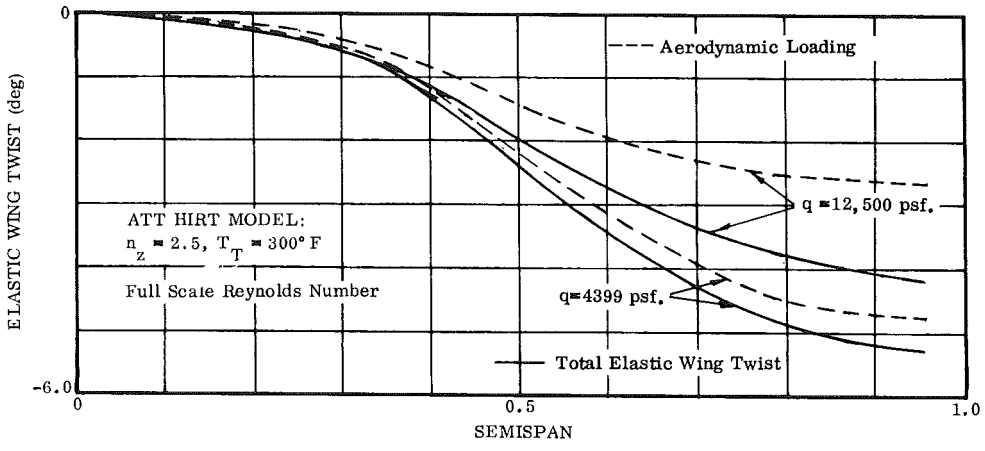

Figure 50. Effect of Dynamic Pressure on the ATT HIRT Model Wing Twist at a Load Factor of 2.5.

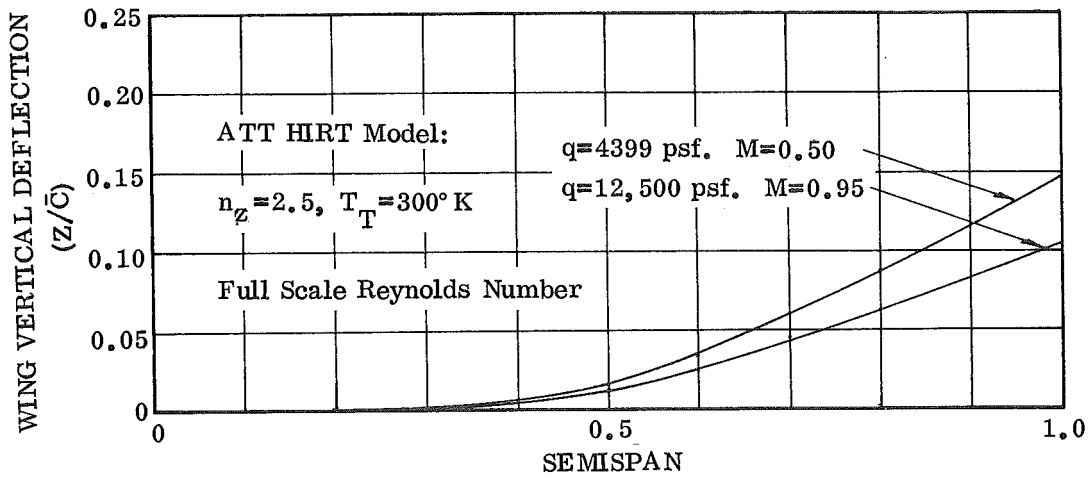

Figure 51. Effect of Tunnel Dynamic Pressure on the ATT HIRT Model Wing Vertical Deflection at Full Scale Reynolds Number.

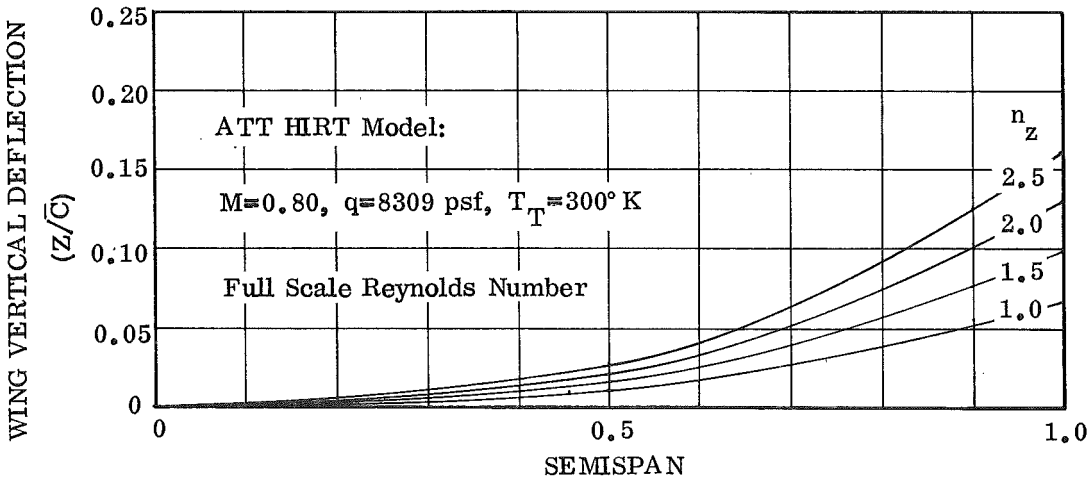

Figure 52. Effect of Load Factor on the ATT HIRT Model Wing Vertical Deflection at Mach 0.80 and Full Scale Reynolds Number (Altitude=25,000 ft).

Figure 53 compares the structural stiffness ratios of the ATT airplane and the ATT HIRT model. The ATT HIRT model wing stiffness ratio is about one half of the ATT airplane wing.

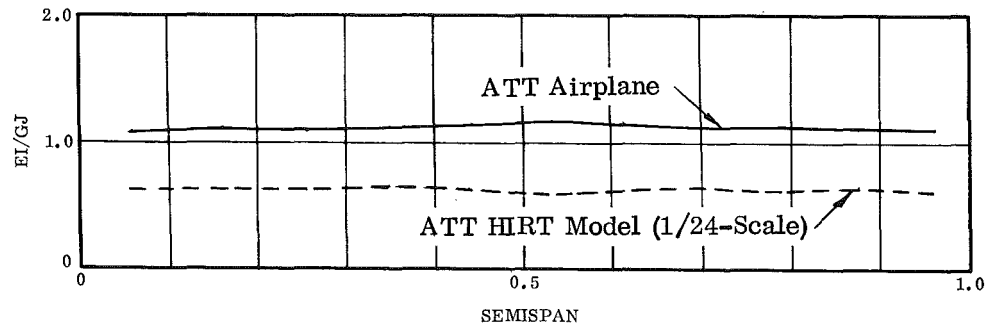

Figure 53. Stiffness Ratio Characteristics of the ATT Airplane and the ATT HIRT Model.

The elastic wing twist for the ATT HIRT model is compared with the ATT airplane elastic wing twist in Figure 54 for the design cruise point. The comparison at equivalent Reynolds number conditions indicates that the model elastic twist distribution may be held within 0.1 degrees angle of attack at each wing section relative to the airplane wing.

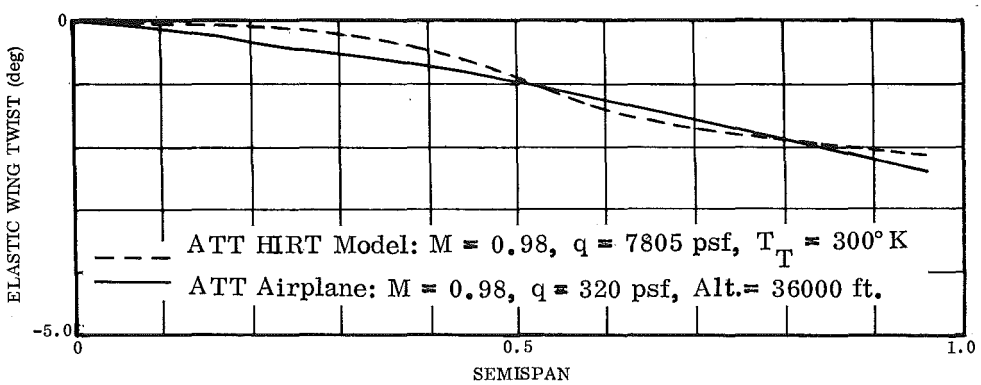

Figure 54. Comparison of the ATT Airplane and the ATT HIRT Model at the Equivalent Reynolds Number for the Design Cruise Point

Table 6 shows the shear load, bending moment and pitching torque for the ATT HIRT model along the wing elastic axis. The flight conditions are presented in Table 1.

Table 6. ATT HIRT Model Shear, Bending Moment and Pitching Torque.

Condition No.	A	B	C	D	E	G
	Shear Load, Air + Inertia (thousands of lb)					
1	5.44	5.89	5.48	5.32	6.06	5.30
2	7.62	8.24	7.66	7.45	8.15	7.67
3	9.81	10.62	9.85	9.59	10.26	10.04
4	13.65	12.99	12.02	13.34	12.35	12.42
	Bending Moment (thousands of in-lb)					
1	96.35	106.32	100.86	92.48	103.58	100.02
2	135.00	148.43	140.09	129.62	139.29	144.23
3	173.87	190.74	179.50	166.96	175.31	188.52
4	241.88	233.06	218.55	232.30	211.02	232.72
	Pitching Torque (thousands of in-lb)					
1	-29.99	-32.61	-31.61	-29.33	-41.42	-22.43
2	-34.72	-37.79	-36.48	-33.81	-45.64	-28.07
3	-39.48	-43.01	-41.37	-38.31	-49.90	-33.73
4	-47.81	-48.22	-46.22	-46.18	-54.12	-39.38

The effect of tunnel storage temperature conditions on the elastic wing twist of the ATT HIRT model is presented in Figure 55 for equivalent Reynolds number test conditions. The reduction in tunnel temperature from 300° K to 240° K results in about a 20 percent reduction in the wing tip twist at a constant load factor. Again the effect of storage temperature as a possible control of model deformation should be noted. Reduction in the tunnel temperature may best be applied to the situation where the steel model is structurally limited in comparison to the airplane which has been designed for high load factors.

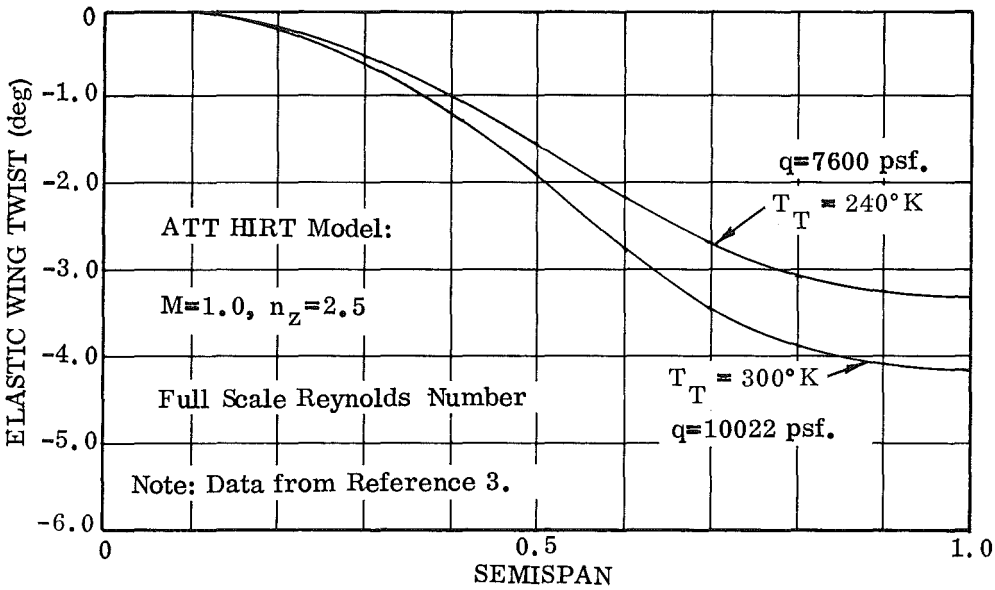

Figure 55. Effect of Tunnel Temperature on the ATT HIRT Model Wing Twist at Full Scale Reynolds Number.

A comparison of the ATT airplane and the HIRT model wing vertical deflection is presented in Figure 56 for an equivalent Reynolds number condition. The nondimensional vertical deflection ratio at the wing tip for the HIRT model is about 31 percent less than the ATT airplane at a constant load factor and an equivalent Reynolds number. The wing deflection is an integral part of the wing twist distribution. For this case, the model wing vertical deflection and twist are less than the airplane at an equivalent Reynolds number.

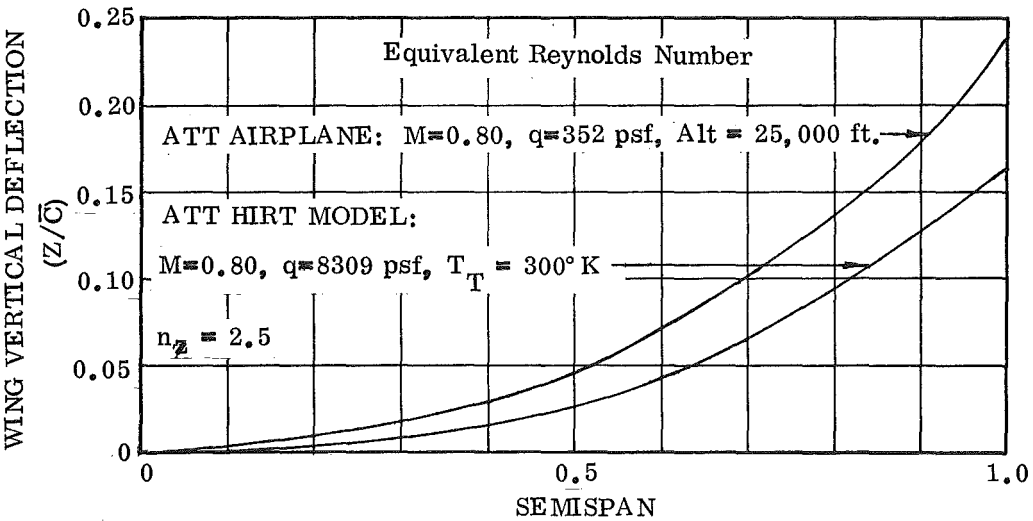

Figure 56. Comparison of the ATT Airplane and the ATT HIRT Model Wing Vertical Deflection at Equivalent Reynolds Number

4.8 ITERATIVE ANALYSIS OF WIND TUNNEL RESULTS

The correlation of the full size analysis with the scale model results will be dependent upon getting the model to deform like the full size vehicle as well as maintaining the Reynolds number. In a real-time testing situation, it may be necessary to change the tunnel dynamic pressure and temperature to achieve the desired deformation for a given angle of attack of the wing root. To reconcile the differences between the theoretical analysis of the model and the observed HIRT results, it will be desirable to iteratively analyze the effects of the aerodynamic spanwise distributions of C_{ℓ_α}, C_{m_o}, and $\partial C_{m_{c/4}} / \partial C_{\ell}$; the structural spanwise distributions of EI and GJ; and, perhaps, the spanwise variation of the elastic axis. As the test series progresses, analyses can identify corrections to the above variables required to match calculations with the model deformations.

Matching the theoretical model analysis to the deformations measured in the HIRT tunnel is important because the aerodynamic distributions of both the model and full size vehicle should be in agreement. The structural characteristics of a full size vehicle are normally reliable for these purposes when the entire structure is considered as opposed to using the wing box alone. Should the full size wing aerodynamics not be in agreement with the model, the deformations will be erroneous. Because of the need to analyze and test the model and full size vehicle simultaneously, it is desirable to perform the analysis rapidly.

This requirement is a natural application for the interactive graphics cathode-ray tube display. The use of a real-time mode rather than a conventional batch mode means that a satisfactory matching of the aerodynamic and structural parameters and deformations can be accomplished in minutes while the test article is in the tunnel, rather than by days of analysis interspersed with tunnel setup and teardown activity.

The cost of HIRT tunnel activity will be much greater than the digital analysis. The latter will be the most useful when operated in the interactive graphics mode.

SECTION V
AERODYNAMIC ANALYSIS

The high loads imposed on the models in the HIRT facility will produce aeroelastic deformation that will be different from those of the flight vehicle due to differences in the material characteristics from which the aircraft and models are constructed. The procedure used during this study considered matching the model wing twist with the flight vehicle wing twist for a selected point, such as a cruising altitude and Mach number. Additional points within the flight envelope were analyzed and the aeroelastic differences determined.

Rigid aerodynamic characteristics were determined for the model and the airplane for each deformed wing shape. The aerodynamic methods did not consider the distortion components due to tunnel constraints for the model. The linearized aerodynamic methods used in the analysis considered the wing twist as a linear twist distribution from a selected point on the wing semispan to the wing tip. Incremental linearized aerodynamic coefficients (ΔC_L, ΔC_D and ΔC_m) were then determined for the study configurations at each of the selected flight conditions.

5.1 DESCRIPTION OF AIRCRAFT AND MODELS

Two types of aircraft have been selected to be analyzed during this study. The aircraft represent typical type vehicles that would be likely candidates for testing in the HIRT facility. The aircraft configurations were:

a. The Advanced Technology Transport (ATT), which is a highly loaded, large, swept-wing transport aircraft.

b. The Convair Aerospace F-111 fighter, which is a swing wing supersonic combat aircraft.

The models designed for the HIRT facility were based on a solid-steel construction for sting mounting.

5.1.1 Advanced Technology Transport (ATT)

The ATT aircraft used in this study was a predesign configuration. The aircraft was a three-jet, low-wing transport with a 44-degree swept-back wing using a supercritical airfoil. The wing had an aspect ratio of 8.0, a theoretical wing area of 2282 square feet and a taper ratio of 0.390. The fuselage was area ruled, with the wing empennage and engines arranged to achieve the optimum cross-sectiontal area distribution for the aircraft cruising at a design Mach number of 0.98. Overall dimensions

of the aircraft included the length, 183.3 feet; height, 51 feet; and span, 135.1 feet. Dimensional characteristics of the ATT are presented in Table 7; a general arrangement is presented in Figure 57.

Table 7. Dimensional Characteristics of the Advanced Technology Transport

Wing	
Area	2282 ft^2
Span	135.1 ft
Root Chord	24.162 ft
Tip Chord	9.416 ft
Aspect Ratio	8.0
Mean Aerodynamic Chord	20.1 ft
Leading Edge Sweep	44.35°
Dihedral	3°
Incidence of the Root	0
Taper Ratio	0.3897
Horizontal Stabilizer	
Area	395 ft^2
Span	46.58 ft
Root Chord	16.33 ft
Tip Chord	6.58 ft
Aspect Ratio	3.00
Mean Aerodynamic Chord	14.1 ft
Leading Edge Sweep	45°
Dihedral	7°
Taper Ratio	0.4065
Vertical Stabilizer	
Area	215 ft^2
Span	18.5 ft
Root Chord	17.0 ft
Tip Chord	6.25 ft
Aspect Ratio	1.59
Mean Aerodynamic Chord	24.36 ft
Leading Edge Sweep	49.5°
Taper Ratio	0.6992

The ATT model designed for the HIRT facility (Reference 3) was a 1/24-scale all steel model. The general arrangement of the model is presented in Figure 58. The wings shown in Figures 57 and 58 are similar except for size. The model wing had allowances for pressure instrumentation, which resulted in a 35 percent degradation in the structural strength of the solid steel wing.

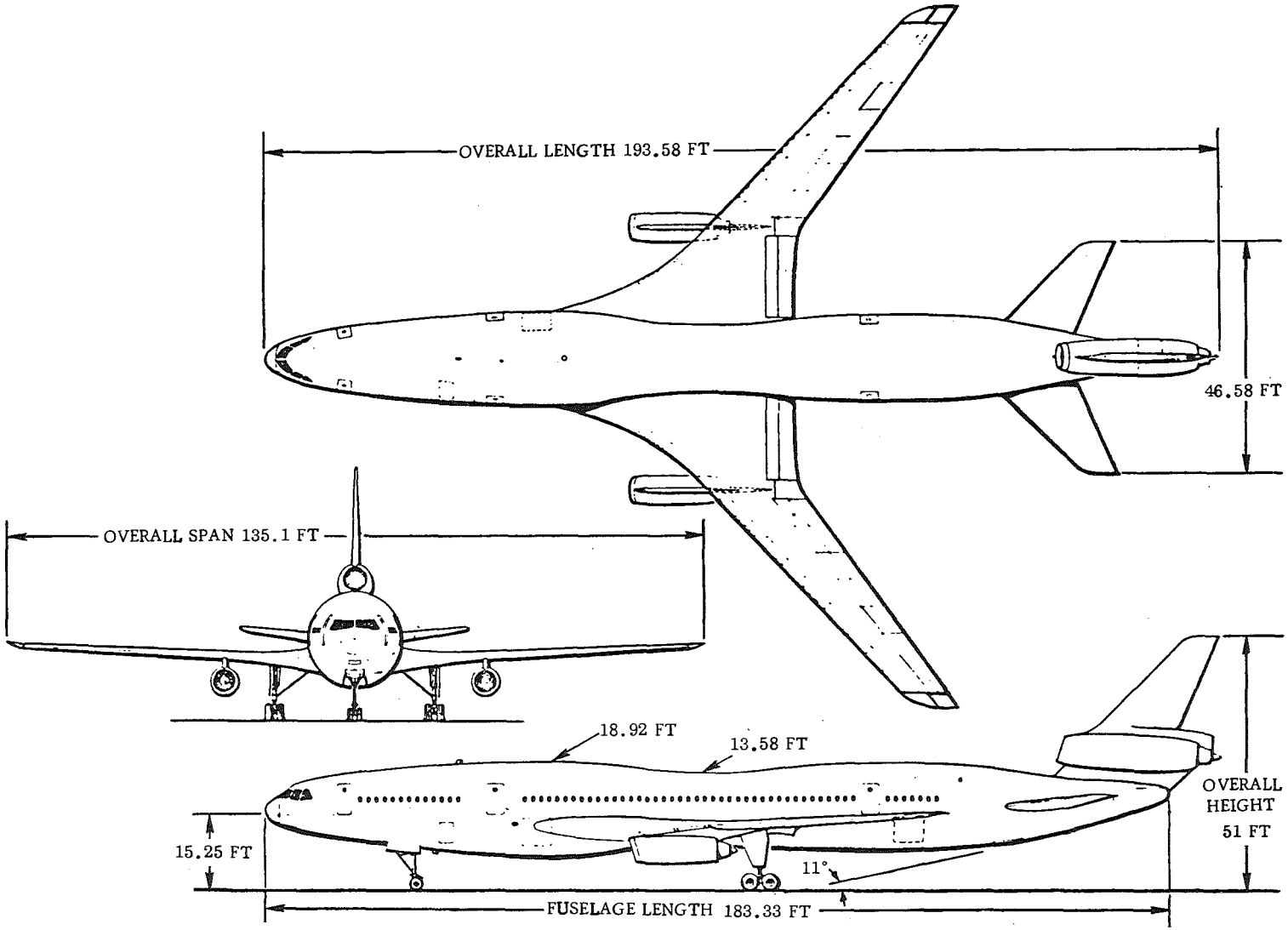

Figure 57. General Arrangement of the Advanced Technology Transport

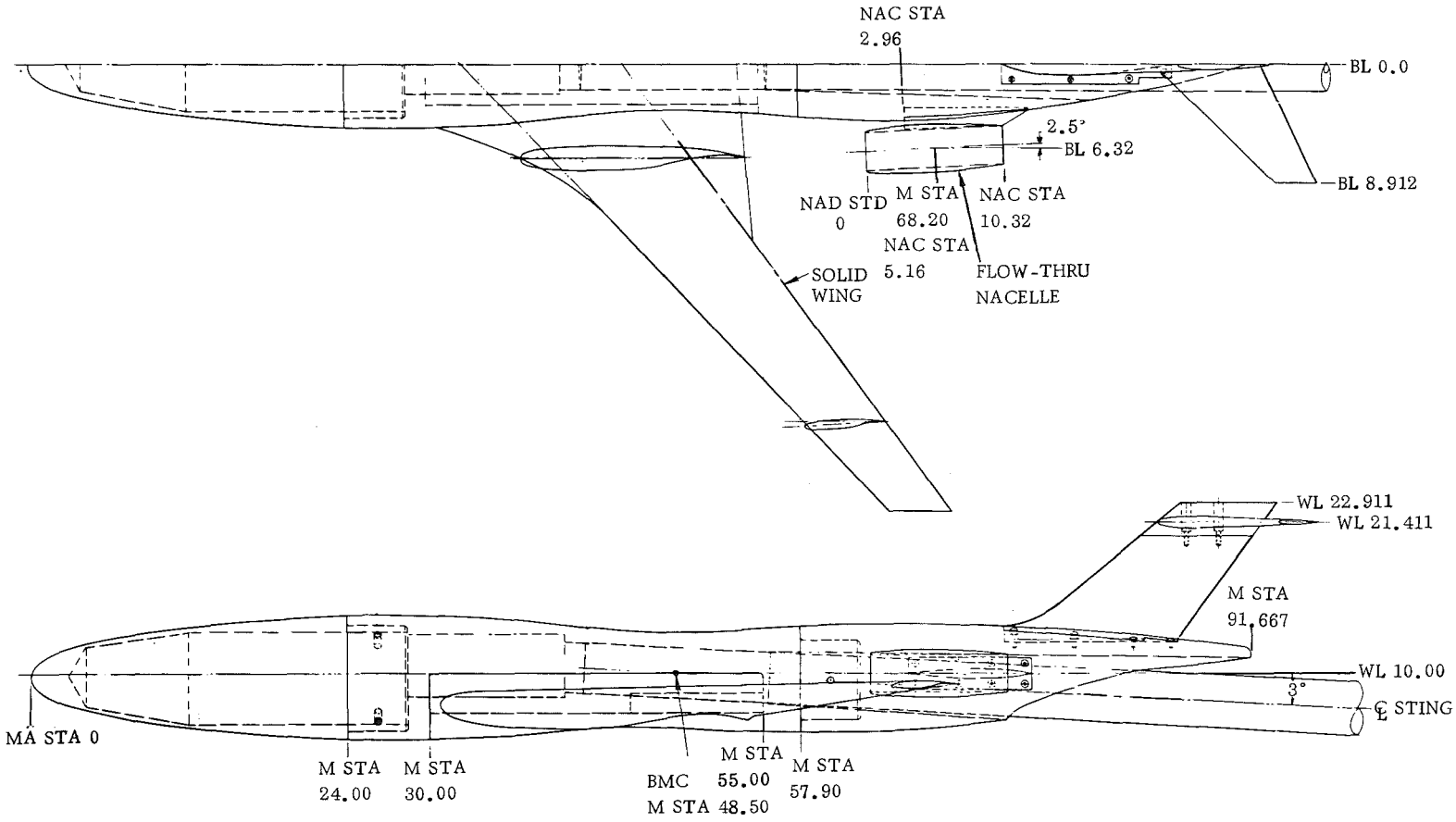

Figure 58. General Arrangement of the Advanced Technology Transport HIRT Model (1/24-Scale)

5.1.2 Variable Swept Wing Fighter (F-111)

The F-111 aircraft used in this study was a production design F-111A airplane. The airplane was a twin jet high wing combat aircraft with a variable swept wing utilizing a 64A series airfoil. The aeroelastic analysis was performed with the wing swept to 50 degrees. The wing has an aspect ratio of 4.325, a taper ratio of 0.325 and a wing area of 537.5 square feet at the 50-degree leading edge sweep position. Overall dimensions of the aircraft included the length, 75.54 feet; height, 17.5 feet; and span, 48.22 feet at the 50-degree leading edge sweep. Dimensional characteristics of the airplane are presented in Table 8; a general arrangement in Figure 9.

Table 8. Dimensional Characteristics of the Convair Aerospace F-111 Aircraft

Wing at 50° L.E. Sweep	
Area	537.5 ft^2
Span	48.22 ft
Root Chord	12.56 ft
Tip Chord	4.07 ft
Aspect Ratio	4.325
Mean Aerodynamic Chord	9.04 ft
Leading Edge Sweep	50°
Dihedral	0°
Incidence at the Root	1.0°
Taper Ratio	0.325

Horizontal Stabilizer		Vertical Stabilizer	
Area	154.2 ft^2	Area	111.7 ft^2
Span	29.33 ft	Span	8.90 ft
Root Chord	15.008 ft	Root Chord	17.79 ft
Tip Chord	5.012 ft	Tip Chord	7.31 ft
Aspect Ratio	2.07	Aspect Ratio	0.709
Mean Aerodynamic Chord	11.46 ft	Mean Aerodynamic Chord	13.28 ft
Leading Edge Sweep	57.5°	Leading Edge Sweep	55°
Dihedral	0°	Taper Ratio	0.411
Taper Ratio	0.334		

The F-111 model that was designed for the HIRT facility was a 1/12-scale all-steel model. The wing was designed as a nonpivoting all-steel structure in Reference 3. A general arrangement of the F-111 model is presented in Figure 60.

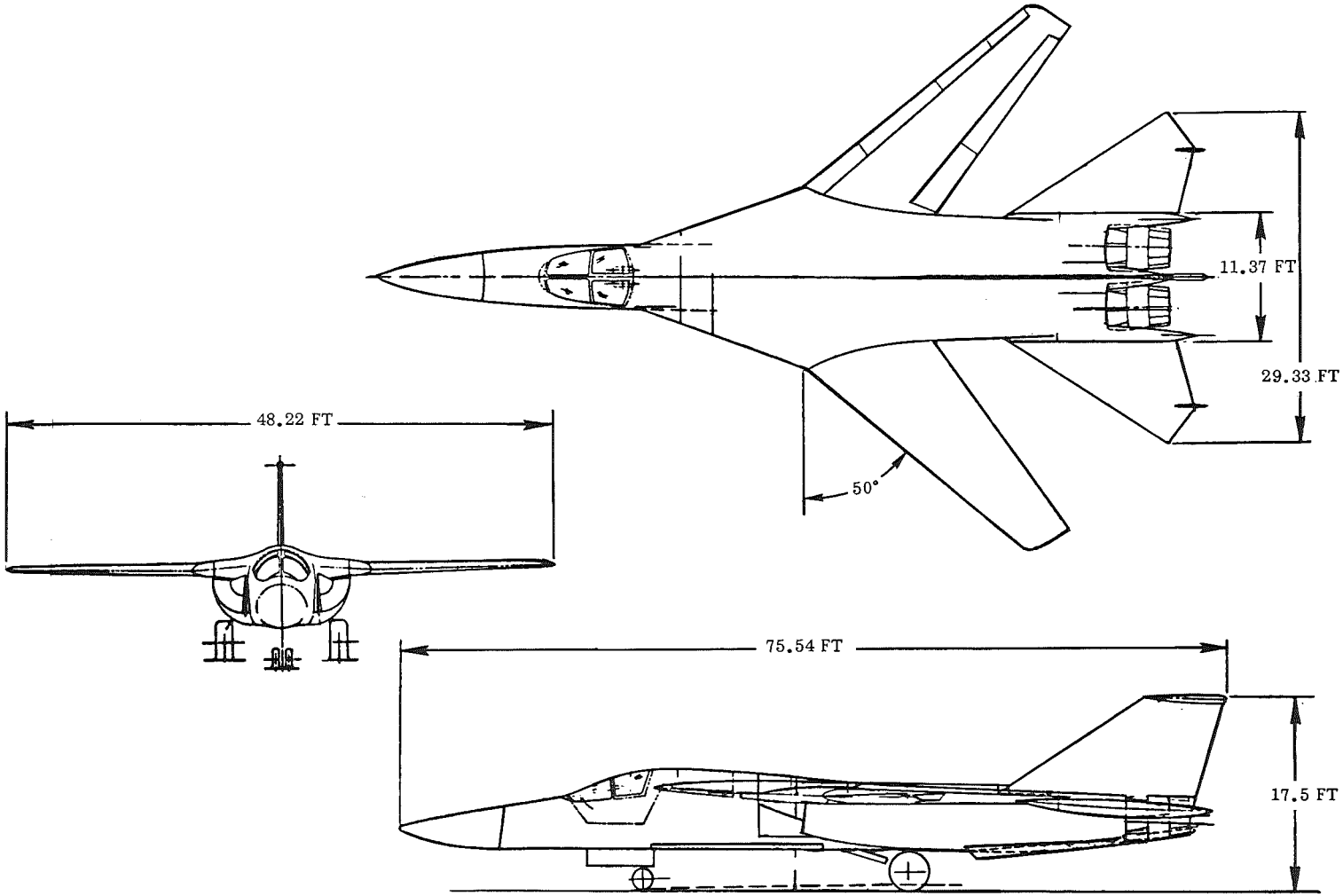

Figure 59. General Arrangement of the Convair Aerospace F-111 Airplane

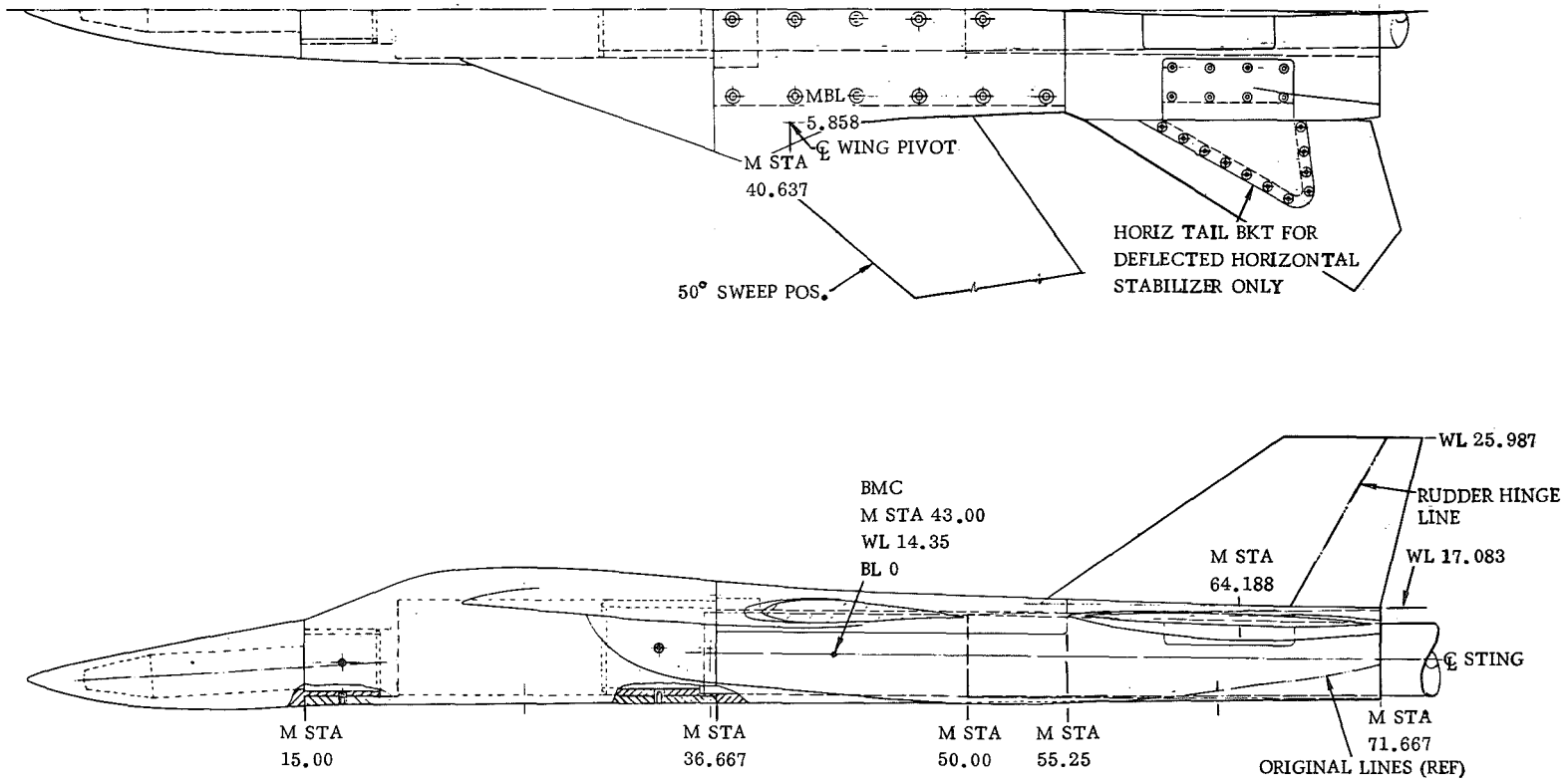

Figure 60. General Arrangement of the F-111 HIRT Model (1/12-Scale)

5.2 AERODYNAMIC METHODS

Several methods have been developed to provide a quick response capability for evaluating an aircraft design and performing some basic trade studies. The methods used for this study employed existing techniques that are applicable to perform a data correlation study. A digital computer program designated the Aeromodule Procedure (Reference 17) has been used to evaluate the lift and drag characteristics of the selected study aircraft. The program features a minimum geometry input, an airfoil section library, several methods for minimum drag prediction and computes a lift curve slope, an angle of attack, minimum drag, drag due to lift, wave drag and transonic drag rise.

Wing lift curve slope was predicted by use of an empirical approach developed to include continuous subsonic, transonic and supersonic application, provide realistic peak lift-curve slope in the transonic region, approximate transonic bucket trends, and provide first-order wing-body interference effects. The total lift curve slope included the contributions from the wing, body, and tail. The wing lift curve slope basically started with the Polhamus equation for trapezoidal wings:

$$C_{L_\alpha} = \frac{\pi \, AR/57.3}{1 + \sqrt{1 + \left[1 - (M \cos \Lambda_{c/2})^2\right]\left[\frac{AR}{2 \cos \Lambda_{c/2}}\right]^2}}$$

Angle of attack at a given lift coefficient was determined by

$$\alpha = \frac{C_L}{C_{L\alpha}} + \left[\alpha_{o_{L_{TWIST}}} + \alpha_{o_{L_{CAMBER}}} + \alpha_{o_{L_{INCIDENCE}}} \right]$$

The incremental term in α_{o_L} due to twist was extrapolated from the results of a parametric study reported by Gilman and Burdges (Reference 18). Their results, which neglect body effects, are valid for wings with linear-element twist.

---

17. "Computer Program Details of Aeromodule Version III: Lift and Drag Analysis of Aerodynamic Configurations," General Dynamics Convair Aerospace Division Report No. MR-A-2089, December 1970.

18. B. G. Gilman and K. P. Burdges, "Rapid Estimation of Wing Aerodynamic Characteristics for Minimum Induced Drag," Journal of Aircraft, Vol. 4, No. 6, November 1969.

Drag due to lift was determined by several techniques, depending on the conditions at which the solution was required. For subsonic Mach numbers, drag due to lift was calculated in the low-lift parabolic region, in the nonlinear stall region, and in the high lift region above stall. The drag due to lift term is basically expressed by

$$C_{D_L} = K(C_L - \Delta C_L)^2 .$$

The polar shape factor, K, was determined from the wing planform geometry, the span efficiency factor, and the wing leading edge suction factor, which was a function of the leading edge radius, Reynolds number, and Mach number. The polar displacement term, ΔC_L, is a function of the wing design lift coefficient, the Mach number, and the span efficiency factor.

Using the output from the Weissinger-L method, which produced lift, pitching moments and aeroelastic deformation of the aircraft, the rigid aerodynamic program was used to determine the drag characteristics of the aircraft at a single deformed point. By determining the rigid aerodynamic characteristics for various wing deformations, the flexible aerodynamic characteristics were determined. This method has been used to evaluate the characteristics of the flight vehicle and the model with the differences being presented and discussed in this study.

5.3 LONGITUDINAL AEROELASTIC/AERODYNAMIC CHARACTERISTICS OF THE ATT

Aeroelastic deformations of the ATT wing were analyzed for several flight conditions of the aircraft and the corresponding conditions of the HIRT model through the use of the modified Weissinger-L method (see Chapter 4). For the ATT model, the deflected wing of the aircraft in level flight ($n_Z \cong 1$) at 36,000 feet and Mach 0.98 was assumed to be the design twist used to determine the model wing jig twist. The resulting jig twist as shown in Figure 42 resulted in matching the model twist distribution to that of the aircraft at the selected condition of Mach number and lift coefficient. The model wing with the thin supercritical airfoil section was designed to be constructed of steel with 35 per cent of the wing section not considered as contributing to the bending and torsional stiffness characteristics because of high lift device considerations or the inclusion of pressure-tube routing channels.

5.3.1 Characteristics at Mach 0.98 and 36,000 Feet

Figure 61 illustrates the comparison of the full-size wing twist with that of the model for HIRT test conditions simulating full-scale Reynolds number at 36,000 feet and

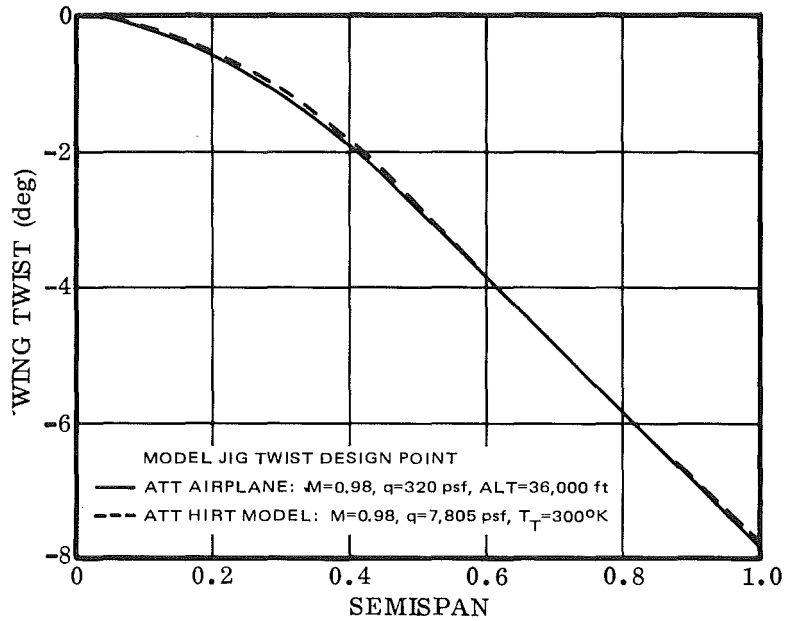

Figure 61. Comparison of the ATT Model Wing Twist with the ATT Airplane Wing Twist for Level Flight at Mach 0.98

Mach 0.98. As the load conditions are varied by pitching from the wing twist matching point, the model wing deflections diverge from the airplane wing deflection. Figure 62 illustrates the comparison of the airplane wing tip twist with that of the model for increasing load factors. The data in Figure 62 show that the airplane wing twists 1.7 degrees per g, while the model wing twists 1.5 degrees per g under the HIRT test conditions. The data indicates that the model is stiffer under the HIRT test conditions than the airplane under flight conditions. A further reduction in the model wing cross sectional properties could possibly result in matching the wing twist through the variation in load factor.

Figure 62 also indicates that the airplane wing twists 0.38 degree more than that of the model at a load factor of 2.5. The additional twist means that the outboard airfoil sections are at a lower angle of attack than the corresponding sections on the wind tunnel model. The increased twist results in a reduced lift, drag, and wing pitching moment relative to the wind tunnel model. The resulting longitudinal incremental aerodynamic coefficients from the differential tip twist are presented in Figure 63 as a function of increased load factor.

Figure 64 illustrates the aerodynamic increments as a function of the model angle of attack. The jig twisted design point corresponds to the point on Figure 64 at 6.0 degrees angle of attack. For this condition, the airplane is flying at a mid-cruise weight of 234,000 pounds, an altitude of 36,000 feet at Mach 0.98, and a C_L of 0.32. The incremental drag coefficient varies from zero at the cruise condition (n_Z= 1.0) to 0.0012 at a

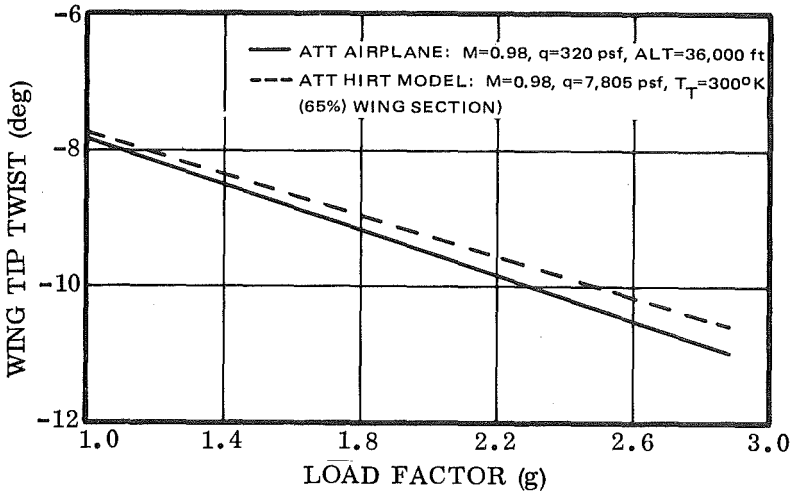

Figure 62 . Effect of Load Factor on the ATT Wing Tip Twist at Mach 0.98

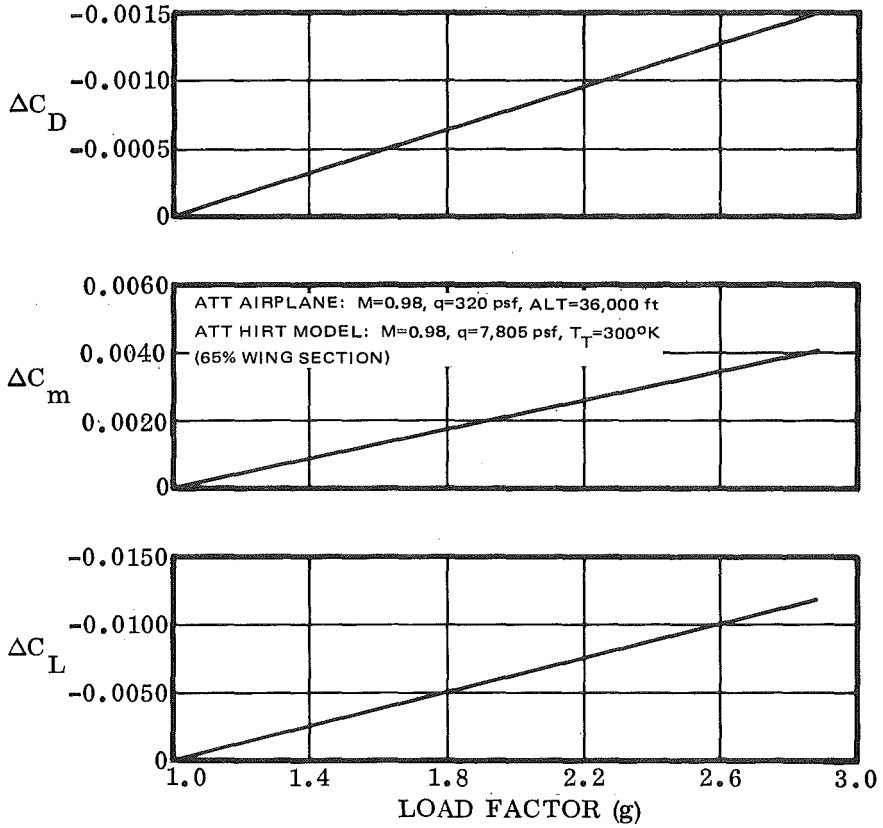

Figure 63. Estimated Effect of Load Factor on the Incremental Aerodynamic Data for the ATT Study Configuration at Mach 0.98

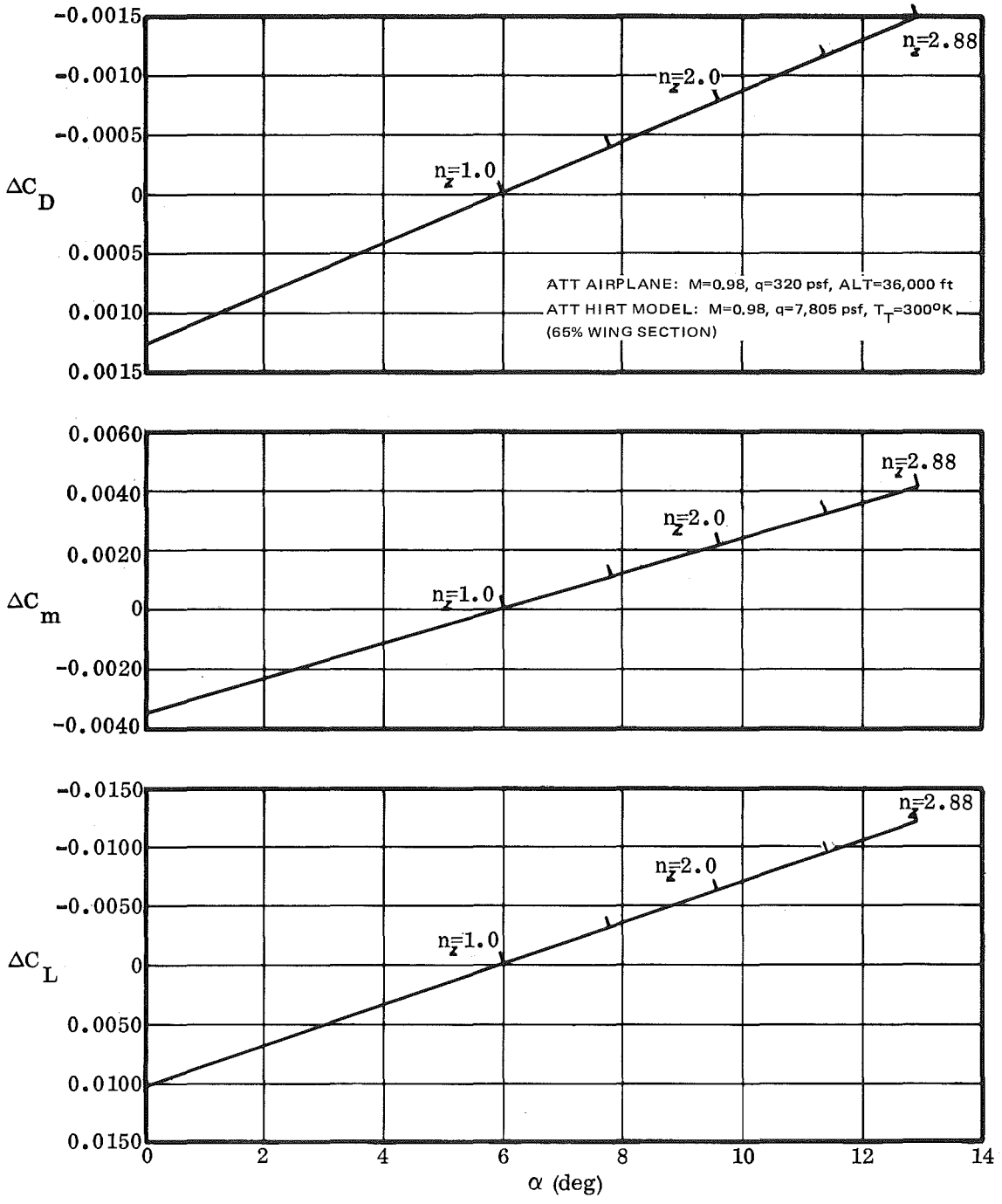

Figure 64. Estimated Effect of Angle of Attack on the Incremental Aerodynamic Data for the ATT Study Configuration at Mach 0.98

load factor of 2.5 at 11.4 degrees angle of attack. A drag increment of 0.0012 results in a drag force of about 37 pounds at tunnel conditions simulating full scale Reynolds number.

The model has been designed to be supported in the HIRT facility on a sting with an internal strain gage balance used to measure the aerodynamic loads. The balance designed for the ATT model (Reference 5) has an estimated maximum normal force capacity of 27,000 pounds with an estimated maximum axial force capacity of 2,700 pounds. The accuracy of the balance has been estimated at about 0.5 per cent of the full-scale load. This results in an accuracy of about ±13.5 pounds of axial force with a full-scale loading. Rotating the drag force increment due to aeroelastic differences with the accompanying lift force increment through the model angle of attack results in an axial force of 22 pounds. This estimated drag difference is within the accuracy of the balance; however, at reduced angles of attack, an incremental drag coefficient of 0.0010 for the ATT model represents the balance accuracy. Below this level, the aerodynamic increments cannot be measured accurately, thus the aeroelastic deformations will not significantly affect the test data up to 10.5 degrees angle of attack for tunnel conditions at full scale Reynolds number and Mach 0.98.

5.3.2 Characteristics with Reduced Wing Cross Sectional Properties

In the preceding discussion, the model wing deflection data indicated that a further reduction in the model wing cross-sectional properties could result in matching the wing twist through the variation in load factor. A model condition has been analyzed with the cross-sectional properties arbitrarily reduced from the 65 percent section to a 52 percent section. The initial 65 percent section was achieved by allowing the aft 35 percent of the wing to be removable. The removable section would allow access to possible wing pressure tubing. By reducing the wing section properties to 52 percent, the model wing will become more flexible. The increased flexibility results in the model wing twisting more than the aircraft wing for increased load factors, as shown in Figure 65. The airplane wing twists 1.7 degrees per g, while the model twists 1.9 degrees per g under the HIRT test conditions. Figure 65 indicates that the model wing twists 0.45 degree more than the airplane at a load factor of 2.5.

The additional model wing twist results in test data with a reduced lift and drag, and increased nose up pitching moment relative to the airplane. The resulting longitudinal aerodynamic increments from the differential tip twist are shown in Figure 66 as a function of load factor. Figure 67 illustrates the estimated difference in drag due to lift as a function of model angle of attack. For a load factor of 2.5, which corresponds to a model angle of attack of 11.3 degrees, the incremental drag coefficient was 0.0016. For this condition, the drag increments, lift increments, and pitching moment increments must be added to the model test data.

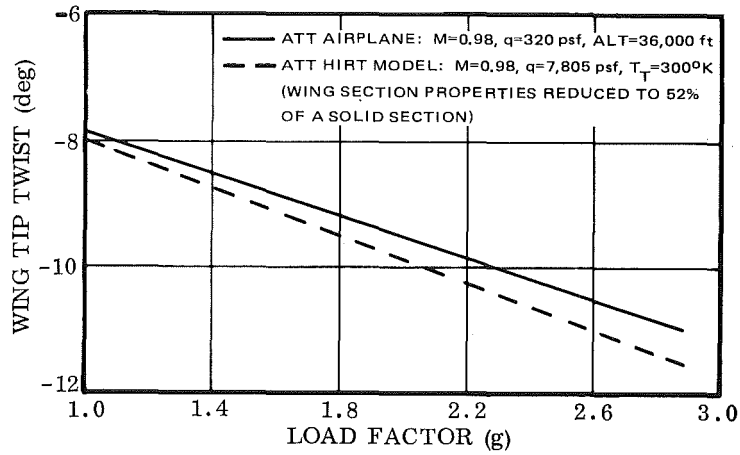

Figure 65. Effect of Load Factor on the ATT Wing Tip Twist at Mach 0.98 (52% Model Wing Section)

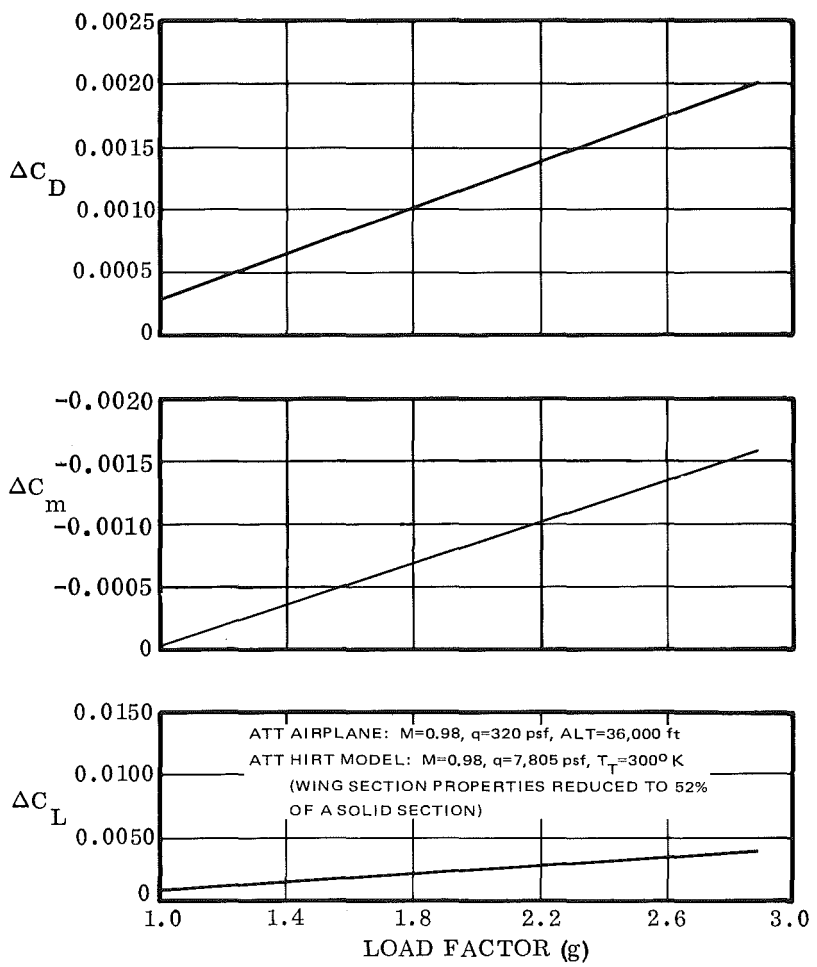

Figure 66. Estimated Effect of Load Factor on the Incremental Aerodynamic Data for the ATT Study Configuration at Mach 0.98 (52% Model Wing Section)

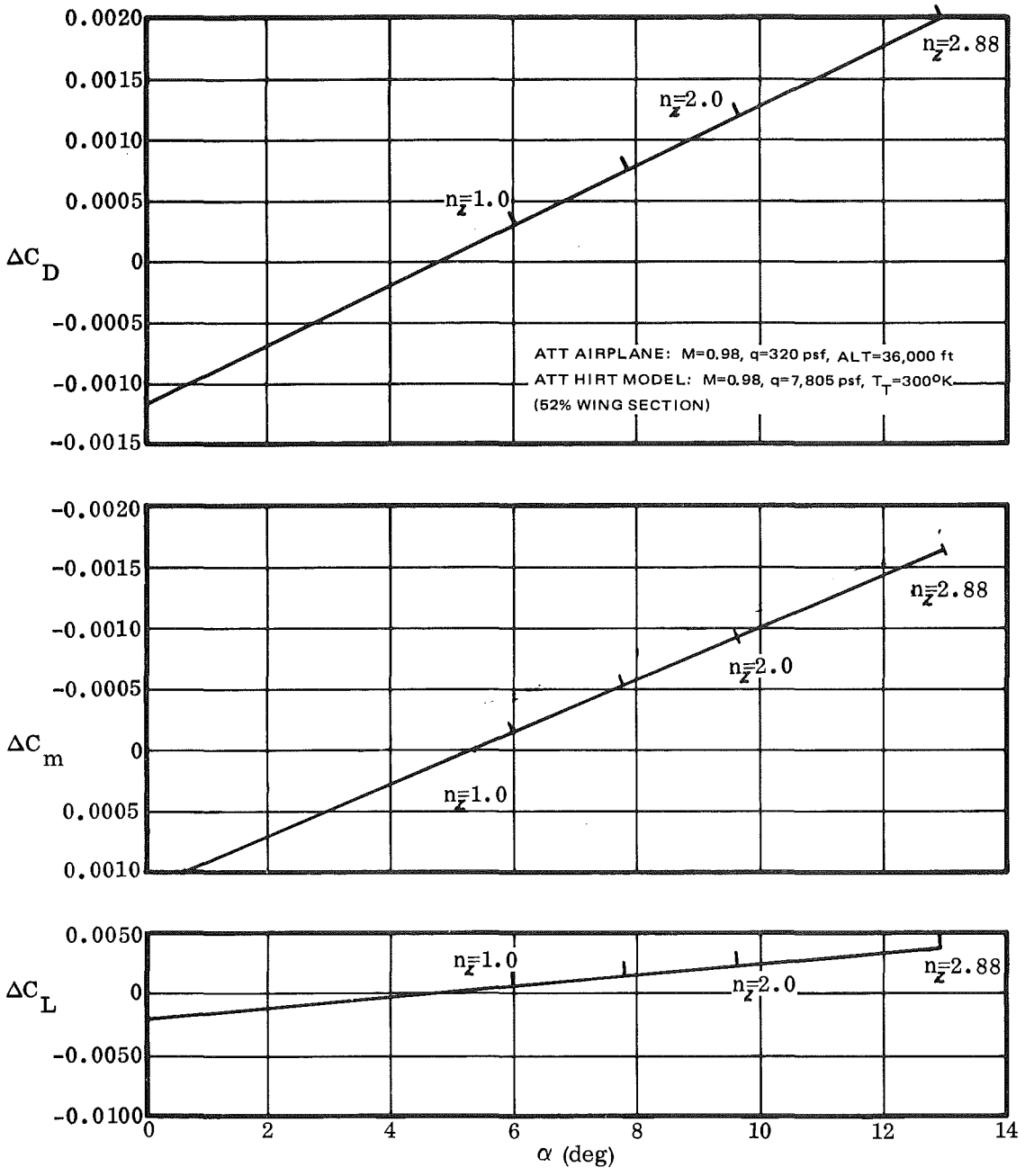

Figure 67. Estimated Effect of Angle of Attack on the Incremental Aerodynamic Data for the ATT Study Configuration at Mach 0.98 (52% Model Wing Section)

The data presented for the two cross-sectional wing properties indicate that, for this transport-type airplane, a possible cross-sectional property of the model wing could be determined and designed into the model, which would cause the model deformation to be the same as that of the flight vehicle. The stress analysis for the reduced cross-sectional properties of the model wing was checked and found to be strong enough for a portion of the flight envelope but not for all critical points within the envelope.

5.3.3 Characteristics at Mach 0.80 and 25,000 Feet

The previous discussion has considered the ATT aircraft operating at a high transonic Mach number and at a high altitude. Four additional points have been analyzed within the flight envelope, based on the model wing jig twist being held the same as the high altitude, high transonic Mach number design condition.

For a flight condition of 25,000 feet and Mach 0.80, the aerodynamic analysis resulted in the wing twist data for the model and airplane as shown in Figure 68 for increasing load factors. The data in Figure 68 indicate that the aircraft wing twists 2.0 degrees per g, while the model twists 1.75 degrees per g under the HIRT test conditions. At a load factor of 2.5, the incremental wing twist was 0.5 degree, with the airplane twisting more than the model wing. Longitudinal aerodynamic increments are presented in Figure 69 as a function of the load factor and as a function of the model angle of attack are in Figure 70. At a load factor of 2.5, the differential drag coefficient was 0.0012, which results in a drag force of about 39.5 pounds at tunnel conditions simulating full scale Reynolds number. The balance accuracy was 13.5 pounds of axial force. Rotating the drag increment through the angle of attack results in an axial force of 51 pounds, which is within the accuracy of the balance. However, with reduced angle of attack, an incremental drag coefficient of 0.0007 represents the balance accuracy for the tunnel conditions in this case.

5.3.4 Characteristics of Mach 0.95 and 20,000 Feet

For a flight condition of 20,000 feet and Mach 0.95, the aeroelastic analysis resulted in the wing twist data shown in Figure 71 for increasing load factor. The data indicate that the aircraft wing twists 1.75 degrees per g, with the model wing twisting 1.40 degrees per g under the HIRT test conditions. In level flight at a C_L of 0.19, the airplane wing tip twists 0.60 degree more than the model wing. At a load factor of 2.5, this airplane wing twists 1.10 degrees more than the model wing. The resulting aerodynamic increments as a function of the load factor are presented in Figure 72, with the data presented in Figure 73 as a function of the model angle of attack. At a load factor of 2.5, the incremental drag coefficient was 0.0015, which results in a drag force of about 74 pounds at tunnel conditions simulating full scale Reynolds number. Rotating the drag increment through the angle of attack results in an axial force of 22 pounds. This is again within the accuracy of the balance; however, with reduced angles of attack an incremental drag coefficient of 0.0014 represents the balance accuracy for the tunnel conditions in this case.

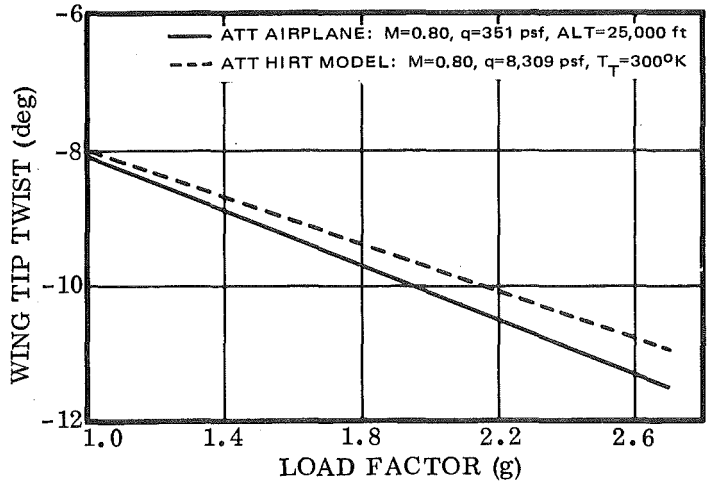

Figure 68 . Effect of Load Factor on the ATT Wing Tip Twist at Mach 0. 8

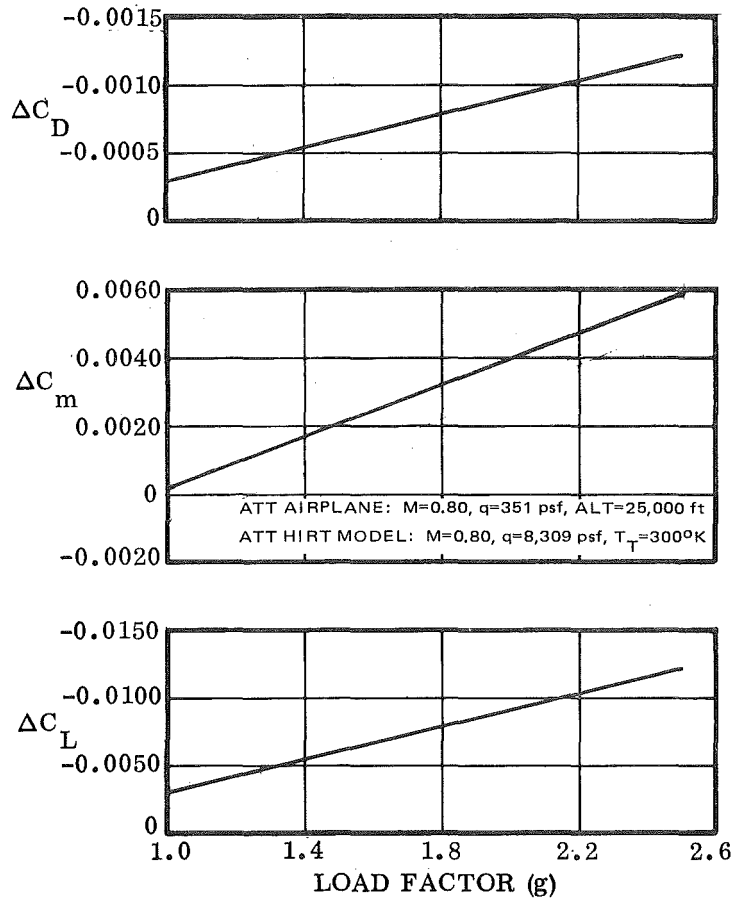

Figure 69. Estimated Effect of Load Factor on the Incremental Aerodynamic Data for the ATT Study Configuration at Mach 0. 8

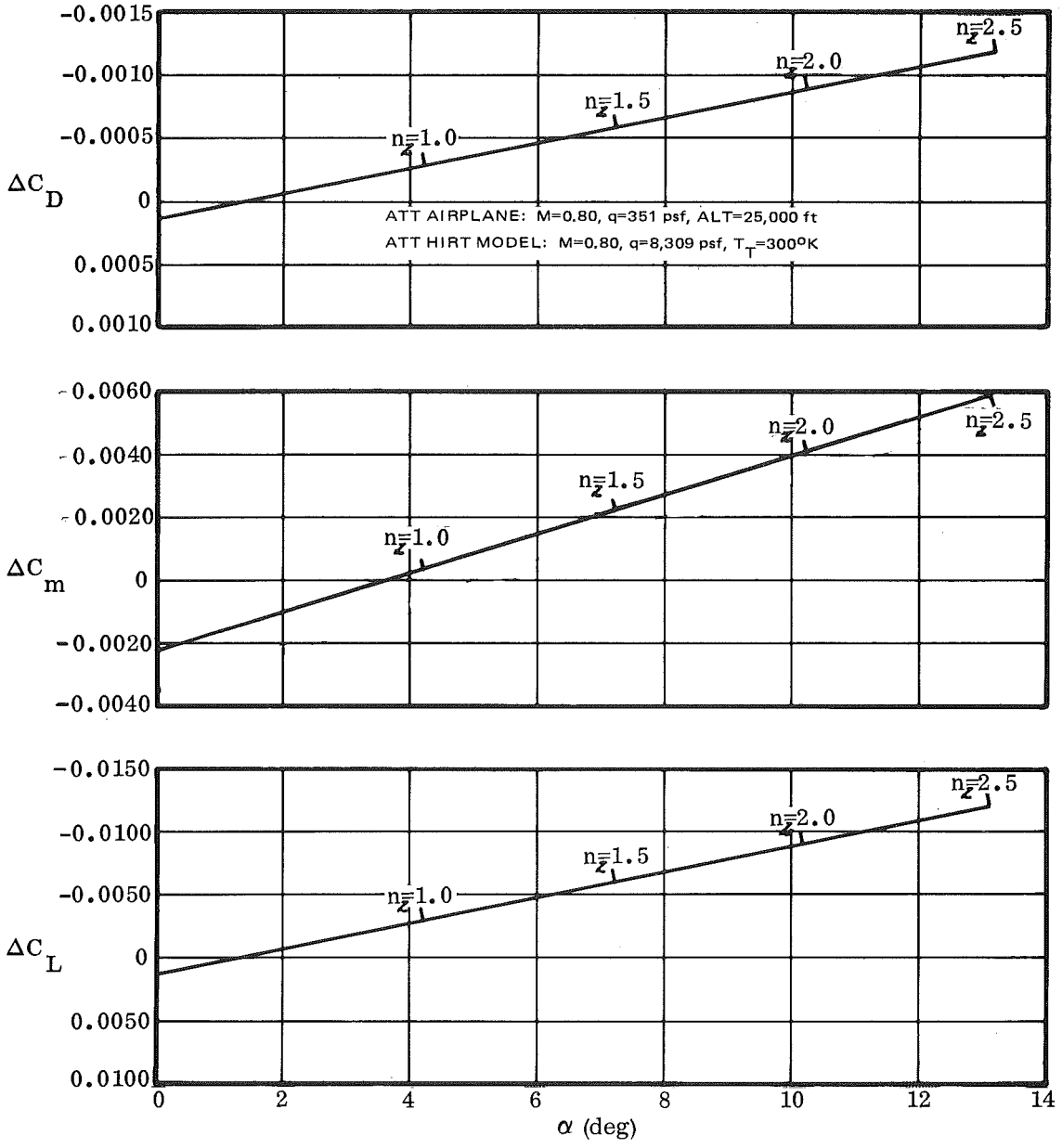

Figure 70. Estimated Effect of Angle of Attack on the Incremental Aerodynamic Data for the ATT Study Configuration at Mach 0.8

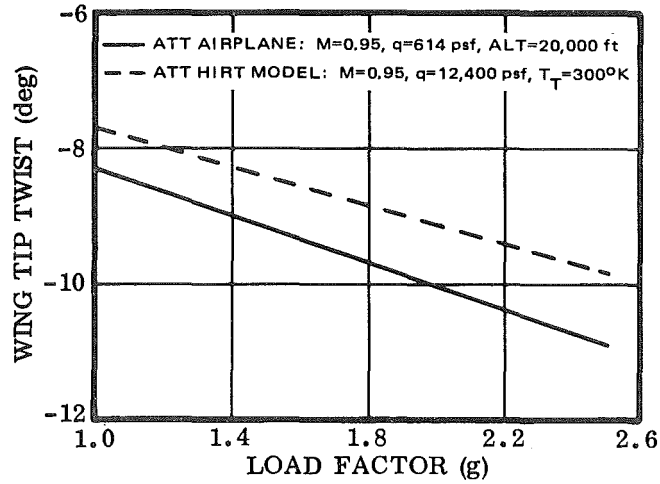

Figure 71. Effect of Load Factor on the ATT Wing Tip Twist at Mach 0.95

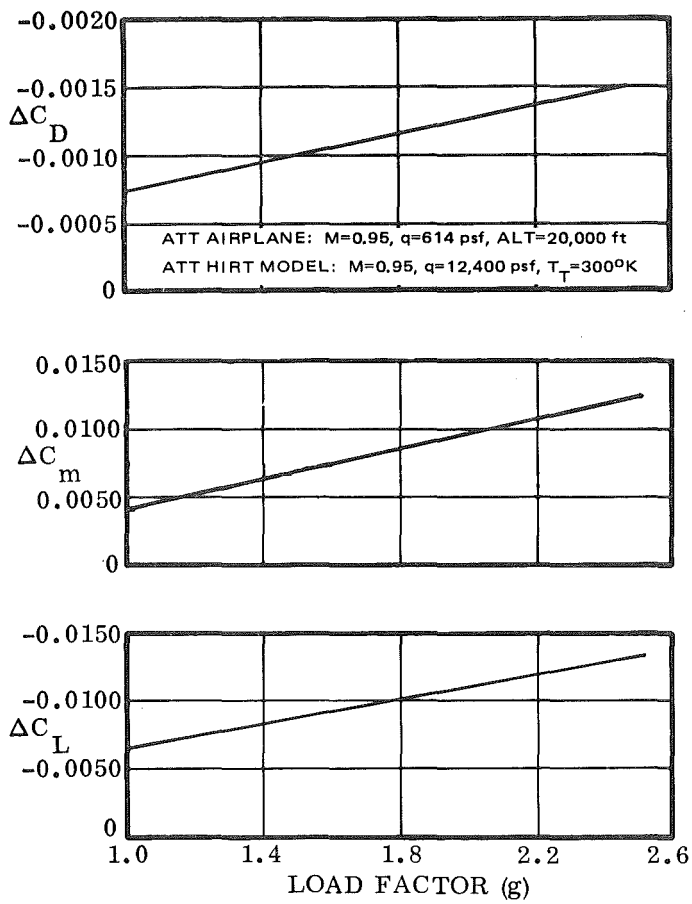

Figure 72. Estimated Effect of Load Factor on the Incremental Aerodynamic Data for the ATT Study Configuration at Mach 0.95

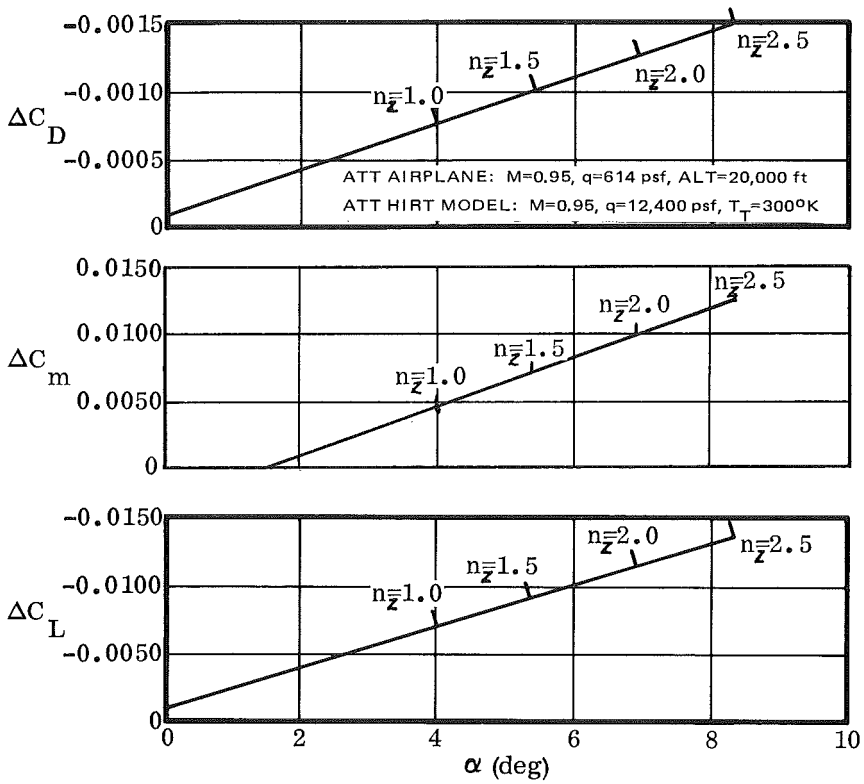

Figure 73. Estimated Effect of Angle of Attack on the Incremental Aerodynamic Data for the ATT Study Configuration at Mach 0.95

5.3.5 Characteristics at Mach 0.60 and 10,000 Feet

A flight condition at 10,000 feet and Mach 0.6 was analyzed. The wing tip twist data are presented in Figure 74 . The data indicate that the aircraft wing twists 2.0 degrees per g, with the model wing twisting 1.70 degrees per g under the HIRT test conditions. At a load factor of 2.5, the incremental tip twist was 0.7 degree, with the aircraft wing deflecting more than the model wing. Aerodynamic increments are presented in Figure 75 as a function of load factor and in Figure 76 as a function of the model angle of attack. For this condition, this drag increment varies from 0.0003 at the level flight condition at a C_L of 0.32, to 0.0015 at a load factor of 2.5 at a C_L of 0.80. The incremental drag coefficient of 0.0015 results in a drag force of 48 pounds at the tunnel conditions simulating full scale Reynold number and at Mach 0.6. Rotating the drag increment through the angle of attack results in an axial force of -55 pounds. This is again within the accuracy of the balance; however, with a reduced angle of attack, an incremental drag coefficient of 0.0009 represents the balance accuracy for the tunnel conditions in this case.

Figure 77 illustrates selected data of the model wing tip twist as a function of Mach number at a constant dynamic pressure. The data indicate only a small effect of Mach number on the wing tip twist.

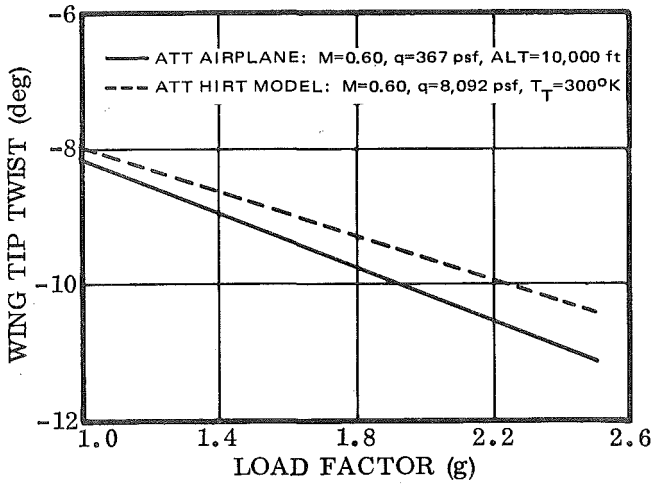

Figure 74. Effect of Load Factor on the ATT Wing Tip Twist at Mach 0.60

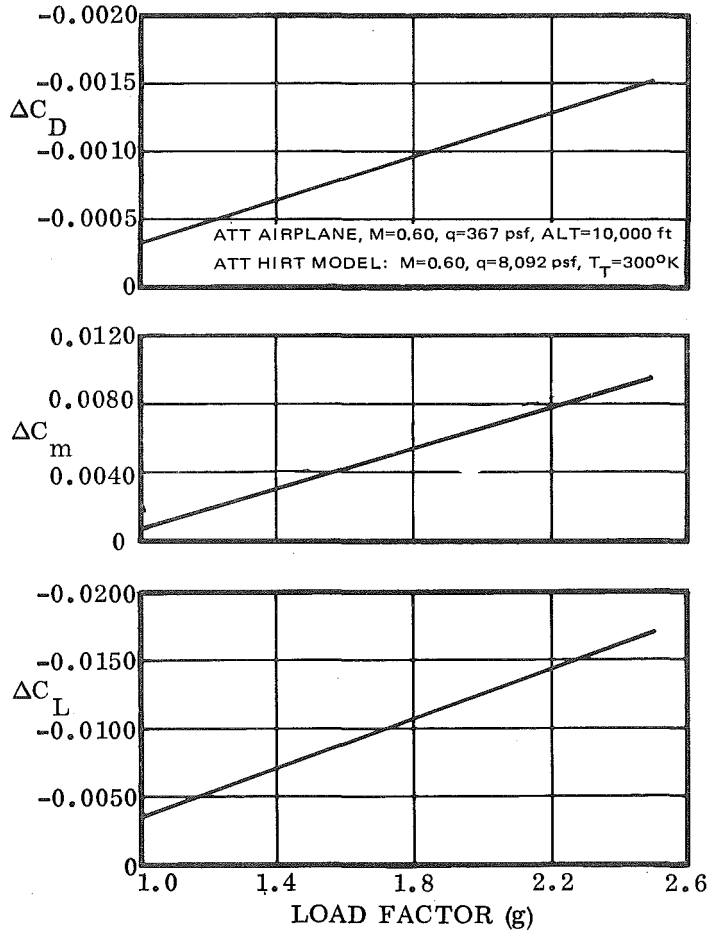

Figure 75. Effect of Load Factor on the Incremental Aerodynamic Data for the ATT Study Configuration at Mach 0.60

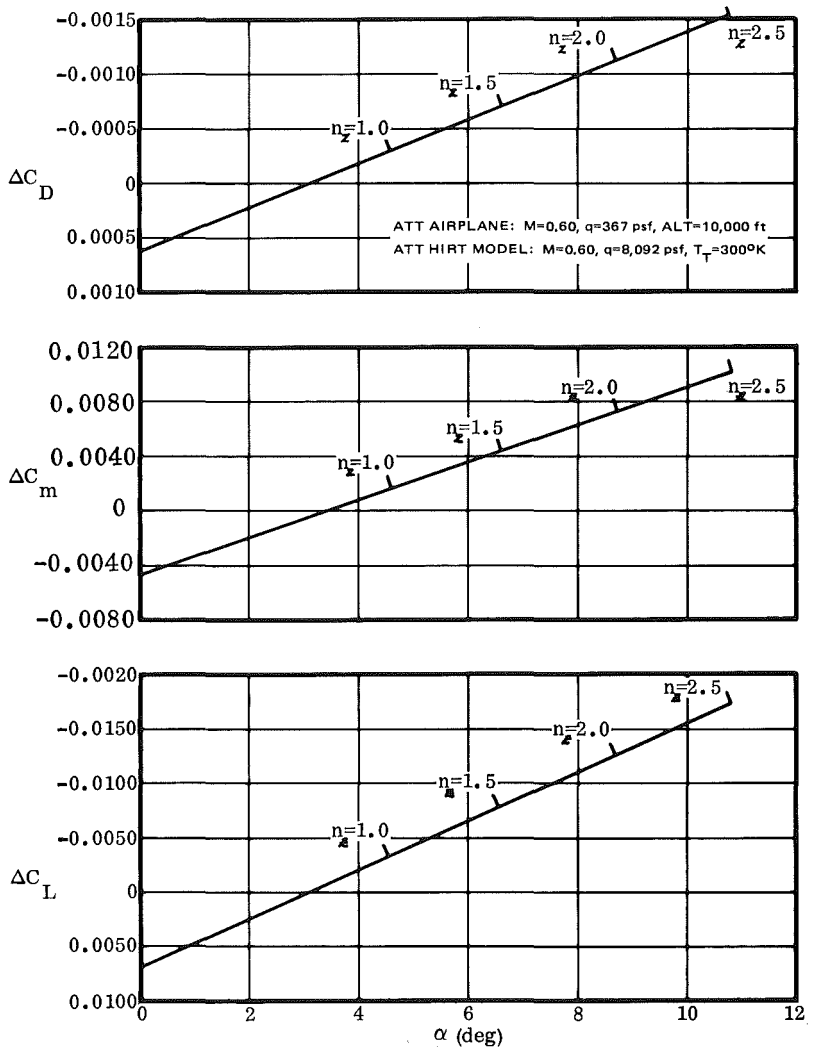

Figure 76. Estimated Effect of Angle of Attack on the Incremental Aerodynamic Data for the ATT Study Configuration at Mach 0.60

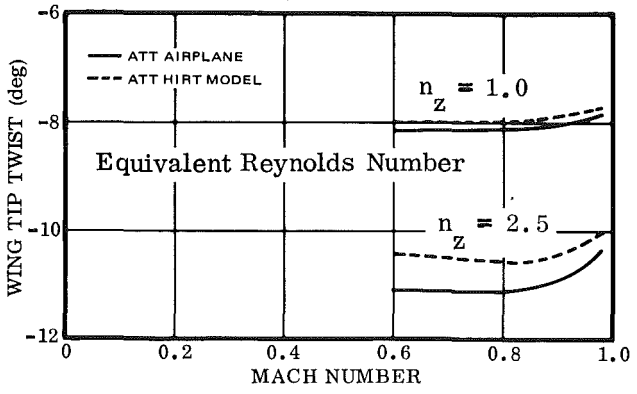

Figure 77. Effect of Mach Number on the ATT Wing Tip Twist

5.3.6 Summary

The ATT transport model used in this study was considered to be designed as an all steel model with 35 percent of the wing section not considered as contributing to the bending and torsional stiffness characteristics because of the inclusion of wing pressure tube routing channels. The aeroelastic analysis of the wing resulted in less model wing twist and vertical deflection than the airplane wing at equivalent Reynolds number conditions as shown in Figures 68 and 56. In the aerodynamic analysis, vertical deflection or the effect of a nonplanar wing was not considered directly but was considered insofar as including the primary effect of vertical deflection on twist. Further effect of a nonplanar wing on the aerodynamic characteristics was considered to be very small.

The deformation differences between the model wing and the airplane do not result in significant differences in the estimated model and airplane aerodynamics. For instance, at the design cruise condition (M=0.98, Alt. =36,000 ft) and at the maximum load factor (2.5) the drag of the model was found to be 0.0012 greater than the airplane. For this test condition, the model force balance accuracy in drag was considered to be about ±0.0010. Thus, the balance accuracy is of as much concern as the aeroelastic effects on the aerodynamic data for this configuration since at least approximate corrections can be made for the aerodynamic differences due to aeroelasticity if the deflection are known.

5.4 LONGITUDINAL AEROELASTIC CHARACTERISTICS OF THE F-111

Aeroelastic deformations of the F-111 wing were analyzed for several flight conditions of the HIRT model through the use of the modified Weissinger L-method. For the F-111 model, the deflected wing shape of the aircraft in level flight ($n_z = 1$) at 10,000 feet and Mach 0.90 was used to determine the model wing jig twist. The resulting jig twist, as shown in Figure 78, resulted in matching the model wing deflection with the aircraft wing deflection. The model wing design (Reference 3) was assumed to be constructed of solid steel without cutouts in the wing cross-sectional characteristics.

5.4.1 Characteristics at Mach 0.90 and 10,000 Feet

Figure 78 illustrates a comparison of the airplane wing twist with that of the model for HIRT test conditions simulating the full scale Reynolds number at 10,000 feet and Mach 0.90. Figure 79 illustrates the comparison of the airplane wing tip twist with that of the model for increasing load factors. The data indicate that the model wing twists 0.7 degree per g under the HIRT test conditions, with the airplane wing twisting 0.6 degree per g under flight conditions. The model wing twists about 0.5 degree more than the airplane wing at a load factor of 5.0. For this case, the model is more flexible under

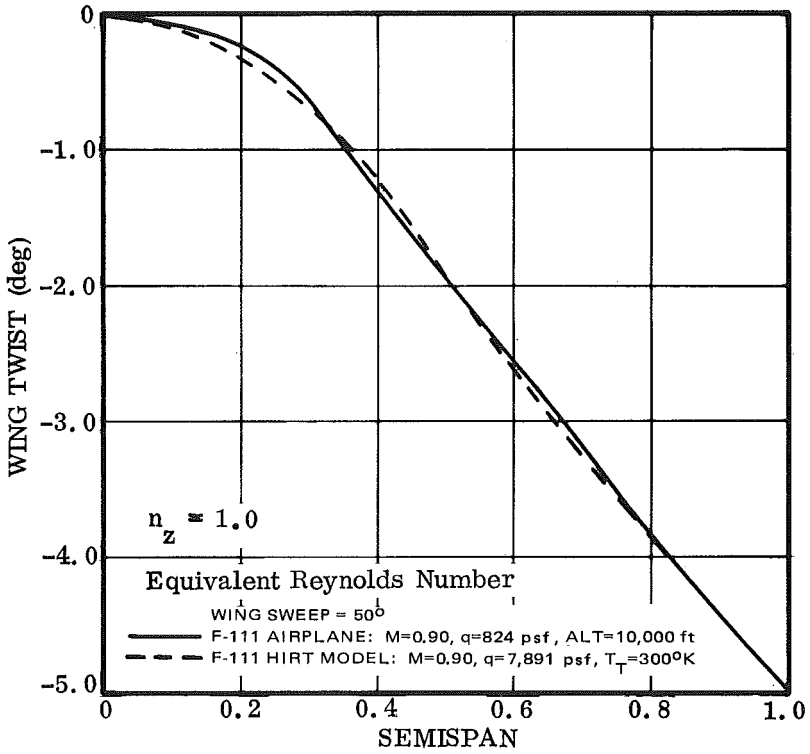

Figure 78. Comparison of the F-111 Model Wing Twist with the F-111 Airplane Wing for Level Flight at Mach 0.90

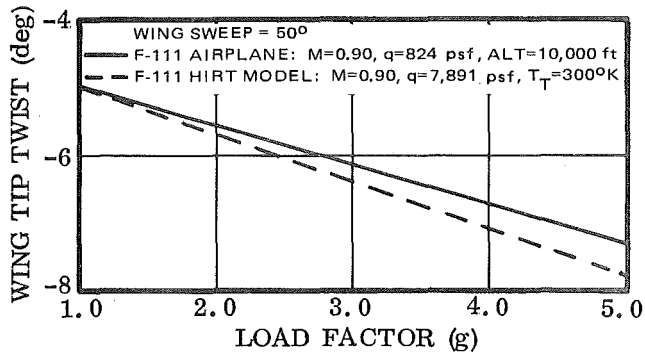

Figure 79. Effect of Load Factor on the F-111 Wing Tip Twist at Mach 0.90 and Full-Scale Reynolds Number (Altitude = 10,000 ft)

the HIRT test conditions than the airplane under flight conditions. From this condition, one of the possible methods of improving the resulting model aeroelastic deformations would be the tunnel dynamic pressure. This condition is discussed later in this section.

The additional twist experienced by the model wing means that the outboard airfoil sections are at a lower angle of attack, which results in a decrease in lift and drag and more nose-up pitching moment relative to the airplane.

The longitudinal aerodynamic increments resulting from the additional tip twist are presented in Figure 80 as a function of the aircraft load factor. Figure 81 illustrates the aerodynamic increments as a function of the model angle of attack.

The jig twist design point corresponds to the point on Figure 81 at 2.4 degrees angle of attack. For this condition, the airplane is flying at a cruise weight of 70,000 pounds, an altitude of 10,000 feet, a speed of Mach 0.90, and a C_L of 0.16. The incremental drag coefficient varies from zero at the matched condition to 0.0010 at a load factor of 5.0 at 10.3 degrees angle of attack. A drag increment of 0.0010 results in a drag force of about 29.4 pounds at tunnel conditions simulating full scale Reynolds number.

The model has been designed to be supported in the HIRT facility on a sting with an internal strain gage balance used to measure the aerodynamic loads. The balance design for the F-111 model (Reference 5) has an estimated maximum normal force capacity of 37,000 pounds, with an estimated maximum axial force of 3,700 pounds. Balance accuracy has been estimated to be about 0.5 percent of the full scale load. This results in an accuracy of about 18.5 pounds of axial force with a maximum axial force loading.

Rotating the drag force increment due to aeroelastic differences with the accompanying lift force through the angle of attack results in an axial force of 23.9 pounds. This is

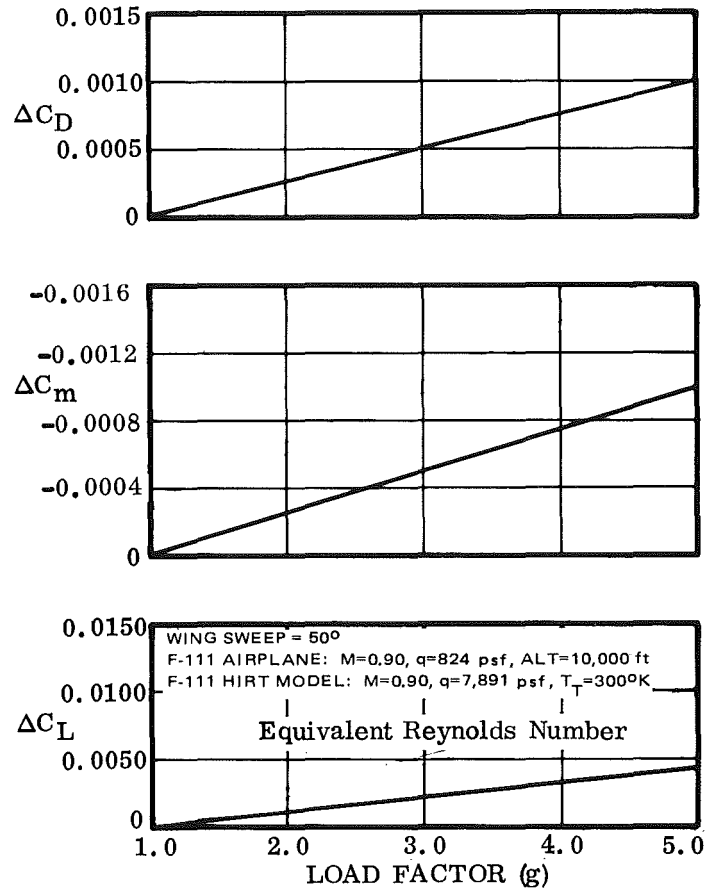

Figure 80. Estimated Effect of Load Factor on the Incremental Aerodynamic Data for the F-111 Study Configuration at Mach 0.90

within the accuracy of the balance; however, with reduced angles of attack, an incremental drag coefficient of 0.0006 represents the balance accuracy. Below this level, the aerodynamic drag increment due to aeroelastic effects cannot be measured accurately, thus the test data will not be affected up to about 7.0 degrees angle of attack.

5.4.2 Characteristics at 75 Percent Full Scale Test Reynolds Number

For certain conditions it may be required to minimize the aerodynamic increments as presented in Figure 80. To achieve this, the HIRT facility offers unique methods of dynamic pressure reduction. First would be simply a reduction in the test Reynolds

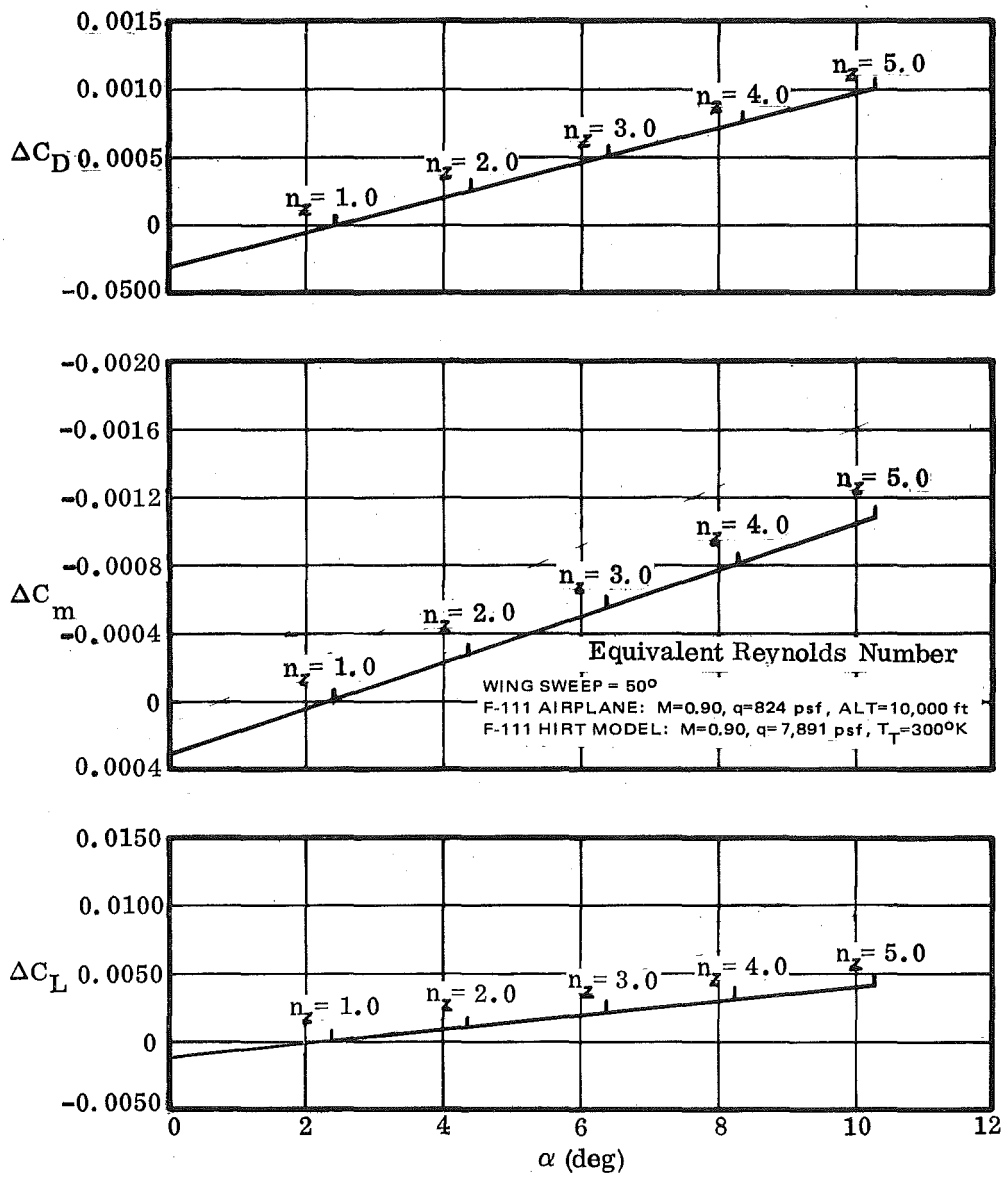

Figure 81. Estimated Effect of Angle of Attack on the Incremental Aerodynamic Data for the F-111 Study Configuration at Mach 0.90

number; secondly would be a decrease in the tunnel operating temperature, which would allow full scale Reynolds number testing at a lower dynamic pressure. Three test conditions have been considered and analyzed for the study design point on the F-111 HIRT model.

For a 25-percent reduction in the test Reynolds number ($R_{e_{test}} = 0.75\ R_{e_{airplane}}$), the incremental wing twist was reduced from 0.5 to 0.25 degree at a load factor of 5.0. Figure 82 illustrates the wing tip twist comparison for a 25-percent reduction in the full scale test Reynolds number as a function of the load factor. For this condition, the model wing does not twist as much as the airplane wing under flight conditions. The outboard sections of the model wing are at a slightly greater angle of attack than the airplane wing. This results in the aerodynamic increments as shown in Figure 83. The test data has been estimated to indicate a higher drag and lift and greater nose-up pitching moment than the airplane would indicate. Figure 84 shows the aerodynamic increments as a function of the model angle of attack. For a 25-percent reduction in the full scale test Reynolds number, the results indicate that the aerodynamic corrections are smaller than for tests performed at full scale test Reynolds number.

5.4.3 Characteristics at 50 Percent Full Scale Test Reynolds Number

For a 50 percent reduction in the test Reynolds number, the estimated difference in the model and the airplane aerodynamic characteristics became significantly greater. The tip twist is presented in Figure 85 as a function of load factor for the 50 percent reduced test Reynolds number case, with the airplane at flight conditions. The differential wing tip twist angle becomes 1.45 degrees at a load factor of 5.0. The incremental aerodynamic terms, as presented in Figures 86 and 87, become greater in magnitude than those in Figures 80 and 81 at full scale test Reynolds number.

Thus, for the F-111 study configuration, a small reduction in test Reynolds number will improve the model simulation in terms of lift and drag due to lift and pitching moment.

5.4.4 Characteristics at Full Scale Test Reynolds Number with Reduced Test Section Temperature

The preceding discussions on reducing the test Reynolds number to help the model loading conditions is one method of minimizing the aeroelastic effects on the test data. A second method proposed for the HIRT facility is to control the tunnel air temperature. This allows a reduction in the tunnel air temperature for testing at full scale Reynolds number with a reduced dynamic pressure. For this tunnel condition, a data point was generated on the F-111 study configuration based on a temperature drop from 300°K to 240°K. The tunnel characteristics from reference 13 were used to determine the tunnel dynamic pressure at the 240°K air temperature. The results produced a dynamic pressure identical to that for the 25-percent reduction in the test Reynolds number case discussed in Section 5.4.2.

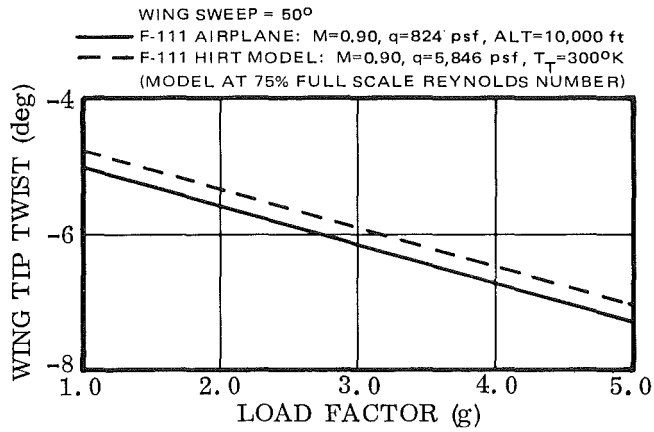

Figure 82. Effect of Load Factor on the F-111 Wing Tip Twist at Mach 0.90 and 75% Full Scale Reynolds Number

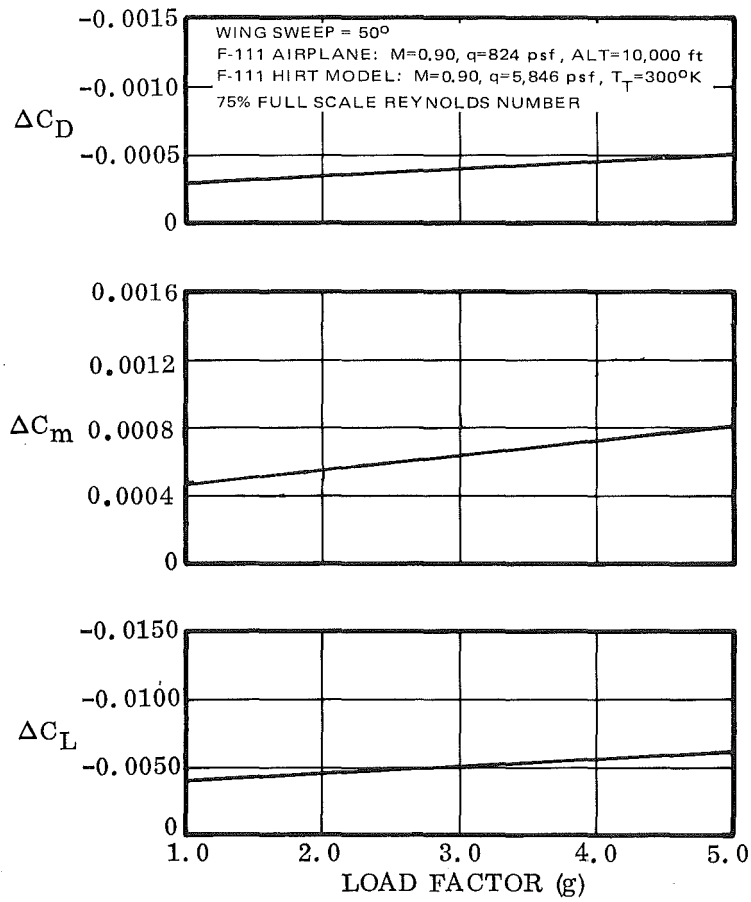

Figure 83. Estimated Effect of Load Factor on the Incremental Aerodynamic Data for the F-111 Study Configuration at Mach 0.90 and 75% Full Scale Reynolds Number

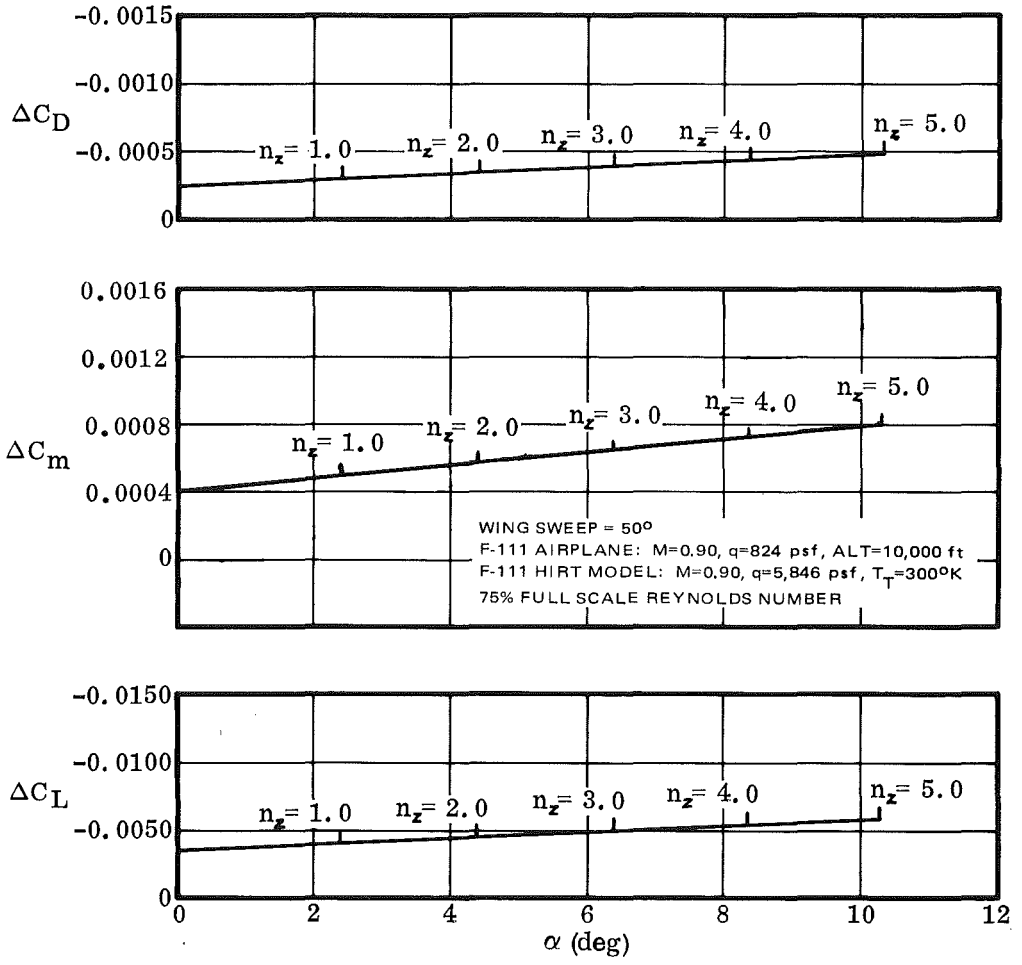

Figure 84. Estimated Effect of Angle of Attack on the Incremental Aerodynamic Data for the F-111 Study Configuration at Mach 0.90 and 75% Full Scale Reynolds Number

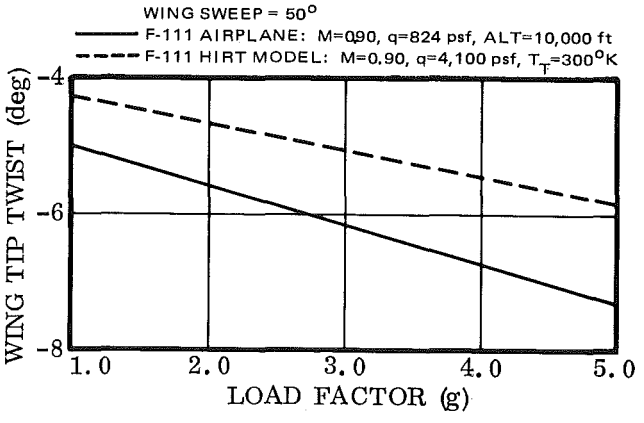

Figure 85. Effect of Load Factor on the F-111 Wing Tip Twist at Mach 0.90 and 50% Full Scale Reynolds Number

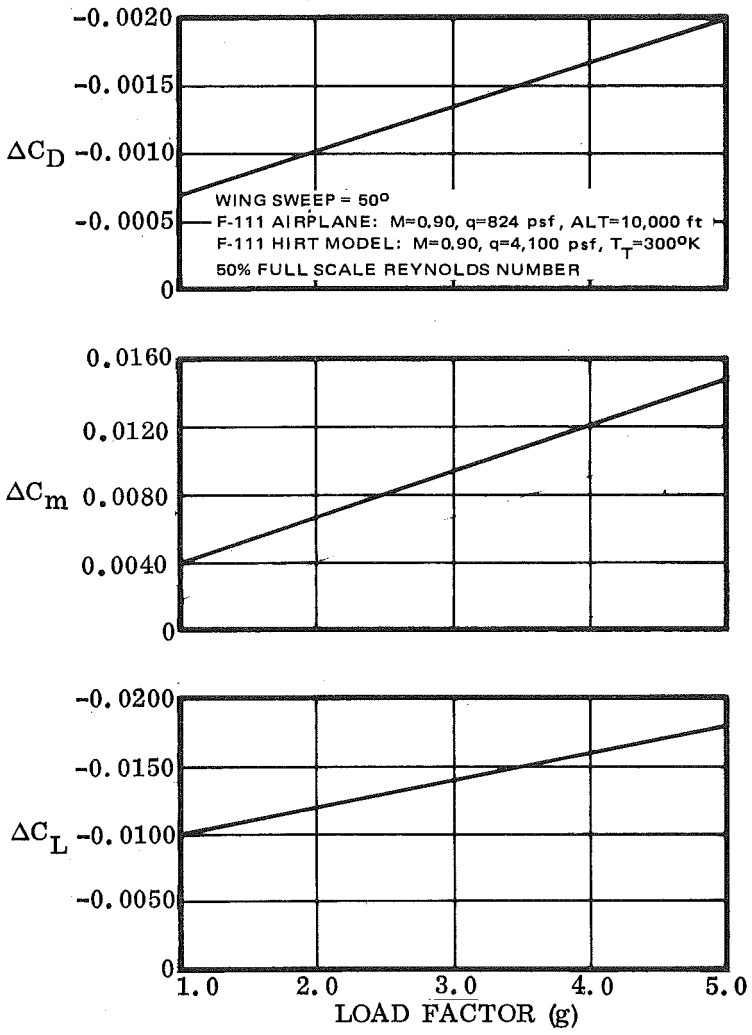

Figure 86. Estimated Effect of Load Factor on the Incremental Aerodynamic Data for the F-111 Study Configuration at Mach 0.90 and 50% Full Scale Reynolds Number

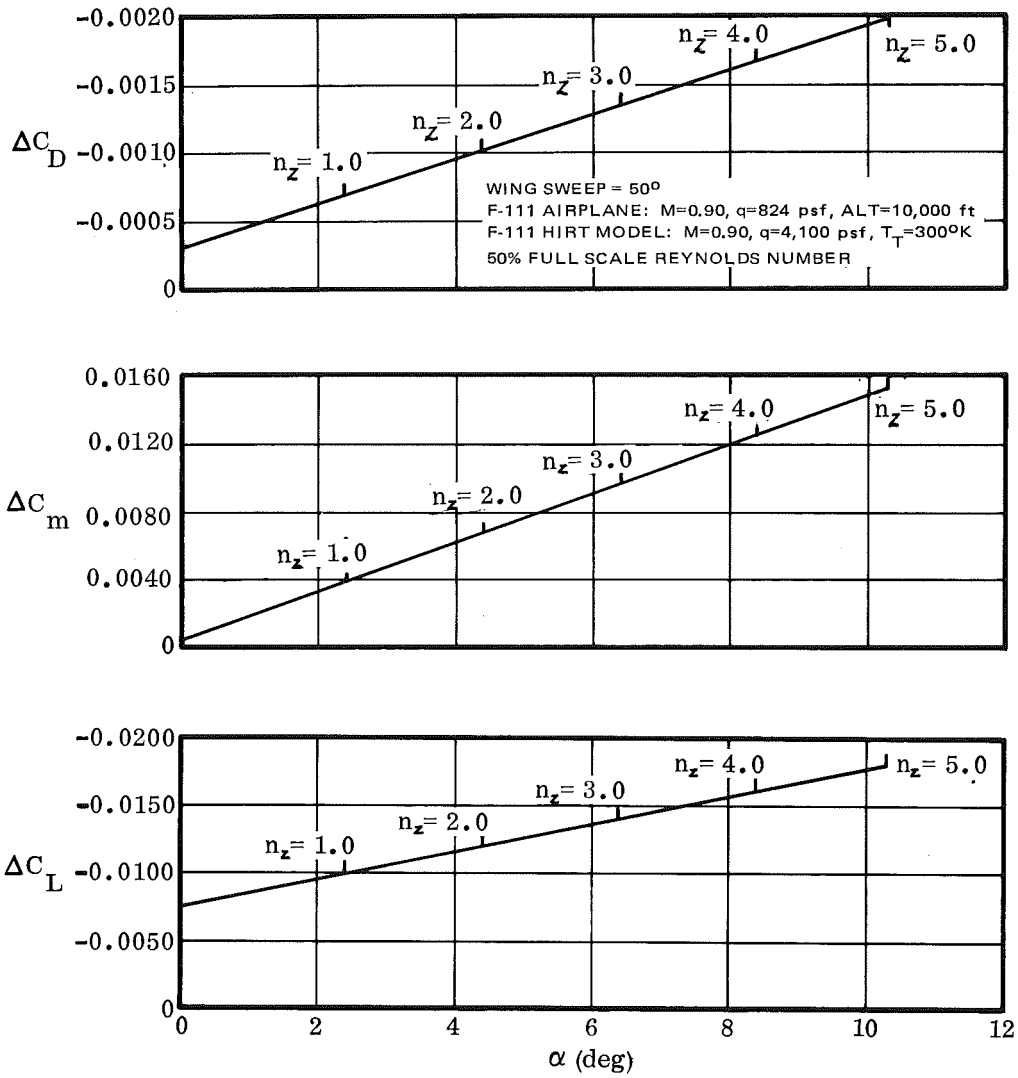

Figure 87. Estimated Effect of Angle of Attack on the Incremental Aerodynamic Data for the F-111 Study Configuration at Mach 0.90 and 50% Full Scale Reynolds Number

The tip twist for the 240° K tunnel temperature condition is presented in Figure 88. The incremental aerodynamic terms are presented in Figures 89 and 90. For this case, the reduction from ambient conditions at 300° K to the cold condition at 240° K results in aerodynamic corrections that are smaller than for tests performed at the 300° K. Thus, for the F-111 study configuration, a reduction in the tunnel temperature would result in improved model simulation in terms of the aerodynamic increments in lift, drag, and pitching moment without a reduction in the test Reynolds number.

The elastic twist data presented in this section, together with the cases at reduced test Reynolds number, indicate an incremental tip twist variation from 0.5 to 1.45 degrees at a load factor of 5.0. The proposed wing twist measuring system for the HIRT facility will definitely be of great importance to the interpretation of the test data over the ranges of variables discussed in Sections 5.4.1 through 5.4.3. The data indicate the sensitivity to the tunnel dynamic pressure due to a reduction in the test Reynolds number or the tunnel operating temperature.

5.4.5 Characteristics at Mach 0.90 and 30,000 Feet

A case at Mach 0.90 and 30,000 feet was analyzed for the F-111 study configuration. The tip twist is compared for the HIRT model and the airplane for flight load factors in Figure 91. The data indicate that the model wing twists 0.9 degree per g under the HIRT test conditions. The airplane wing twists 0.7 degree per g under flight conditions. The model wing twists 0.4 degree more than the airplane wing at a load factor of 2.0. The incremental aerodynamic terms are presented in Figure 92 as a function of load factor and in Figure 93 as a function of the model angle of attack.

5.4.6 Characteristics at Mach 0.90 and 20,000 Feet

A flight condition at Mach 0.90 and 20,000 feet was analyzed for the F-111 airplane and the HIRT model under the HIRT test conditions corresponding to full scale Reynolds number and Mach number. The tip twist is compared for the model and the airplane in Figure 94. The data indicate that the model wing twists 0.80 degree per g under the HIRT test conditions, while the airplane wing twists 0.53 degree per g under the flight conditions. The model wing twists 0.65 degree more than the airplane wing at a load factor of 4.0. The incremental aerodynamic terms that result from the differential tip twist are presented in Figure 95 as a function of the load factor. Figure 96 illustrates the incremental terms as a function of the model angle of attack.

5.4.7 Characteristics at Mach 0.70 and 10,000 Feet

A flight condition at Mach 0.70 and 10,000 feet was analyzed for the F-111 airplane and the model under the HIRT test conditions corresponding to full scale Reynolds number and Mach number. The tip twist is compared for the model and the airplane in Figure 97. The data indicate that the model wing twists 0.80 degree per g under the HIRT test conditions while the airplane wing twists 0.50 degree per g under flight

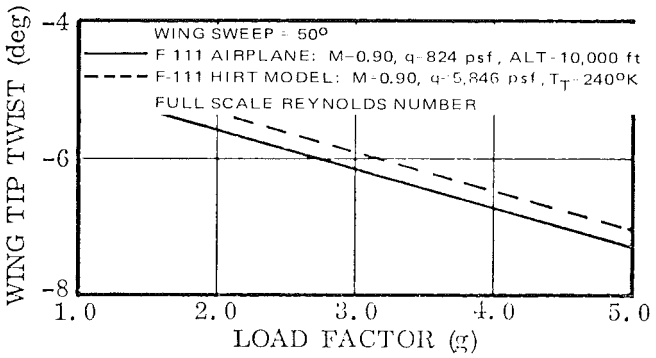

Figure 88. Effect of Load Factor on the F-111 Wing Tip Twist at Mach 0.90 and Full Scale Reynolds Number with the HIRT Tunnel Temperature Reduced to 240°K

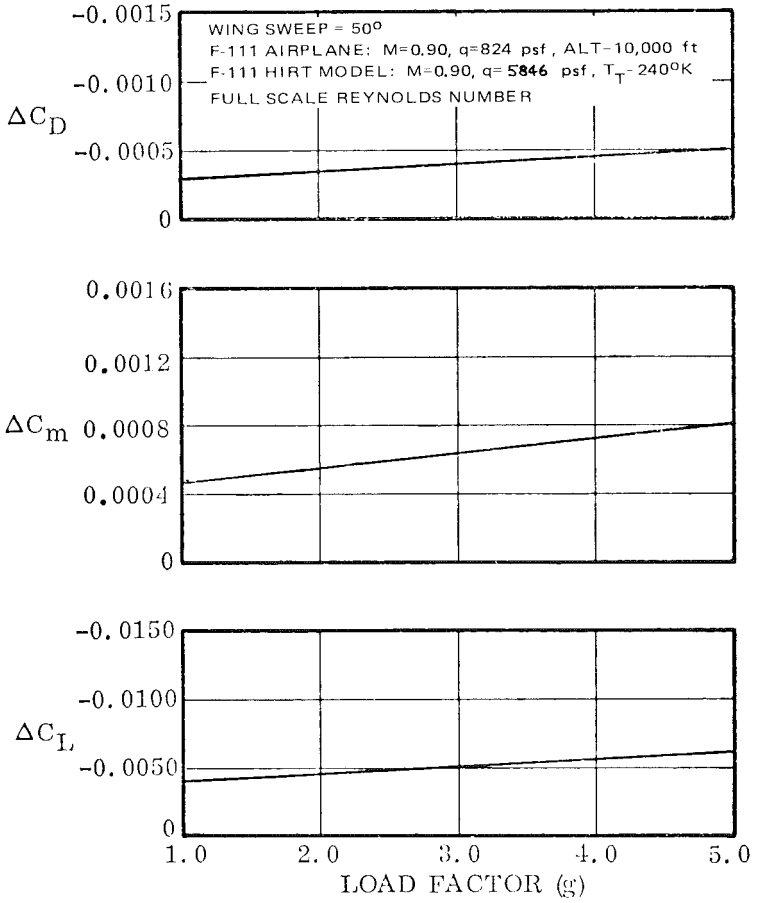

Figure 89. Estimated Effect of Load Factor on the Incremental Aerodynamic Data for the F-111 Study Configuration at Mach 0.90 and Full Scale Reynolds Number with the HIRT Tunnel Temperature Reduced to 240°K

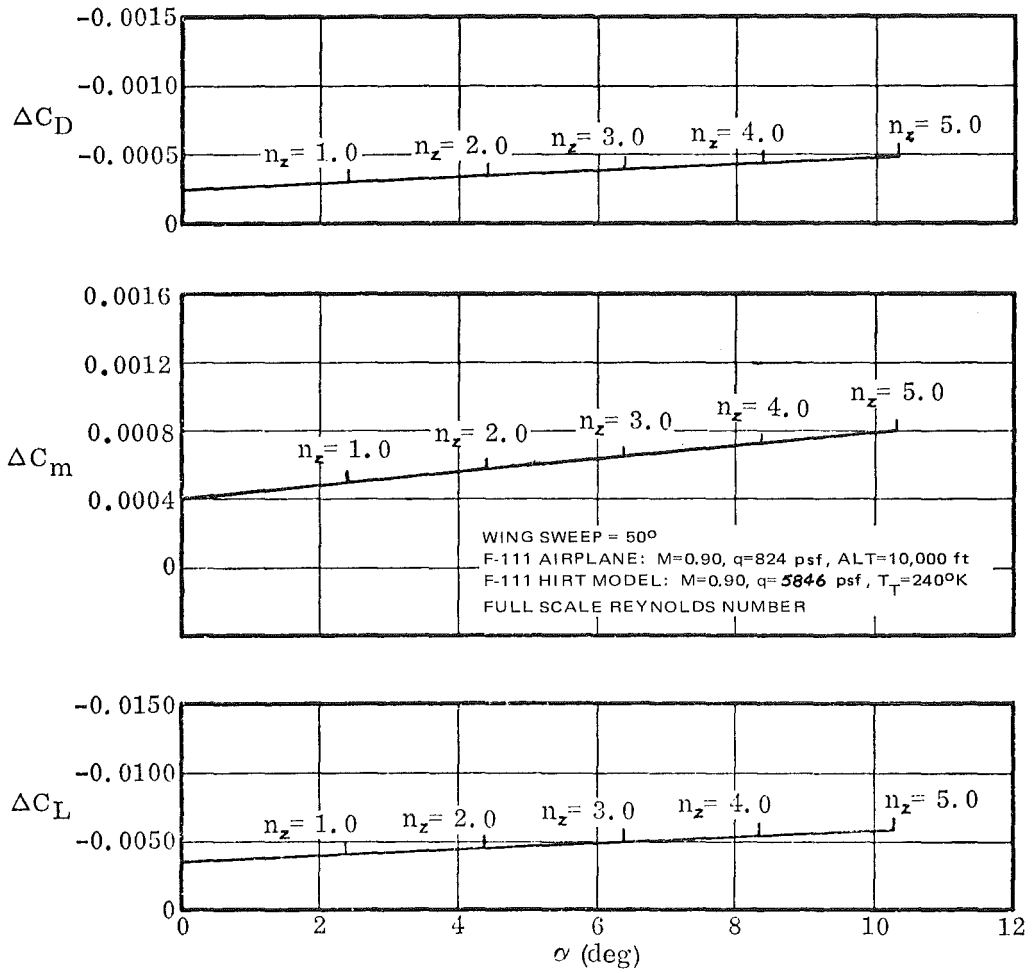

Figure 90. Estimated Effect of Angle of Attack on the Incremental Aerodynamic Data for the F-111 Study Configuration at Mach 0.90 and Full Scale Reynolds Number with the HIRT Tunnel Temperature Reduced to 240°K

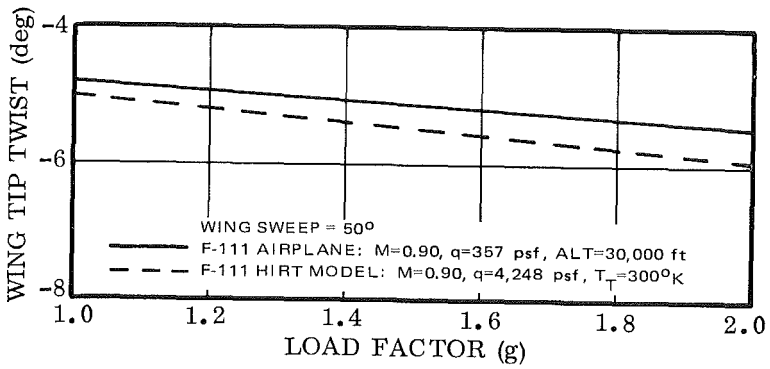

Figure 91. Effect of Load Factor on the F-111 Wing Tip Twist at Mach 0.90 and Full Scale Reynolds Number (Altitude = 30,000 ft)

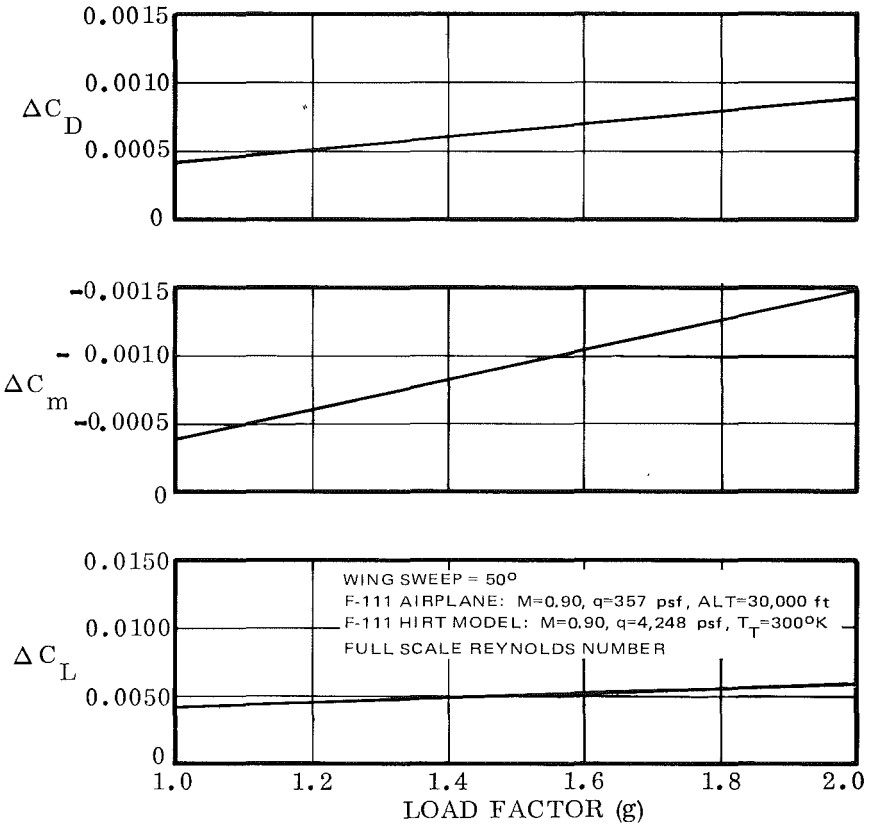

Figure 92. Estimated Effect of Load Factor on the Incremental Aerodynamic Data for the F-111 Study Configuration at Mach 0.90 and Full Scale Reynolds Number (Altitude = 30,000 ft)

conditions. The model wing twists 0.60 degree more than the airplane wing at a load factor of 3.4. The incremental aerodynamic terms that result from the differential tip twist are presented in Figure 98 as a function of the load factor. Figure 99 illustrates the incremental terms as a function of the model angle of attack.

5.4.8 Tip Twist Characteristics as a Function of Dynamic Pressure

Figure 100 illustrates the wing tip twist as a function of dynamic pressure for the F-111 HIRT model at a constant Mach number. For the condition of level flight, the wing tip twist remains relatively constant with increasing dynamic pressure. At load factors greater than 1.0, the tip twist decreases with increasing dynamic pressure.

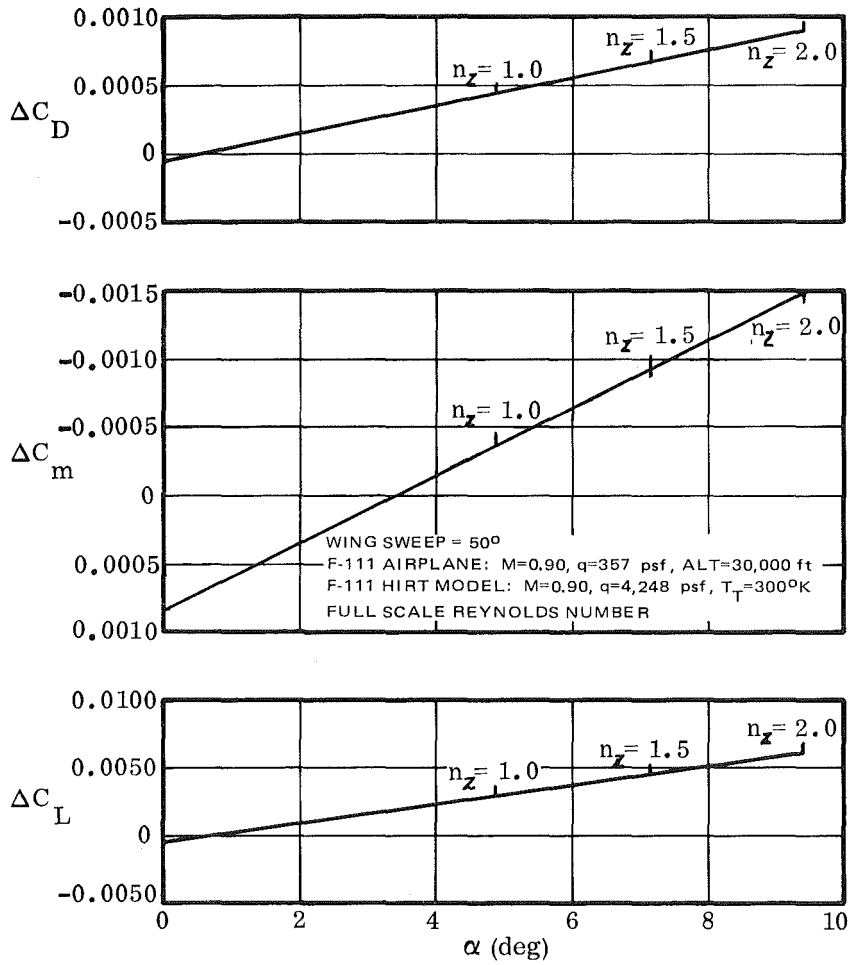

Figure 93. Estimated Effect of Angle of Attack on the Incremental Aerodynamic Data for the F-111 Study Configuration at Mach 0.90 and Full Scale Reynolds Number (Altitude = 30,000 ft)

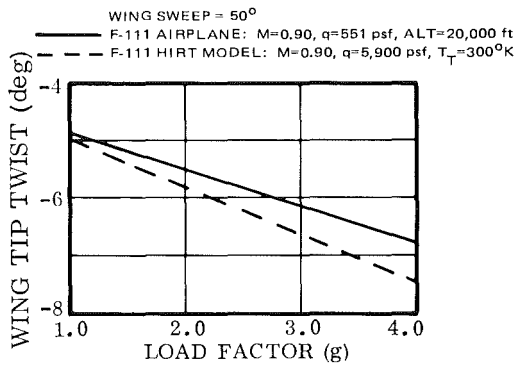

Figure 94. Effect of Load Factor on the F-111 Wing Tip Twist at Mach 0.90 and Full Scale Reynolds Number (Altitude = 20,000 ft)

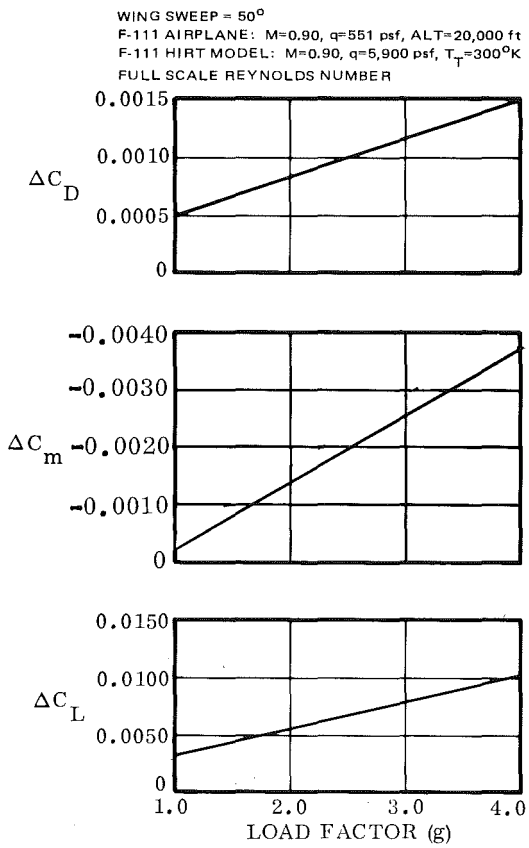

Figure 95. Estimated Effect of Load Factor on the Incremental Aerodynamic Data for the F-111 Study Configuration at Mach 0.90 and Full Scale Reynolds Number (Altitude = 20,000 ft)

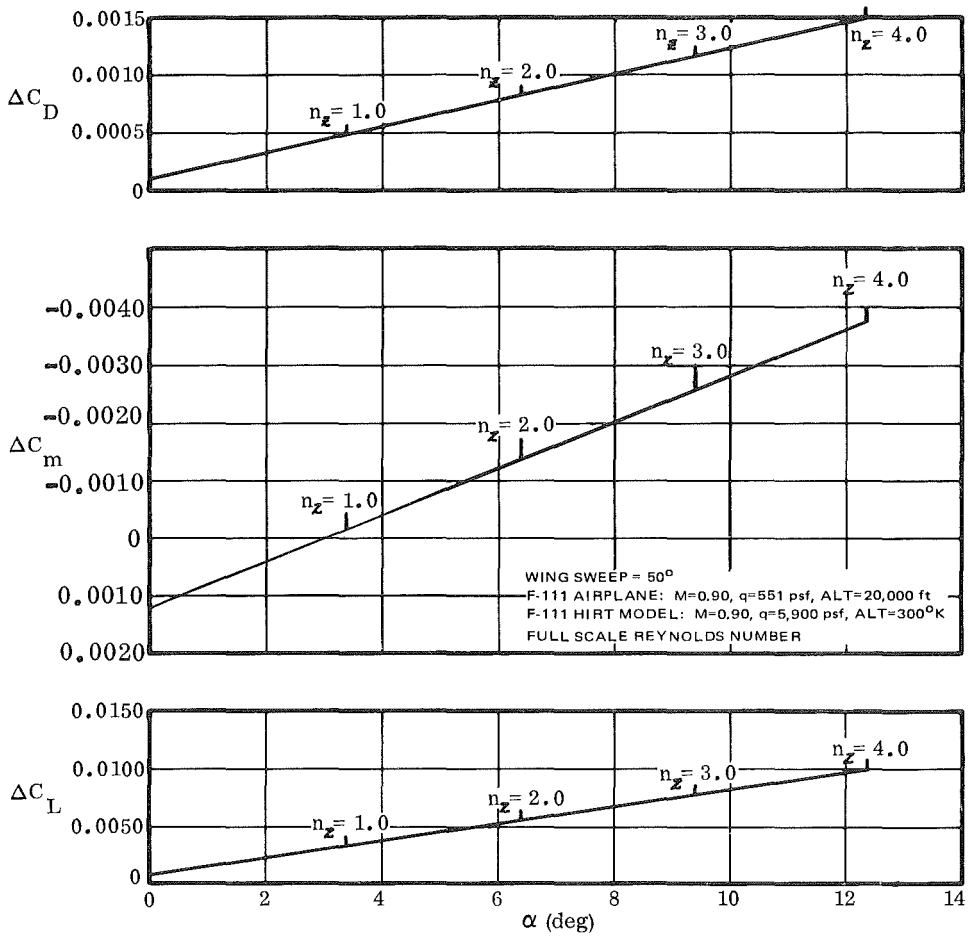

Figure 96. Effect of Angle of Attack on the Incremental Aerodynamic Data for the F-111 Study Configuration at Mach 0.90 and Full Scale Reynolds Number (Altitude = 20,000 ft)

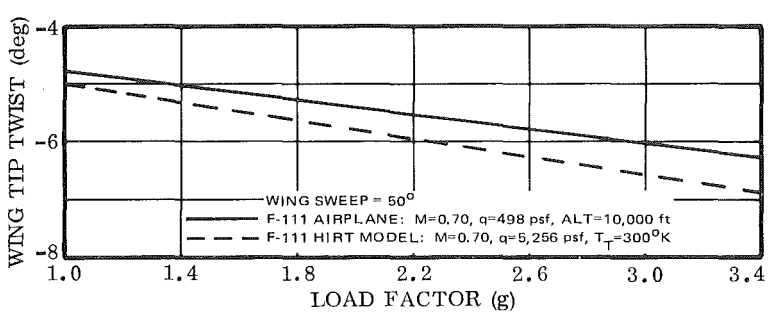

Figure 97. Effect of Load Factor on the F-111 Wing Tip Twist at Mach 0.70 and Full Scale Reynolds Number (Altitude = 10,000 ft)

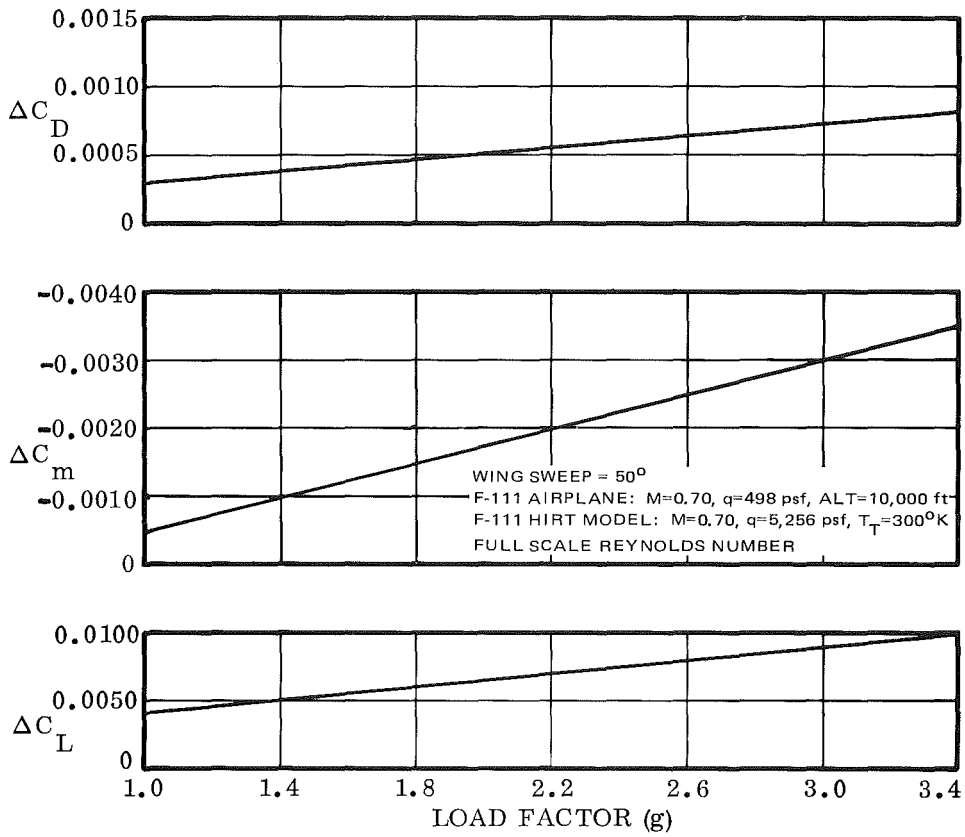

Figure 98. Estimated Effect of Load Factor on the Incremental Aerodynamic Data for the F-111 Study Configuration at Mach 0.70 and Full Scale Reynolds Number (Altitude = 10,000 ft)

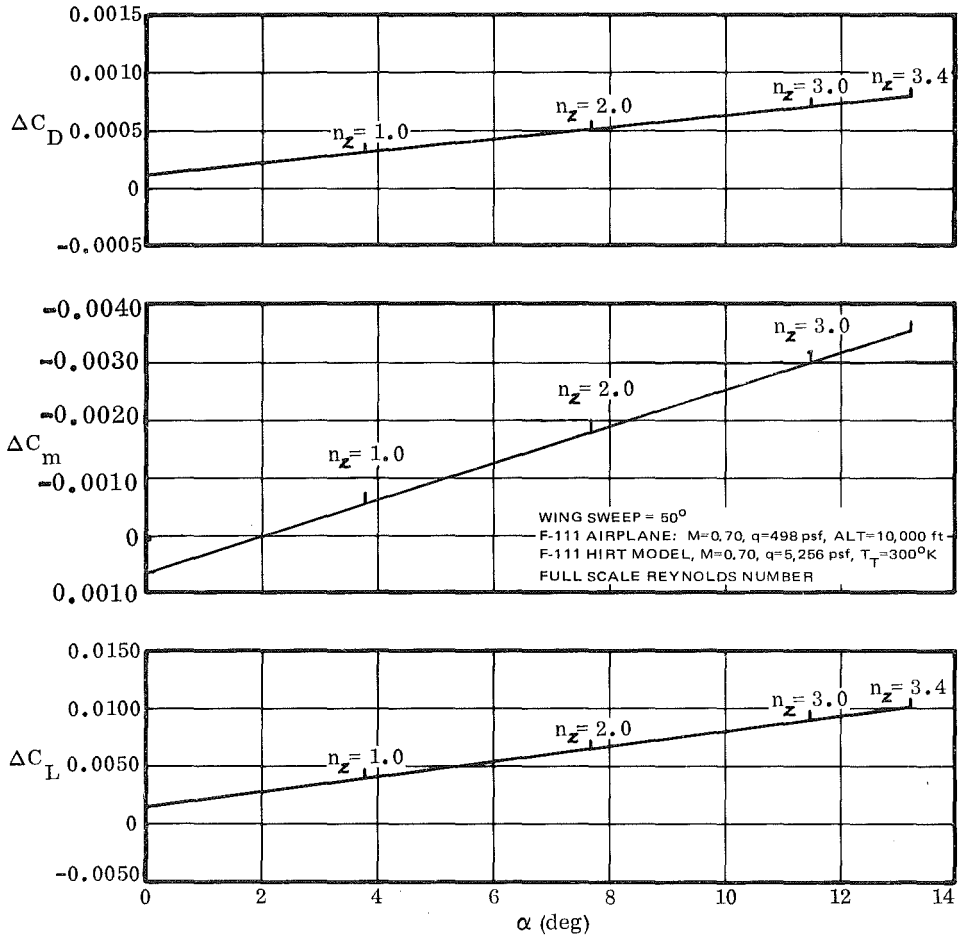

Figure 99. Estimated Effect of Angle of Attack on the Incremental Aerodynamic Data for the F-111 Study Configuration at Mach 0.70 and Full Scale Reynolds Number (Altitude = 10,000 ft)

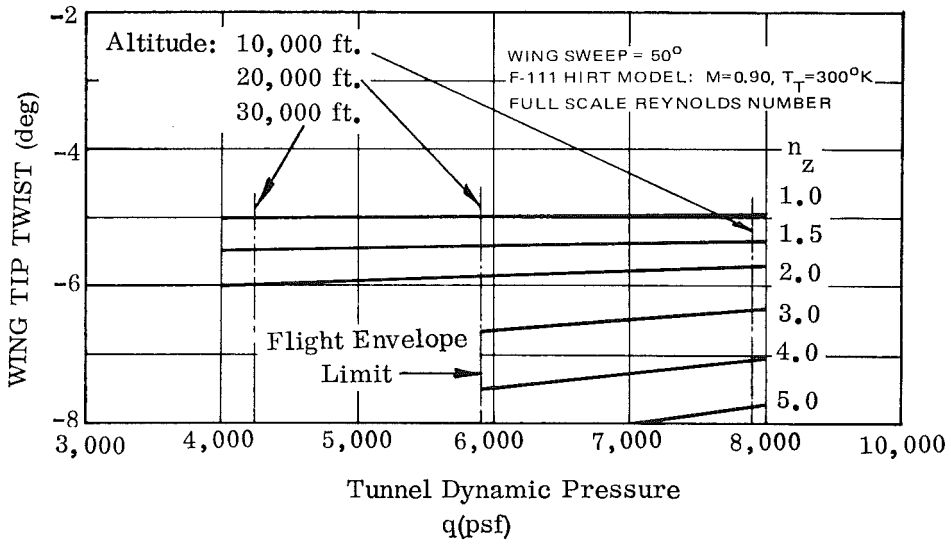

Figure 100. Effect of Tunnel Dynamic Pressure on the F-111 HIRT Model Wing Tip Twist at Mach 0.90 and Full Scale Reynolds Number.

5.4.9 Summary

The F-111 model used in this study was considered to be designed as an all steel model with solid steel wings. The aeroelastic analysis of the wing resulted in greater model wing twist and vertical deflection than the airplane wing at equivalent Reynolds number conditions as shown in Figures 79 and 40. In the aerodynamic analysis, vertical deflection of the wing was not considered directly but was considered insofar as including the primary effect of vertical deflection on twist. The further effect of a nonplanar wing on aerodynamic characteristics was considered to be very small. The deformation differences between the model wing and the airplane do not result in significant differences in the estimated model and airplane aerodynamics. For instance, at the design cruise condition (M=0.90, Alt. =10,000 ft) and at a high load factor (5.0) the drag of the model was 0.0010 less than the airplane. For this test condition, the model force balance accuracy in drag was considered to be about ±0.0006. Thus, as was stated for the ATT model, the balance accuracy is of as much concern as the aeroelastic effects on the aerodynamics data.

The effect of mismatching test Reynolds number and reduced tunnel temperatures were analyzed for the F-111 model. The data at a level of 75% full scale Reynolds number as shown in Figures 82, 83 and 84 decreased the model/airplane deformation differences and also the incremental aerodynamic terms. For a 50% full scale Reynolds number test condition, the data as shown in Figure 85, 86 and 87 indicates increased model/airplane deformation differences and increased incremental aerodynamic terms. Thus, only slight mismatching of Reynolds number will bring the model/airplane deformations into agreement along with the aerodynamic terms.

The effect of reducing tunnel storage temperature from 300° K to 240° K was analyzed for the F-111 model. The data indicates smaller model/airplane deformation and aerodynamic differences can be achieved through the tunnel storage temperature control. For this configuration, where the model deformations are greater than the airplane deformations at equivalent Reynolds number conditions, the control of tunnel temperature may be the only method of improving the model/airplane deformations and thus the aerodynamic terms.

SECTION VI

CONCLUSIONS

This study indicates that for the two study configurations, a model wing jig twist can be selected such that the elastic deformation of the model wing will be similar to the airplane for a wide range of conditions within the flight envelope. The resulting aeroelastic differences (i.e. twist) between the model and the airplane at an equivalent Reynolds number will not result in significant effects on the aerodynamic test data.

The HIRT facility will provide more accurate test data because of the model flexibility than current "rigid" model test techniques will provide. The proposed model deformation measuring system will be essential since accurate measurement of the model deflection will provide information for correct interpretation of the test data.

The study further indicated that three options are available to produce close similarity of the model/airplane wing deformation over a broad range of operating conditions. These include mismatching Reynolds number, variation in the tunnel operating temperature, and construction of more than one wing. For configurations where model aeroelastic deformations are excessive, dynamic pressure reduction through a reduction in the test Reynolds number reduces the model wing deformations so that geometric similarity between the model and airplane may be attained. Reduction in the tunnel temperature such as from 300° K to 240° K, reduces the model wing deformations so that geometric model/airplane similarity is attained at equivalent Reynolds numbers. For cases where model aeroelastic deformations are excessive after reduction in tunnel dynamic pressure conditions, the fabrication of an additional wing may be required. The additional wing with a new jig twist distribution would allow improvement in the model/airplane similitude for these conditions.

Finally, based on the HIRT balance study, (Reference 5), the balance accuracy will be as significant as the estimated aerodynamic differences due to aeroelastic differences between a model and the airplane.

REFERENCES

1. J. D. Whitfield, C. J. Schueler, and R. F. Starr, ARO, Inc., "High Reynolds Number Transonic Wind Tunnels — Blowdown or Ludwieg Tube", AGARD-CP-83 -71, April 1971.

2. R. G. Roepke, "The High Reynolds Number Transonic Wind Tunnel HIRT Proposal as Part of the National Aeronautical Facilities Program,"AIAA Paper No. 72-1035, September 1972.

3. W. K. Alexander, S. A. Griffin and R. L. Holt, General Dynamics Convair Aerospace Division, "Wind Tunnel Model Parametric Study for Use in the Proposed 8 Ft × 10 Ft High Reynolds Number Transonic Wind Tunnel (HIRT) at Arnold Engineering Development Center," AEDC Report TR-73-47, March 1973.

4. W. K. Alexander, A. E. Brady and S. A. Griffin, "Study of Multipiece Flow-through Wind Tunnel Model for HIRT" AEDC Report TR-75-60, July 1974.

5. M. L. Kuszewski, P. J. Mole and S. A. Griffin, "Study of Six-Component Internal Strain Gage Balances for Use in the HIRT Facility," AEDC Report TR-75-63, July 1974.

6. J. Picklesimer, and W. H. Lowe, "A Study of Expected Precision In the Proposed AEDC HIRT Facility," AEDC Report TR-75-61, July 1974.

7. "Application of Lifting Line Theory to Aircraft Aeroelastic Loads Analysis," General Dynamics Convair Report No. GDC-ERR-AN-1178, February 1968.

8. W. L. Gray and K. M. Schenk, Boeing Aircraft Co., "A Method for Calculating the Subsonic Steady-State Loading on an Airplane with a Wing of Arbitrary Planform and Stiffness," NACA TN 3030, December 1953.

9. L. H. Schindel, "An Evaluation of Procedures for Calculating Aerodynamic Loads," AFFDL-TR-65-18, May 1965.

10. C. J. Borland, "Methods of Calculating Aerodynamic Loads on Aircraft Structures," AFFDL-TR-66-37, August 1966.

11. J. A. Blackwell, Jr., "A Finite Stop Method for Calculation of Theoretical Load Distribution for Arbitrary Lifting — Surface Arrangements of Subsonic Speeds," NASA TND-5335, 1969.

12. "USAF Stability and Control DATCOM," AFFDL.

13. "Curves of Flow Properties for HIRT Operation," USAF, June 1972.

14. "F-111 Wing Aeroelastic Analysis for the Safe Life Steel Wing Carry-Through-Box," General Dynamics Convair Aerospace Division, Report No. FZS-12-1030, January 1970.

15. "F-111C Wing Aeroelastic Analysis for the Safe Life Steel Wing Carry-Through-Box," General Dynamics Convair Aerospace Division, Report No. FZS-12-5003, April 1971.

16. "F-111 A/B Basic Data Report," General Dynamic Convair Aerospace Division, Report No. FZS-12-157, January 1966.

17. "Computer Program Details of Aeromodule Version III: Lift and Drag Analysis of Aerodynamic Configurations," General Dynamics Convair Aerospace Division, Report No. MR-A-2089, December 1970.

18. B. G. Gilman and K. P. Burdges, "Rapid Estimation of Wing Aerodynamic Characteristics for Minimum Induced Drag," Journal of Aircraft, Vol. 4, No. 6, November 1969.

APPENDIX A

A STUDY OF HIRT MODEL AEROELASTIC CHARACTERISTICS IN REFERENCE TO THE AEROELASTIC NATURE OF AN AIRPLANE COMPOSITE WING

The main part of this study was concerned with determining and assessing the differences in model/airplane wing deformations and the effects of these differences on the longitudinal aerodynamic characteristics. Both study configurations were considered to have conventional aluminum structures for the flight article, while the wind tunnel models were constructed from steel.

Future aircraft designers are likely to depart from total aluminum construction and make use of composite materials such as graphite/epoxy or boron/aluminum. In this appendix, the representation of a full-scale composite wing by a steel wind tunnel model wing is analyzed to determine the wing deformations under load and assess the effect of these differences on the aerodynamics. The analysis has been performed for the F-111 configuration with the wing designed to an expected value of structural properties for an anisotropic (composite) structure. Section A1 of this appendix describes the aeroelastic characteristics of the selected composite wing. Section A2 describes the resulting incremental aerodynamic characteristics of the study configuration. Section A3 describes the analytical results for simulating a composite wing with a solid steel model wing. Section A4 states conclusions of this study.

A1. AEROELASTIC CHARACTERISTICS OF A COMPOSITE WING FOR THE F-111 AIRPLANE

Aeroelastic deformations of the F-111 wing were analyzed for one flight condition using the same approach and methods previously identified in this report. The wing was analyzed with assumed values of structural properties, EI and GJ, for an anisotropic structure. Anisotropicity causes the wing to be more flexible in accommodating all of the applied loads but leads to an increase in the complexity of the structural wing design due to the large combinations of ply orientation. Ply orientation can be selected to produce positive or negative elastic wing twist in contrast with a wing constructed from isotropic materials. For this analysis, three locations of the elastic axis have been selected and examined.

Table A-1 depicts the structural properties, E and G, for steel, aluminum, boron/aluminum and graphite/epoxy materials with crossply percentages ranging from 20 to 100 percent for the graphite/epoxy.

Figure A-1 illustrates the E/G ratio graphically for the percentage of crossplies in a graphite/epoxy structure. Figure A-2 illustrates several airplane wing stiffness ratios that have been fabricated or proposed (Reference 1). It is expected that future wing designs will tend toward higher E/G ratios since anisotropic structures may allow a design of the structure to obtain the best compromise of the flutter and structural divergence characteristics with a low structural weight. The advanced fighter attack

Table A-1. Material Structural Properties

Material	E (millions of psi)	G (millions of psi)	E/G
Aluminum	10.5	4.0	2.62
Steel	29.5	11.0	2.63
Boron/Aluminum	32.0	8.0	4.00
Graphite/Epoxy			
20% Crossplies	14.0	1.50	9.33
38% Crossplies	11.8	2.34	5.05
67% Crossplies	7.7	2.90	2.66
80% Crossplies	5.5	4.00	1.37
100% Crossplies	1.9	5.30	0.36

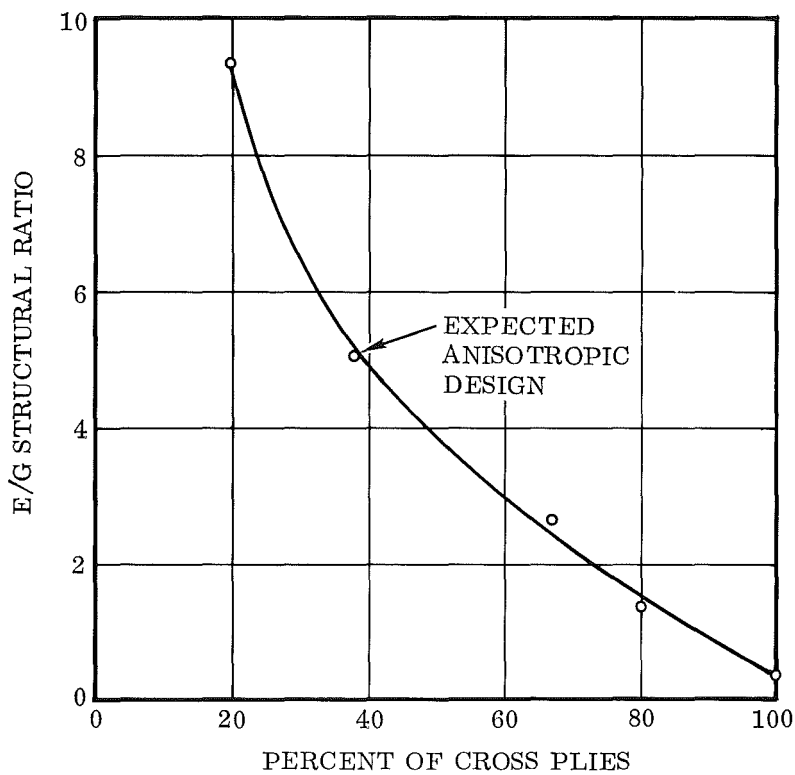

Figure A-1. Characteristics of Graphite/Epoxy Structure

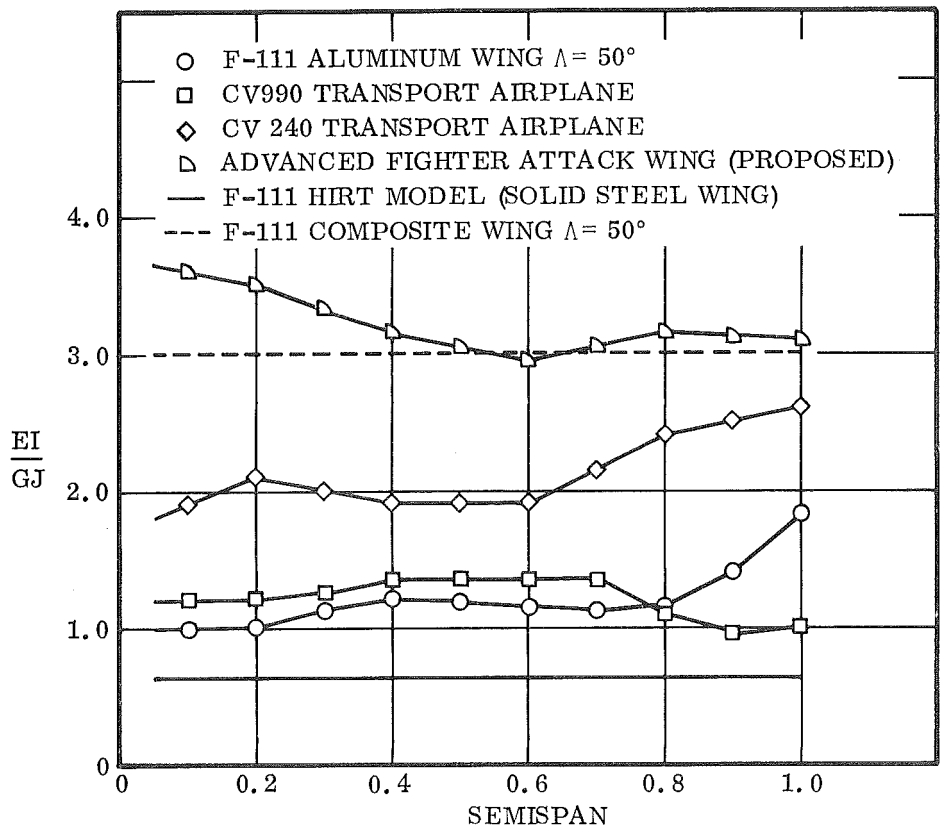

Figure A-2. Stiffness Ratio Characteristics of Existing Airplanes and Proposed Designs

wing characteristics (Reference 1) illustrated in Figure A-2 have a nominal stiffness ratio of 3.0. This level of nominal stiffness was selected to represent the composite wing for this study. The stiffness ratio of 3.0 corresponds to a graphite/epoxy structure with 38 percent of the laminates crossplied relative to a 0° axis located along the wing center spar. The crossplied laminates may be adjusted to any orientation, such as ±45° or ±60° relative to the 0° axis. By appropriate adjustment of the proportions and orientation, virtually any design requirement can be met. The E/G ratio for the graphite/epoxy was about 5.0 and the I/J ratio for the airplane wing was about 0.6, which resulted in the stiffness ratio (EI/GJ) ratio of 3.0.

The HIRT wind tunnel model wing was jig twisted and analyzed in Section IV of this report, based on the design twist and isotropic characteristics of the F-111 aluminum wing. For this effort, the model wing twist was not changed. The composite wing jig twist distributions for three locations of the elastic axis was determined by holding the loaded wing twist distribution identical to the aluminum wing for level flight at Mach 0.90 and at an altitude of 10,000 feet. The resulting wing jig twist distributions are shown in Figure A-3. The final wing twist distribution for the Mach 0.90 level flight condition is presented in Figure A-4.

F-111 AIRPLANE: WING SWEEP = 50°

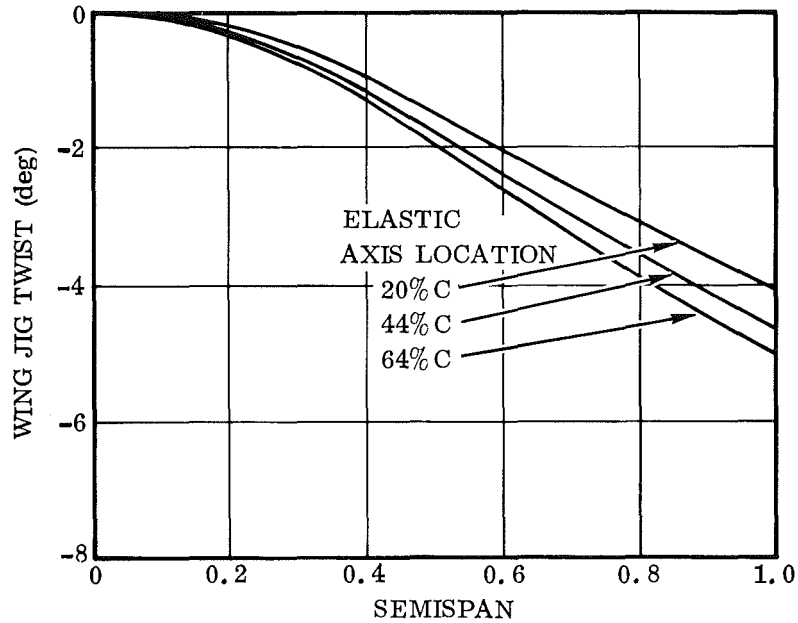

Figure A-3. Wing Jig Twist Distribution for the F-111 Composite Wings

F-111 AIRPLANE: M = 0.90, q = 824 PSF, ALT = 10,000 FT
WING SWEEP = 50°

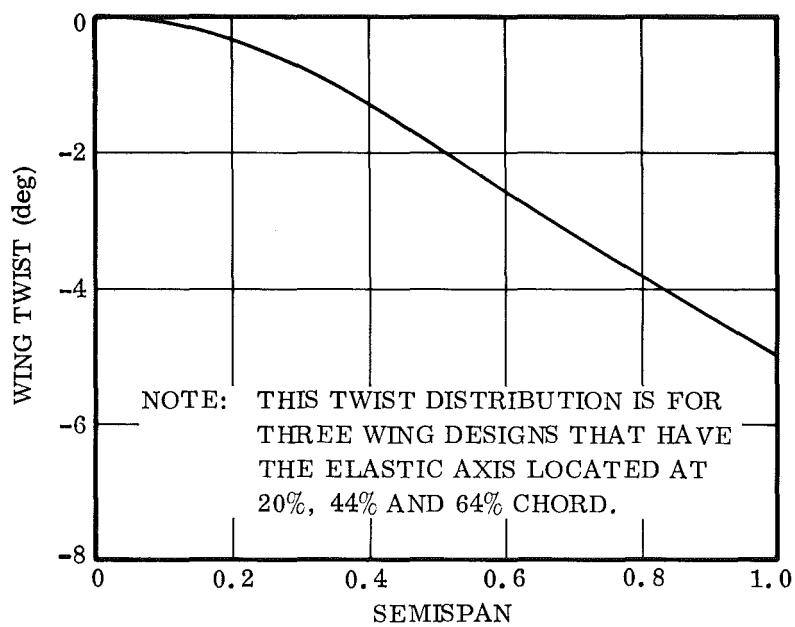

Figure A-4. Wing Twist Distribution for the F-111 Airplane with a Composite Wing in Level Flight at Mach 0.90

Figure A-5 illustrates the shear load distribution on the composite wings for the elastic axis locations of 20, 44, and 64 percent of the wing chord at load factors of 1.0 and 5.0. Movement of the elastic axis as the crossply orientation is changed will cause the spanwise distribution of shear to increase with increasing load factor. The shear load distribution for the three elastic axis locations at the level flight Mach 0.90 condition does not change, because the sum of the elastic twist and the wing jig twist is identical for each elastic axis location as shown in Figure A-4.

The effect of the elastic axis location on the wing bending moment and pitching torque perpendicular and parallel to the elastic axis, respectively, is presented in Figure A-6.

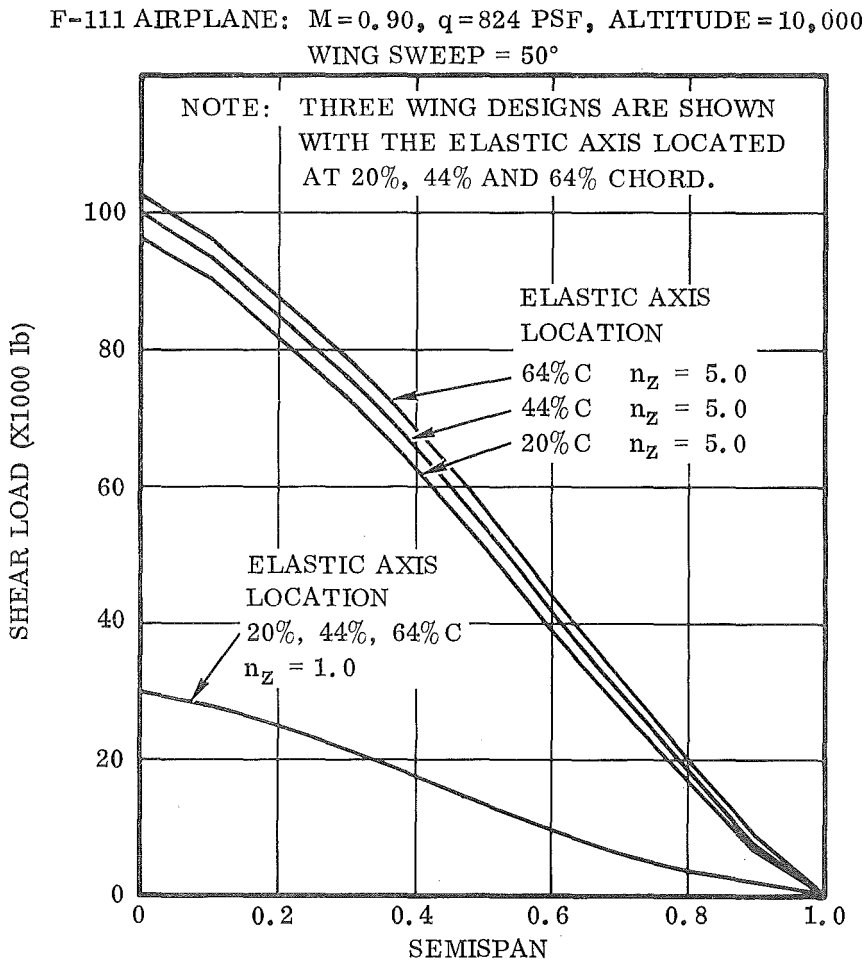

Figure A-5. Shear Load Distribution for the F-111 Airplane with a Composite Wing at Load Factors of 1.0 and 5.0

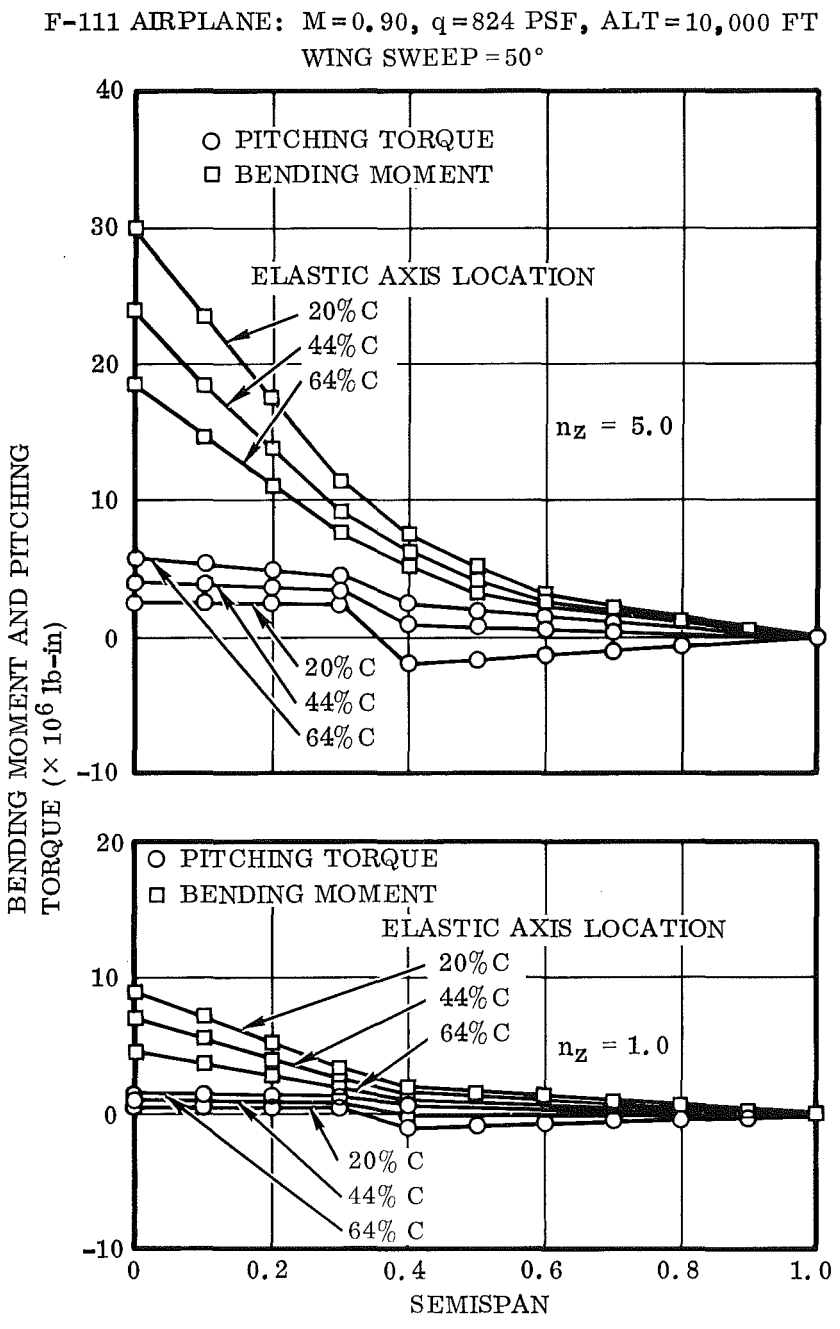

Figure A-6. Composite Wing Bending Moment and Pitching Torque for the F-111 Wing at Load Factors of 1.0 and 5.0

The distribution of span loading over the wing is presented in Figure A-7 for Mach 0.90, 10,000 feet and load factors of 1.0 and 5.0. For the level flight condition, the span load is identical for the wings with the elastic axis located at the 20, 44, and 64 percent chordline. For increased load factors, the aft movement of the elastic axis leads to slightly higher loading conditions near the tip.

The wing bending moment of inertia and the wing polar moment of inertia are presented in Figure A-8 as a function of the wing semispan. The ratio of bending moment of inertia to the polar moment of inertia was 0.60 along the wing semispan.

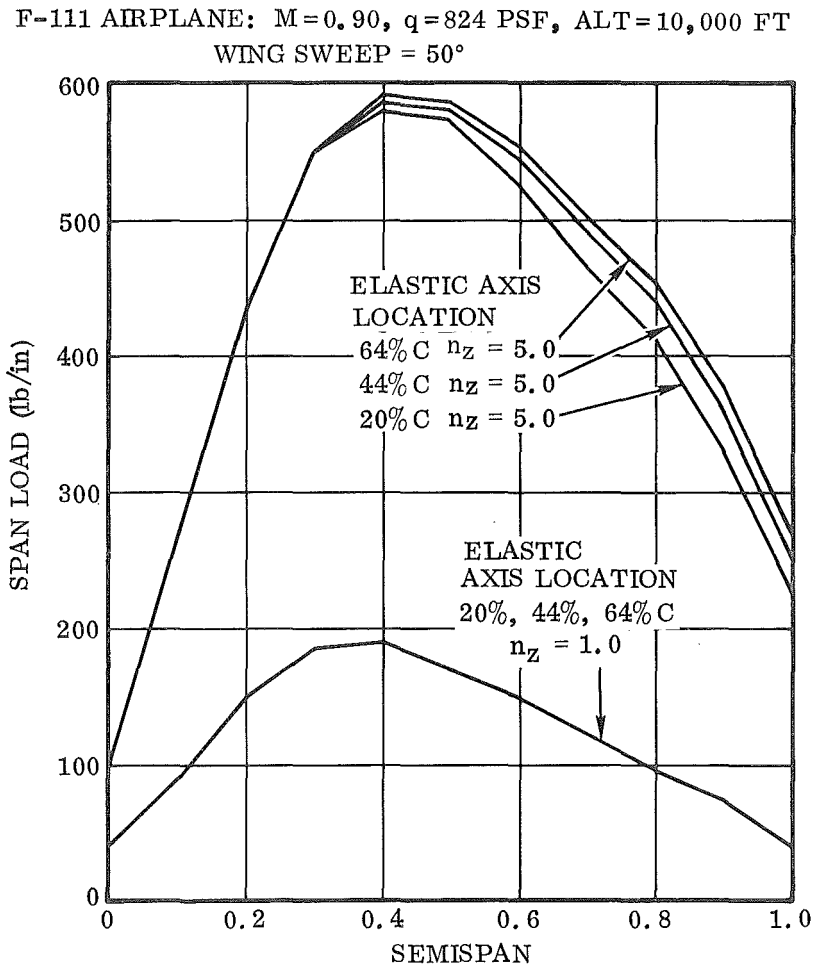

Figure A-7. Span Load Distribution Over the F-111 Wing with a Composite Wing at Load Factors of 1.0 and 5.0

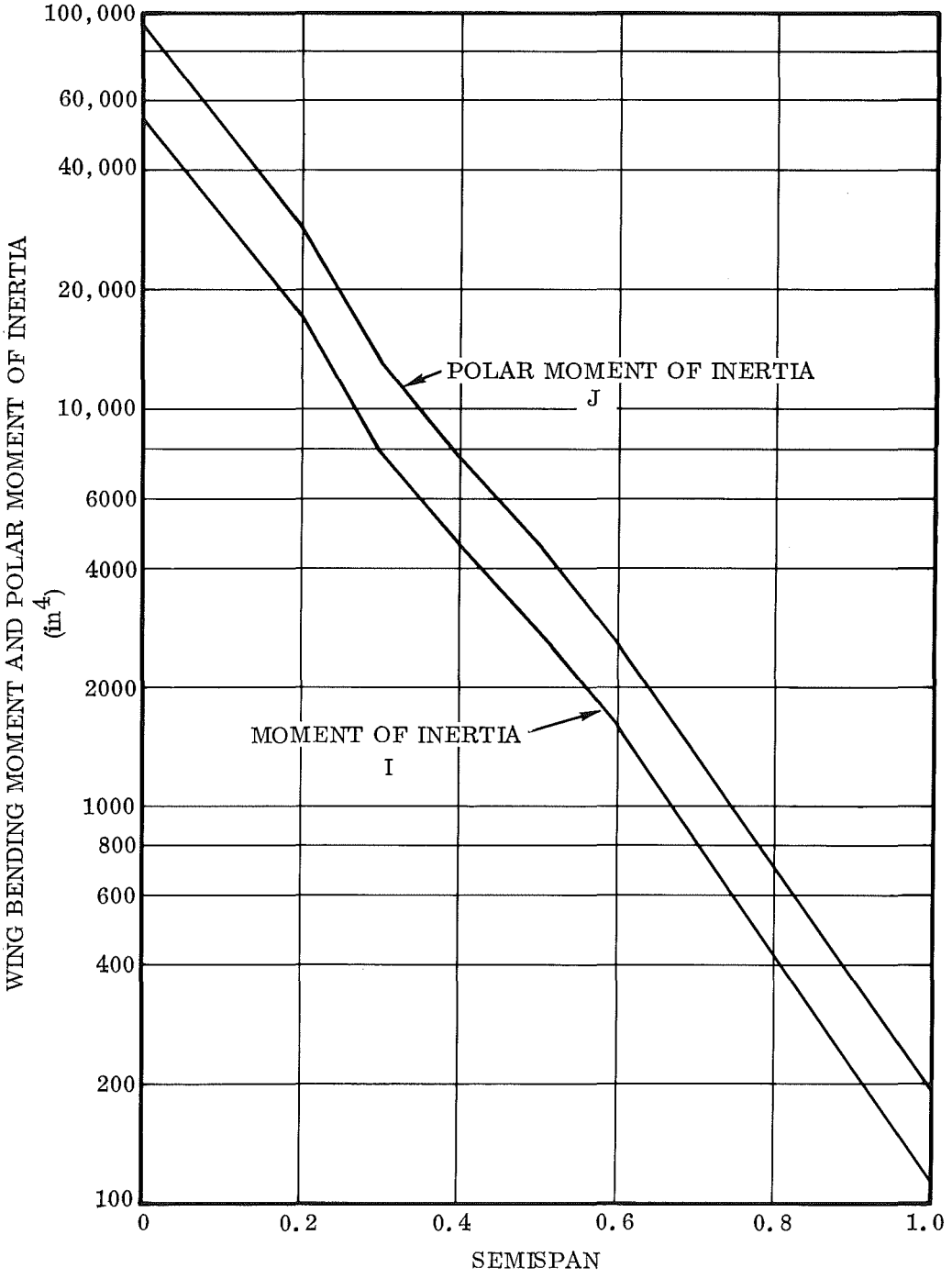

Figure A-8. Wing Bending Moment of Inertia and Polar Moment of Inertia for the F-111 Composite Wings

The elastic wing twist for the composite wing becomes more positive as the elastic axis is moved aft. Wing section pitching moment does not change with the location of the elastic axis; however, the aerodynamic loading due to angle of attack induces a positive elastic twist increment as the elastic axis moves aft, as shown in Figure A-9.

Figure A-10 illustrates the comparison of an aluminum and graphite/epoxy wing elastic twist distribution for the F-111 airplane at Mach 0.90. The elastic axis was located at the 44% chordline of the wings. For a constant load factor, the effect of increasing the EI/GJ ratio of the wing structure leads to reduced wing twist due to the increased bending strength of the wing.

Vertical deflection of the composite wing is affected by the location of the elastic axis. Figure A-11 illustrates the nondimensional vertical deflection of the three composite wings at load factors of 1.0 and 5.0 for a flight condition of Mach 0.90. The wing deflection measured along the elastic axis, which has been nondimensionalized with respect to the wing mean aerodynamic chord, decreases with an aft movement of the elastic axis.

A.2 LONGITUDINAL AEROELASTIC AERODYNAMIC CHARACTERISTICS OF THE F-111 AIRPLANE WITH A COMPOSITE WING

The aerodynamic methods used to evaluate the aerodynamic consequences of the aeroelastic differences between the airplane with a composite wing and the solid steel HIRT model are the same as used in the preceding analysis of this report. The assumption of a linear twist distribution was made to be consistent with the aerodynamic methods.

For this effort, a composite F-111 wing has been analyzed and compared with the solid steel HIRT model wing. Three locations of the elastic axis were evaluated. Figure A-12 illustrates the effect of load factor on wing tip twist for the composite wings, the aluminum wing, and the steel model wing. For the composite wing with the elastic axis located at the 20% chordline, the tip twist is almost identical to the aluminum wing. For the 44% chord and 64% chord locations of the elastic axis, the maneuvering elastic twist is much smaller in magnitude than that of the aluminum wing. For the 64% chord elastic axis location, the maneuvering elastic twist is positive with increasing load factor; this can also be seen from Figure A-10. From Figure A-12, the wing tip twist for a load factor of 5.0 results in a difference of about 3.5 degrees between the composite wing under flight conditions at Mach 0.90 and the solid steel wing of the HIRT model under equivalent Reynolds number testing.

For a composite wing with the elastic axis located at the 20% chordline, the differential tip twist between the model and the airplane results in the aerodynamic differences presented in Figure A-13. At a one-g flight condition, the model wing and airplane were matched at a lift coefficient of about 0.16. Since the model wing, under equivalent Reynolds number testing, twists more under the increased load factors than the

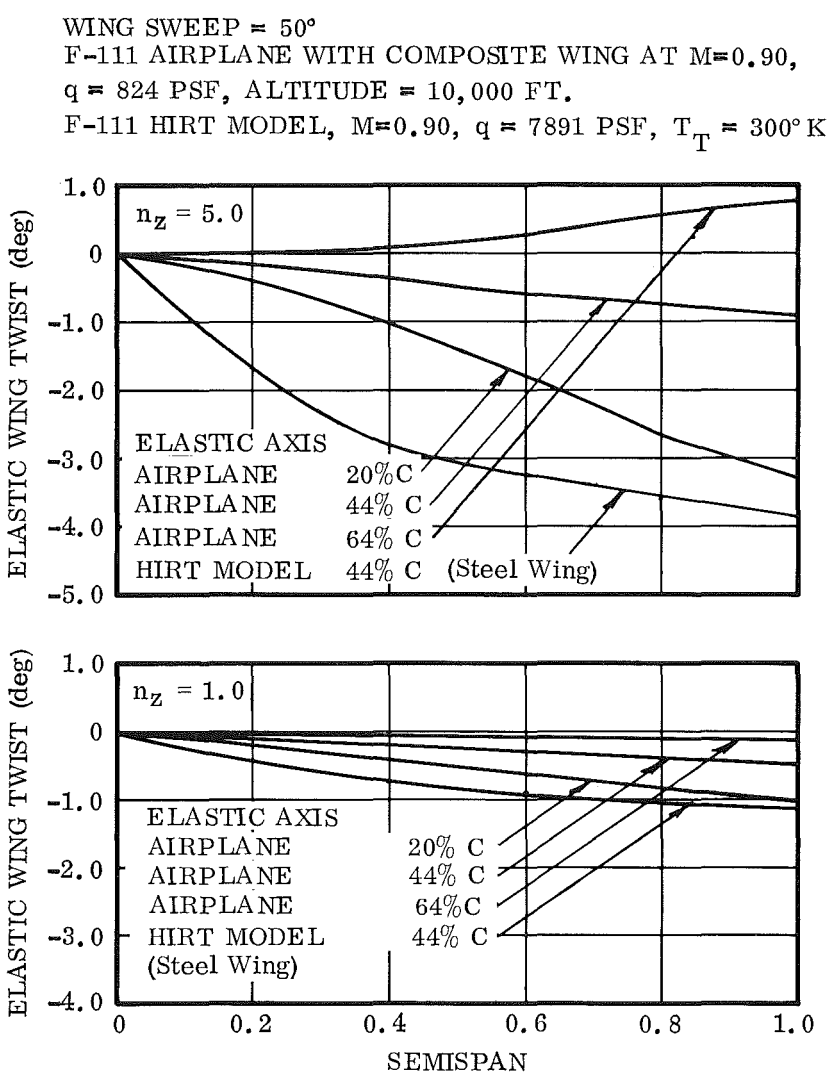

Figure A-9. Elastic Wing Twist for the F-111 Composite Wings at Load Factors of 1.0 and 5.0

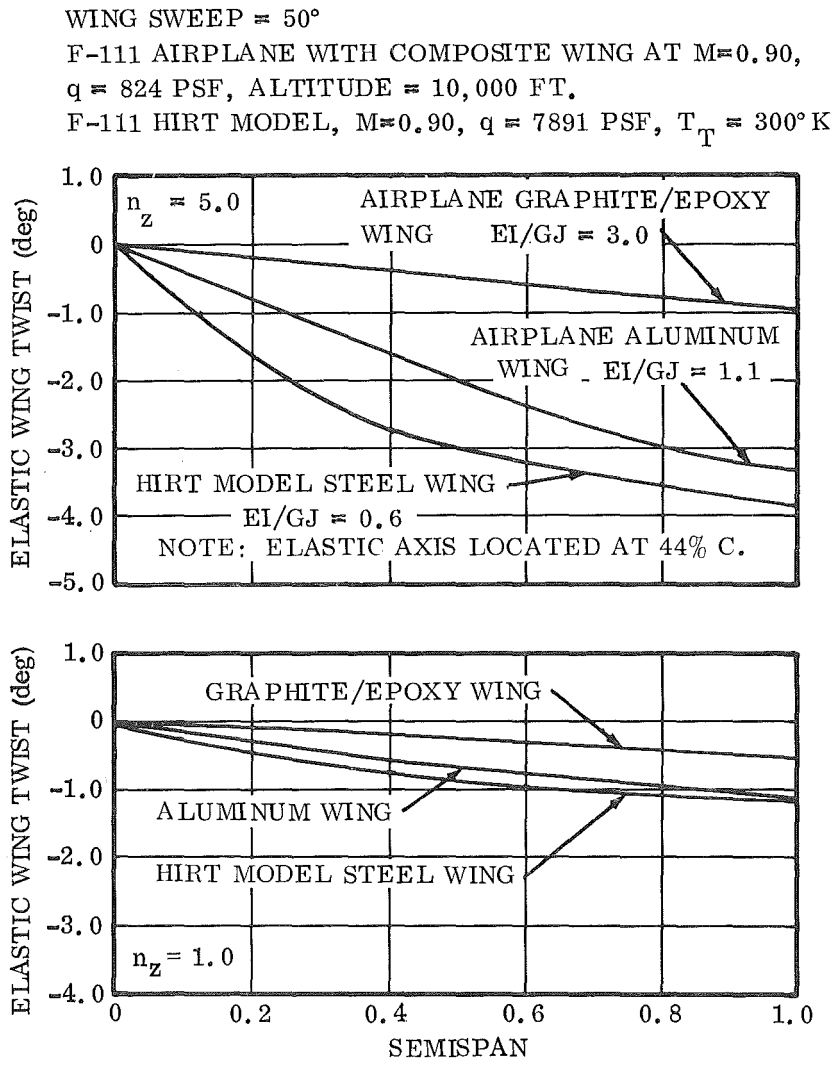

Figure A-10. Comparison of Elastic Twist Distribution for a Composite and Aluminum Wing on the F-111 Airplane at Load Factors of 1.0 and 5.0

WING SWEEP = 50°
F-111 AIRPLANE WITH COMPOSITE WING AT M=0.90,
q = 824 PSF, ALTITUDE = 10,000 FT.
F-111 HIRT MODEL, M = 0.90, q = 7891 PSF, T_T = 300° K

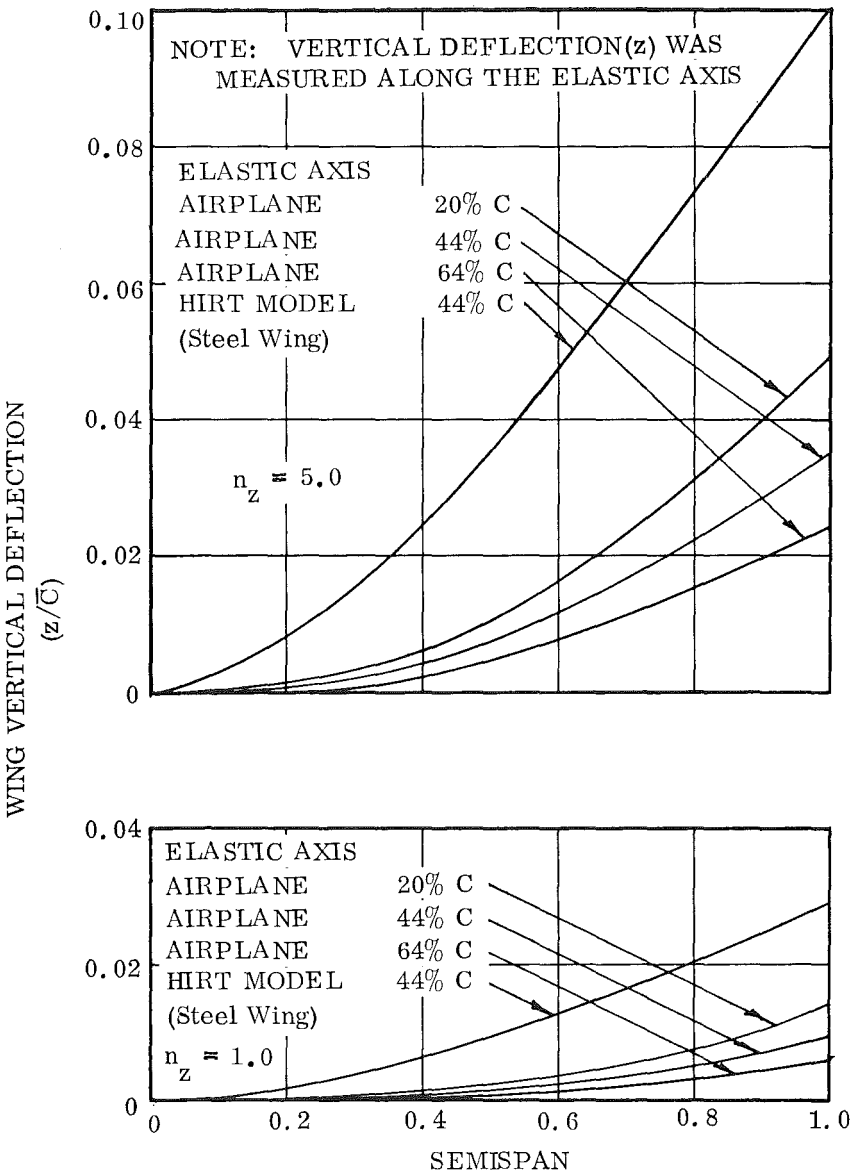

Figure A-11. Vertical Deflection for the F-111 Composite Wings at Load Factors of 1.0 and 5.0

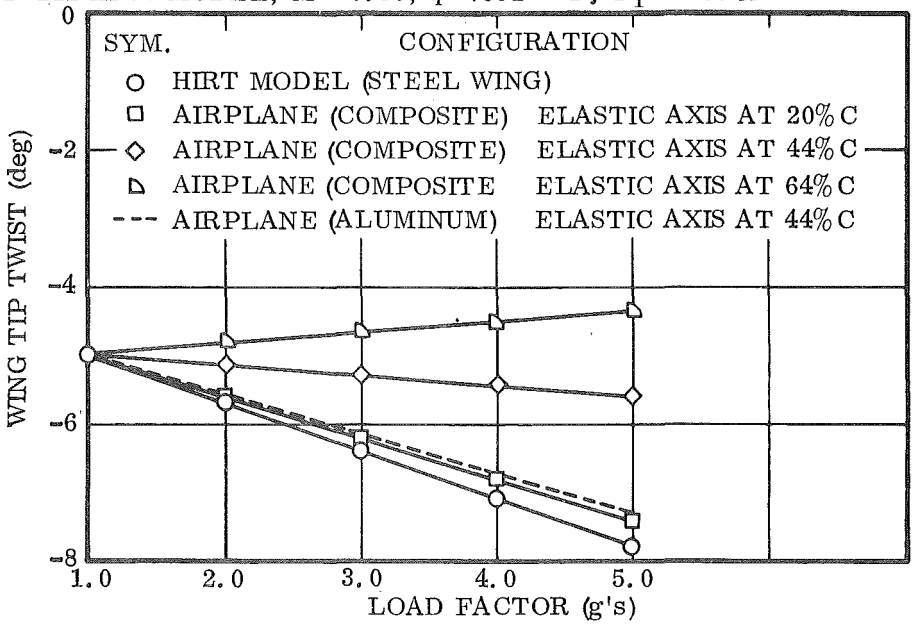

Figure A-12. Effect of Load Factor on the F-111 Tip Twist at Mach 0.90 and Full Scale Reynolds Number

composite wing at the equivalent flight condition, the model test data would indicate a lower lift, drag, and pitching moment by the amount shown in Figure A-13. These differences are considered inconsequential and are probably within the balance accuracy band. Figure A-14 shows the same aerodynamic increments as a function of the angle of attack for the composite wing designed with the elastic axis at 20% chord.

Incremental aerodynamic coefficients are presented in Figure A-15 for the composite wing with the elastic axis located at the 44% chord location. From Figure A-12, the differential tip twist was about 2.2 degrees. At a load factor of 5.0, the lift increment due to the differential tip twist is about 0.0120, with the drag increment increased to 0.0032. The aerodynamic increments as a function of angle of attack are presented in Figure A-16.

Figure A-17 illustrates the incremental aerodynamic coefficients for the condition of the composite wing with the elastic axis located at the 64% chord. The differential tip twist of 3.5 degrees at a load factor of 5.0 results in a lift increment of 0.0220 and a drag increment of 0.0054. Figure A-18 illustrates the aerodynamic characteristics as a function of angle of attack.

WING SWEEP = 50°
F-111 AIRPLANE WITH COMPOSITE WING AT M = 0.90, q = 824 PSF, ALTITUDE = 10,000 FT
F-111 HIRT MODEL, M = 0.90, q = 7891 PSF, T_T = 300°K
SOLID STEEL WING. FULL SCALE REYNOLDS NUMBER

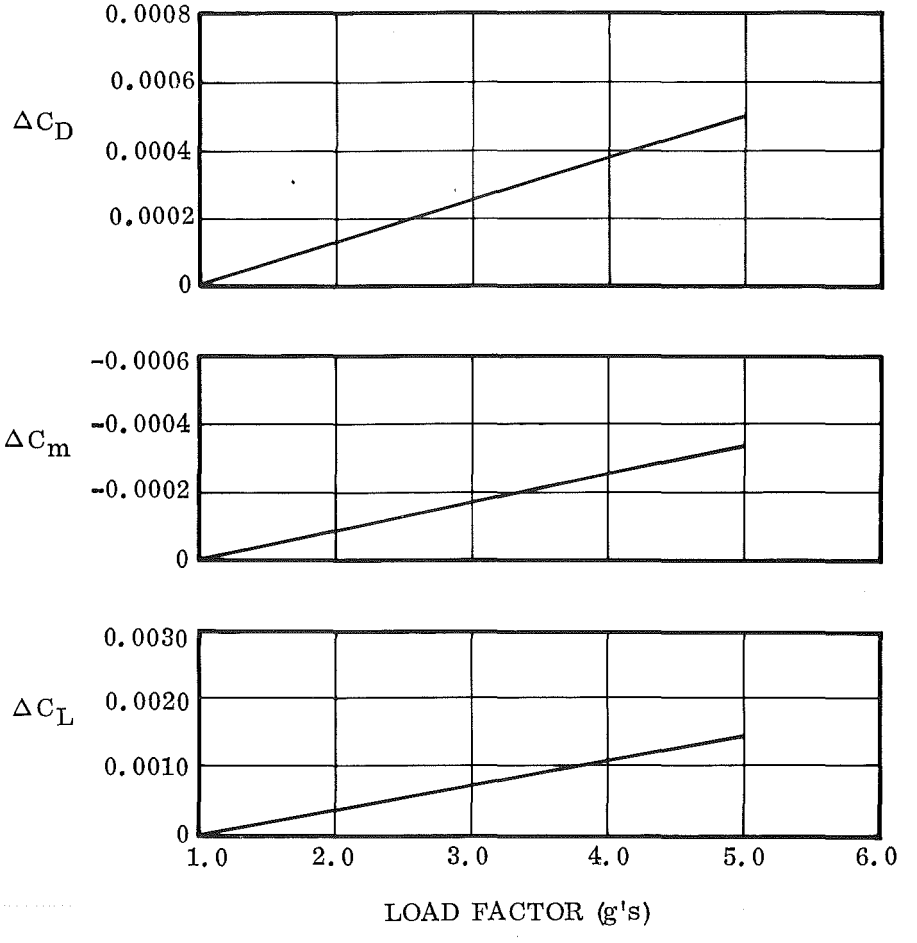

Figure A-13. Estimated Effect of Load Factor on the Incremental Aerodynamic Data for the F-111 Study Configuration at Mach 0.90 and Full Scale Reynolds Number (Altitude = 10,000 ft) (Composite Airplane Wing with Elastic Axis at 20% Chord)

WING SWEEP = 50°
F-111 AIRPLANE M = 0.90, q = 824 PSF, ALT = 10,000 FT
COMPOSITE WING WITH ELASTIC AXIS AT 20% CHORD
F-111 HIRT MODEL M = 0.90, q = 7891 PSF, T_T = 300°K
SOLID STEEL WING. FULL SCALE REYNOLDS NUMBER

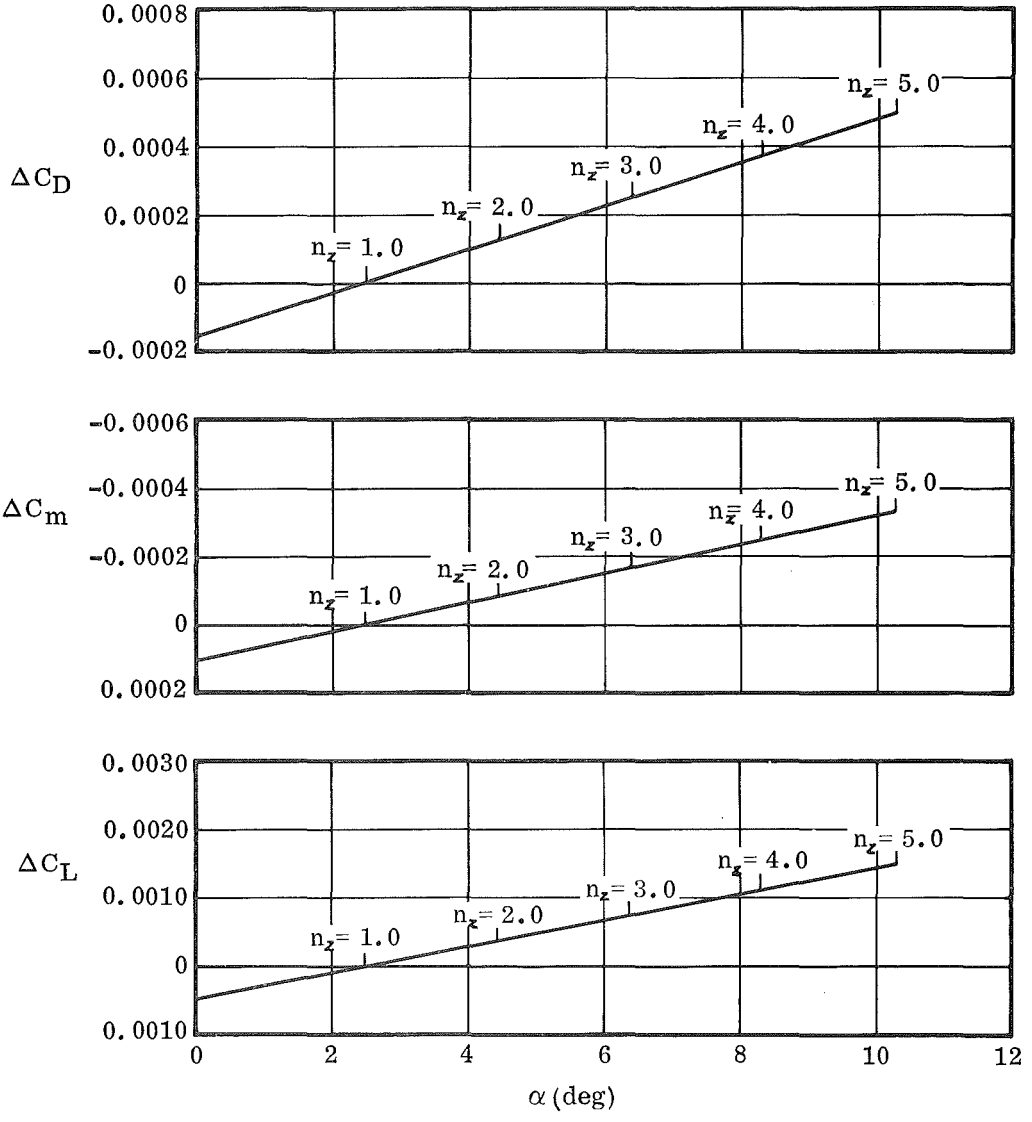

Figure A-14. Estimated Effect of Angle of Attack on the Incremental Aerodynamic Data for the F-111 Study Configuration at Mach 0.90 and Full Scale Reynolds Number (Altitude = 10,000 ft) (Composite Airplane Wing With Elastic Axis at 20% Chord)

WING SWEEP = 50°
F-111 AIRPLANE M = 0.90, q = 824 PSF, ALT = 10,000 FT
COMPOSITE WING WITH ELASTIC AXIS AT 44% CHORD
F-111 HIRT MODEL M = 0.90, q = 7891 PSF, T_T = 300°K
SOLID STEEL WING, FULL SCALE REYNOLDS NUMBER

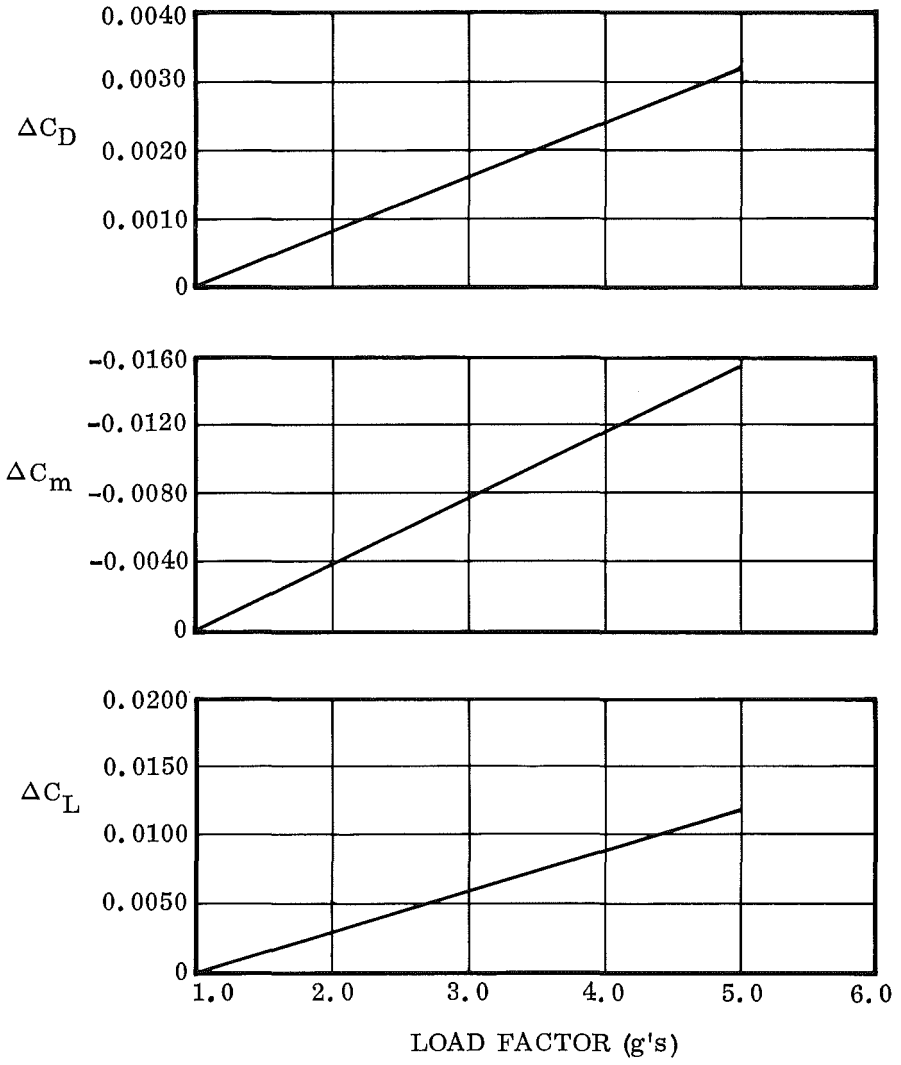

Figure A-15. Estimated Effect of Load Factor on the Incremental Aerodynamic Data for the F-111 Study Configuration at Mach 0.90 and Full Scale Reynolds Number (Altitude = 10,000 ft) (Composite Airplane Wing with Elastic Axis at 44% Chord)

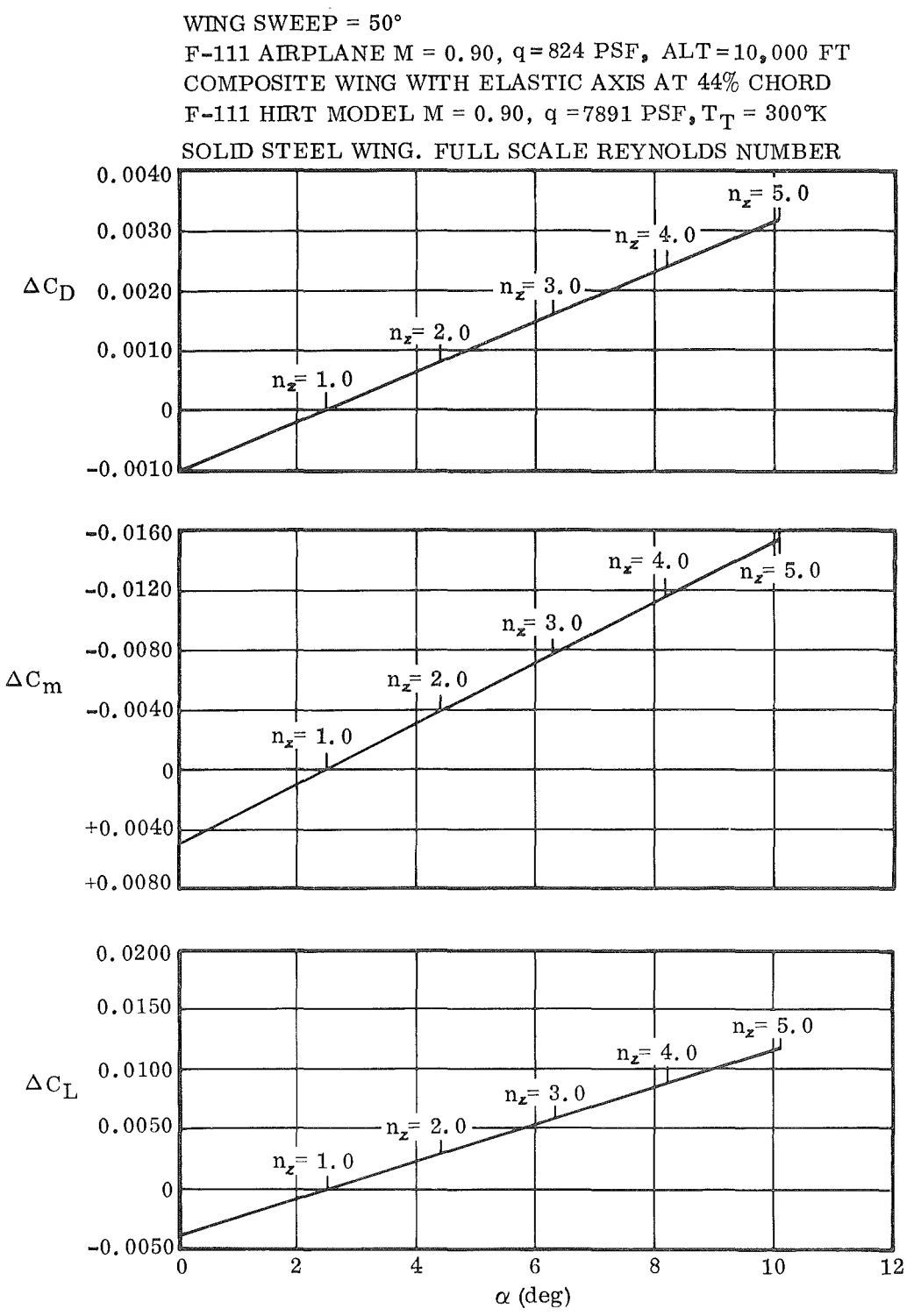

Figure A-16. Estimated Effect of Angle of Attack on the Incremental Aerodynamic Data for the F-111 Study Configuration at Mach 0.90 and Full Scale Reynolds Number (Altitude = 10,000 ft) (Composite Airplane Wing With Elastic Axis at 44% Chord)

WING SWEEP = 50°
F-111 AIRPLANE M = 0.90, q=824 PSF, ALTITUDE = 10,000 FT
COMPOSITE WING WITH ELASTIC AXIS AT 64% CHORD
F-111 HIRT MODEL, M = 0.90, q=7891 PSF, T_T = 300°K
SOLID STEEL WING. FULL SCALE REYNOLDS NUMBER

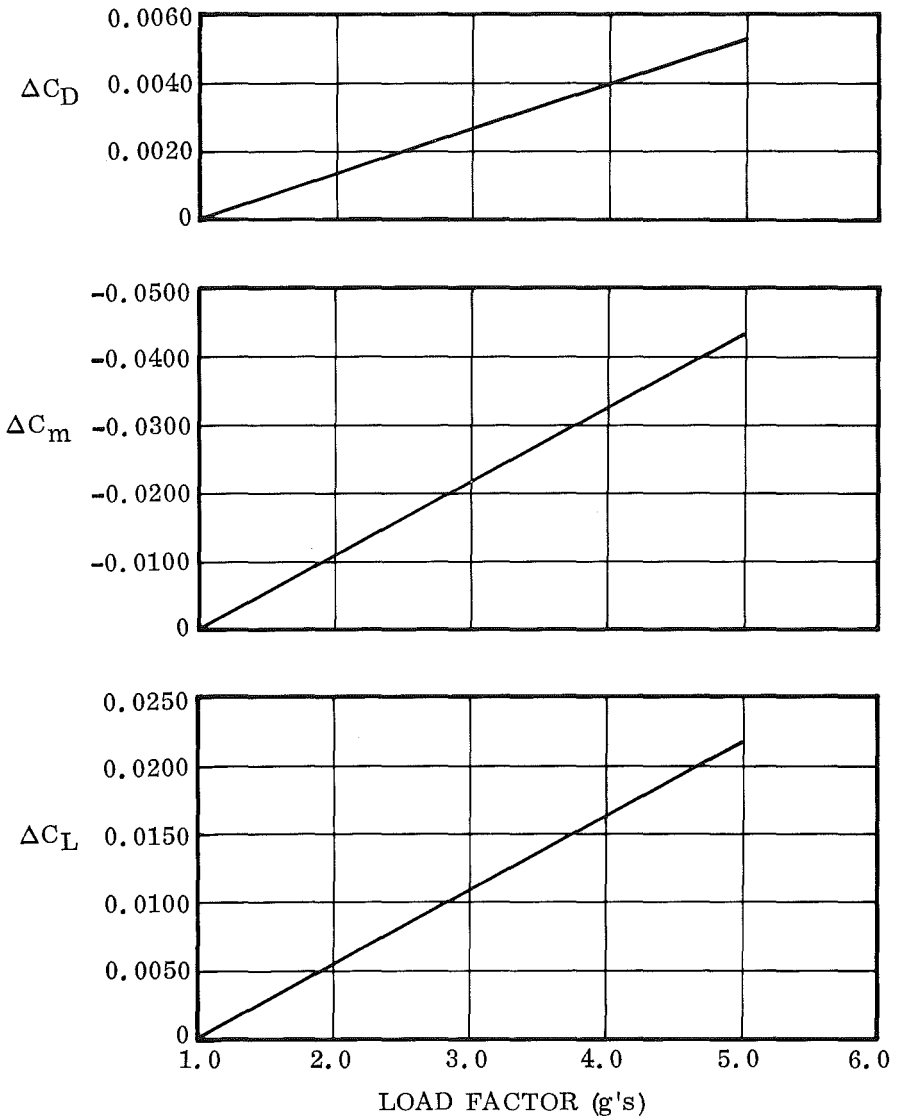

Figure A-17. Estimated Effect of Load Factor on the Incremental Aerodynamic Data for the F-111 Study Configuration at Mach 0.90 and Full Scale Reynolds Number (Altitude = 10,000 ft) (Composite Airplane Wing with Elastic Axis at 64% Chord)

WING SWEEP = 50°
F-111 AIRPLANE M = 0.90, q = 824 PSF, ALT = 10,000 FT
COMPOSITE WING WITH ELASTIC AXIS AT 64% CHORD
F-111 HIRT MODEL, M = 0.90, q = 7891 PSF, T_T = 300°K
SOLID STEEL WING, FULL SCALE REYNOLDS NUMBER

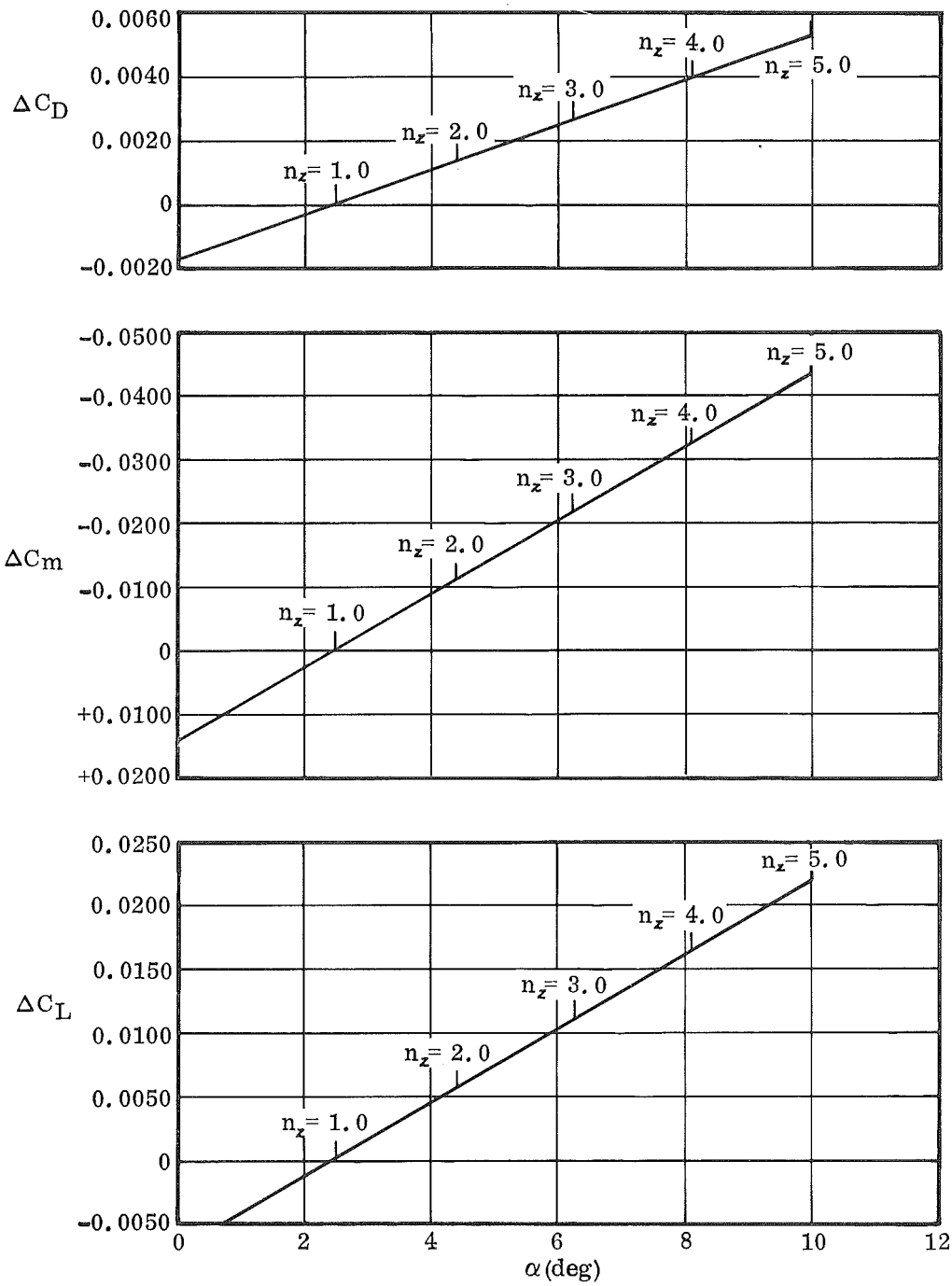

Figure A-18. Estimated Effect of Angle of Attack on the Incremental Aerodynamic Data for the F-111 Study Configuration at Mach 0.90 and Full Scale Reynolds Number (Altitude = 10,000 ft) (Composite Airplane Wing With Elastic Axis at 64% Chord)

A3. ANALYTICAL RESULTS

The results of this analysis indicate that the simulation of a composite wing by means of a solid steel model wing for equivalent Reynolds number testing will require an additional wing or wings to be jig twisted to obtain the desired level of model/airplane similarity at a particular flight condition. This will of course depend on the importance of the maneuvering aerodynamic characteristics for various concepts tested, as well as the importance of maintaining the similarity in Reynolds number.

From this analysis, the wing stiffness ratio (EI/GJ) and the location of the elastic axis simulated by the solid steel model wing will influence the number of wings required to simulate the airplane through the performance envelope. For a composite wing with the elastic axis located near the forward portion of the airfoil section, a single wing may be jig twisted to provide good test data through an angle-of-attack range that would be equivalent to load factors up to 5.0 for a combat airplane. As the elastic axis is moved aft, the simulation by a solid steel model wing becomes more unacceptable. The incremental aeroelastic deformations between the solid steel wing and the composite wing result in moderate effects on the aerodynamic data.

The elastic axis of future composite structures should move aft of the isotropic position to achieve the best compromise of flutter and divergence speeds. The flutter speed will increase with the aft movement of the elastic axis, all other flutter variables remaining unchanged, and the divergence speed will decrease. Current isotropic designs are rarely critical in divergence when a satisfactory flutter margin over the flight envelope has been attained.

The optimum amount of aft movement of the elastic axis can only be determined by examining both the flutter and divergence speeds for two or more elastic axis locations. The aft position (64%C) considered in this work was selected for the purpose of studying the effects on the aerodynamic response and represents an extreme position. It may well be that a practical limit of shifting the elastic axis aft will be between 44 and 64 percent of the local chord. It is clear from the results of this report that, if a large aft movement of the elastic axis of the full size anisotropic structure is needed to reduce wing weight, one or more additional model wings could be required to obtain the desired level of model/airplane simularity.

From the previous study, several testing techniques may be used to improve the simulation of the composite wing with a steel model wing. Tunnel temperature reduction will allow the full-scale Reynolds number to be simulated with a reduced dynamic pressure. This would result in reducing the model wing deflection at a selected equivalent flight condition. Mismatching Reynolds number would be the second method, which again results in reducing the tunnel dynamic pressure and thus the model wing deflections.

The composite wing deflections that have been analyzed during this study were based on a wing stiffness ratio of 3.0. For conditions with reduced wing stiffness ratios, the wing deformations will begin to approach the aluminum wing characteristics. The increased wing bending will lead to an increased wing twist. This condition will improve the ability to maintain model wing similarity with the flight vehicle at the equivalent Reynolds number condition.

Chordwise bending of the wing structure has not been considered in the study. The aerodynamic analysis is based on the twist distribution of the wing only. As stated previously, the wing bending characteristics are an integral part of the wing twist distribution, thus the aerodynamic characteristics resulting from a nonplanar wing are not considered directly.

A4. CONCLUSIONS

This study indicates that, for equivalent Reynolds number testing in HIRT, multiple steel wings may be required to simulate the composite wing shape accurately and thus obtain good experimental data. Several considerations qualify this result. First, when there is a close agreement between the model wing and the airplane composite wing elastic axis location, appreciable twist differences occur, producing aerodynamic data that does not accurately represent the characteristics of the aircraft. For the subject configuration, the composite wing had a stiffness ratio (EI/GJ) of 3.0, which is high relative to an aluminum structure of about 1.1. As the composite wing stiffness ratio is reduced to levels of the aluminum structure, one model wing may be sufficient to maintain wing shape similarity throughout the pitch range. For the condition where appreciable twist differences occur, drag is most affected, followed by pitching moment and lift. A second consideration is the importance of high g maneuver performance. For a transport design at load factors of 2.5, one model wing may be sufficient. Military maneuvering designs have emphasis on sustained maneuver performance (L/D) and instantaneous maneuverability (C_{Lmax}, buffet onset, controlability). This type of design is the most likely to require multiple wing testing.

The model deformation can be traded against Reynolds number to get model wing shape similarity for nonsimilar test Reynolds numbers by constraining the test dynamic pressure as a function of model wing shape rather than Reynolds number. Control capability of tunnel operating temperature would provide an additional dimension for the control of dynamic pressure, model shape, and test Reynolds number.

A5. REFERENCES

1. "A Proposal to Investigate the Conceptual Design of Navy Composite Wings", Vol. I, General Dynamics Convair Report No. CM72-2107.

NOMENCLATURE

Symbol	Description	Units
AEAD	Slope of the wing elastic axis	deg.
ALED	Slope of the wing leading edge	deg.
ATED	Slope of the wing trailing edge	deg.
AR	Wing aspect ratio	dim.
$\begin{bmatrix} A_W \end{bmatrix}$	Wing downwash matrix	in^{-1}.
$\begin{bmatrix} A_F \end{bmatrix}$	Wing image-vortex matrix	in^{-1}.
BL	Buttock line	in.
b	Wing span	in.
$\bar{C}$	Wing mean aerodynamics chord	in.
C_D	Drag coefficient	dim.
$C_{DE\alpha}$	Drag coefficient of external store	deg^{-1}.
C_{D_L}	Induced drag coefficient	dim.
ΔC_D	Incremental drag coefficient due to airplane/model wing twist differences	dim.
C_L	Lift coefficient	dim.
$C_{LE\alpha}$	External store lift curve slope	deg^{-1}.
$C_{LF\alpha}$	Fuselage lift curve slope	deg^{-1}.
$C_{L\alpha}$	Wing lift curve slope	deg^{-1}.
ΔC_L	Incremental lift coefficient due to airplane/model wing twist differences	dim.
C_ℓ	Wing section lift coefficient	dim.
C_M	Pitching moment	dim.
$C_{MF\alpha}$	Fuselage pitching moment curve slope	deg^{-1}.

NOMENCLATURE (cont'd)

Symbol	Description	Units
C_{m_o}	Wing section pitching moment at zero lift.	dim.
ΔC_m	Incremental pitching moment coefficient due to airplane/model wing twist differences	dim.
C_R	Wing root chord	in.
C_T	Wing tip chord	in.
E	Modulus of elasticity	lb/in^2.
EA	Elastic axis location (% chord)	-
$[E_A]$	External store matrix	lb^{-1}.
ETA(η)	Location of wing strip along the Y-axis (% semispan)	-
G	Shear modulus of elasticity	lb/in^2.
H	Wing strip halfwidth	in.
I	Wing section moment of inertia	in^4.
$[I]$	Moment of inertia matrix	in^4.
I_{YCG}	Moment of inertia of the airplane about the pitch axis through the center of gravity.	$in\text{-}lb\text{-}sec^2$.
J	Wing section polar moment of inertia	in^4.
ℓ	Span load	lb.
M	Mach number	dim.
MS	Model station	in.
m	Bending moment per unit pitching moment	dim.
m_o	Lift curve slope including compressibility effects	deg^{-1}.
n	Number of strips on the wing semispan	dim.
n_z	Load factor along Z axis	dim.
P_T	Horizontal tail load	lb.
Q(q)	Free stream dynamic pressure	lb/ft^2.

NOMENCLATURE (cont'd)

Symbol	Description	Units
R_e	Reynolds number	dim.
S	Wing area	in^2.
$[S]$	Wing elasticity matrix	in^{-1}.
T_T	Tunnel storage temperature	°K
t	Torsional moment around the elastic axis per unit pitching moment	dim.
V	Free stream velocity	ft/sec.
$[\Delta V_Z/V_Z]$	Overspeed effect matrix	dim.
W	Airplane gross weight	lb.
WL	Waterline	in.
w_p	Induced velocity normal to the wing chord plane	ft/sec.
XC4	Fuselage location of the 25% station of the wing mean aerodynamic chord	in.
YC4	Buttock line location of the 25% station of the wing mean aerodynamic chord	in.
ZC4	Waterline location of the 25% station of the wing mean aerodynamic chord	in.
ds	Differential distance along the elastic axis	in.
$\frac{d\epsilon}{d\alpha}$	Downwash at the horizontal stabilizer	dim.
α	Angle of attack of the airplane	deg.
α_F	Angle of attack of a wing section including aeroelastic effects	deg.
α_{inc}	Incidence angle	deg.
α_{oL}	Wing section zero lift line angle of attack	deg.
α_r	Wing root section angle of attack	deg.
α_s	Elastic angle of attack due to bending and torsional moments along the elastic axis	deg.

NOMENCLATURE (cont'd)

Symbol	Description	Units
α_r	Wing jig twist relative to the root chord	deg.
Γ	Circulation	$ft^3/sec.$
δ_{FL}	Flap deflection	deg.
δ_{SL}	Slat deflection	deg.
δ_{SP}	Spoiler deflection	deg.
$\ddot{\Theta}_{CG}$	Pitch acceleration of airplane	$deg/sec^2.$
Λ	Wing sweep angle	deg.
ρ	Fluid density	$lb\ sec^2/ft^4.$